Effect of Surface Treatment and Recycling on the Mechanical Properties of E-glass

UNIVERSITY OF BIRMINGHAM

By

Samuel Olukunle Ojo

A thesis submitted to the University of Birmingham for the degree of

DOCTOR OF PHILOSOPHY

School of Metallurgy and Materials
College of Engineering and Physical Sciences
University of Birmingham, UK
July 2016

ABSTRACT

The primary focus of this study was to investigate the effect of removing the binder, by specified method, on the tensile strength of E-glass fibre bundle and composites. The methods investigated for removing the binder from E-glass fibres were: (i) fibre spreading; (ii) acetone-based treatment; and (iii) heat treatment in air and in a vacuum.

In the first phase of the research, the effect of the above mentioned binder removal methods were investigated using the single-bundle tensile test. Binder removal via fibre spreading did not cause any reduction in the properties of E-glass fibre bundles. However, binder removal by acetone extraction led to a decrease of 37% in the tensile strength. The most detrimental effect on the tensile strength was found to be when E-glass was exposed to temperatures in excess of 450 °C. The percentage reduction in tensile strength for E-glass fibre bundle for 450 °C, 550 °C and 650 °C were 60%, 66% and 90% respectively.

In the second phase of the research, E-glass bundles that were subjected to the above-mentioned treatments were used to fabricate single bundle composites. The procedure for manufacturing these composites was developed. It was established that the reduction in the strengths of the E-glass composites after specified treatment could be correlated to the reduction in properties experience by the fibre bundles. Attempts were made to analyse the treated fibres using a range of analytical techniques such as X-ray diffraction, thermographic analysis, differential scanning calorimetry and infrared spectroscopy analysis. Heat treating E-glass fibres in the absence of air was shown to bring about a reduction in the tensile strength by 58% as compared to 78% when the fibres were previously heated in air at 650 °C.

DEDICATIONS

This thesis is dedicated to:

To my Saviour, Jesus Christ who gave His life for me. He is a loving Father and lifter of my head. He is the unchangeable changer, the immortal and the invisible. The ancient of days, the One who knows the end from the beginning.

(For His unconditional love and goodness over my family)

ACKNOWLEDGEMENTS

I thank the University of Birmingham, the School of Metallurgy and Materials and the Engineering and Physical Sciences Council (EPSRC) for providing the necessary funding to finance my studentship and other expenses incurred during the course of this research works. I would like to express my deepest appreciation to my Supervisor, Prof. Gerard F. Fernando, who gave me the opportunity to embark on this journey. I am thankful for his aspiring guidance, invaluably constructive criticism and friendly advice during the course of this research work. His assistance, kindness, and positive attitude displayed during the course of this work cannot be over emphasised. I am eternally grateful. I would like to thank the Deputy Head of School, Dr. Stephen Kukureka, who is my second Supervisor for his contribution at the initial stage of this programme. I am grateful.

Also, I am indebted to Dr Mayorkinos Papaelias and Dr. Surya Pandita, who both assisted me at different stages of this work. Despite their tight schedules, they were able to spend time with me in order to give valuable advise and provided tools to make my work easier. I wish to thank Dr. Winson Kuo of Johnson Matthey and a colleague in the department, Mr. Rayan Mohammed Ameen, who attempted to examine some of the samples used in this work by SEM when the author was in desperate need of answers to some mind boggling questions. I will always be grateful to such kind gesture. I am also grateful to my colleagues Dr. Shafique Irfan, Dr. Claire Wait, Messrs. Richard Murray and Nikolaos Angelopoulos whose support whilst working together in the laboratory for countless hours are immeasurable. Dr. Wait and Murray provided some of the materials used in this research and micrographs used in this thesis. I appreciate their good will. I have to appreciate my

beloved Brother, ‘Kunle Oyediran and Mr. Mark Paget who both read through my manuscript. I am eternally grateful to you both. I am also grateful for the assistance I received from Messrs. Frank Biddlestone, Andy Bradshaw, Carl Meggs and Stephen Williams. I am immensely grateful to you all.

A special gratitude to my family, especially my wife (Mrs Stella Ojo), whom without her support and understanding I would not have completed this work. I am also grateful to family members and friends for their supports and encouragement. My appreciation goes to my senior brother and his wife Pastor and Dr (Mrs) Philip Ojo for their prayers and encouragement from time to time. I would like to thank my spiritual fathers and mothers Dr. & Dr (Mrs) U. Obed, and Pastor Grace Edem, for their prayers and encouragement. Above all, may all the glory be unto the Lord, the One who is the controller of everything. He is a wonderful God and I give Him all the glory.

TABLE OF CONTENTS

LIST OF FIGURES

LIST OF TABLES

1 INTRODUCTION

1.1 Background to the Research

A review of the literature revealed that approximately 90-95% of all fibre reinforced composite products contain glass fibres (Kalidass and Balaji, 2014; Thomason *et al.*, 2014b; Colorado *et al.*, 2013; Lopez *et al.*, 2012a; Lopez *et al.*, 2012b; Feih *et al.*, 2009; Bunsell and Renard, 2005; Zinck *et al.*, 2001). In the past five decades, composite materials have become a preferred choice of material for manufacturing military and leisure boats, aircraft and helicopter components, marine structures, land transport vehicles, electrical/electronic appliances, sporting goods and other consumer products due to their high specific properties (property of interest normalised to the density). It is predicted that the use of glass fibres will grow as they penetrate deeper into existing markets (Blair *et al.*, 2015) and find new applications in emerging markets such as rail and other civil infrastructures (Blair *et al.*, 2015).

The continued increase in the use of fibre reinforced composites in recent years has increased the volume of waste. This has motivated significant research into the recycling and reuse of fibre reinforced composites (Hamad *et al.*, 2013; Job, 2013; Halliwell, 2006; Leterrier, 2000).

The recycling and re-use of fibre reinforced composite waste needs to be addressed to satisfy various European Union legislation and those specified by regional authorities (Job, 2013; Lopez *et al.*, 2012a; Lopez *et al.*, 2012b; Oliveux *et al.*, 2012; Gerard and Kandlikar, 2007; Williams *et al.*, 2005). For example, COM 666 (EC, 2005) is an act that seeks to

promote recycling in order to reintroduce end-of-life waste materials into the economic cycle in the form of quality products, whilst minimising the negative environmental impacts (DeRosa *et al.*, 2004).

It has been projected that the total global production of composite materials will exceed 10.3 million tonnes by 2015; this is estimated to occupy an area of about 60 million cubic metres (Witten, 2014; Yang *et al.*, 2015; Lopez *et al.*, 2012a; Lopez *et al.*, 2012b; Kinsella *et al.*, 2001). Since glass fibre composites based on thermosets constitute approximately 90% of composite currently produced globally, the difficulties and costs involved in recycling these products must be addressed. Recycling of materials thrive where it is cost-effective to do so. For example, the metal recycling industry. On the contrary, fibre reinforced composite waste materials are generally more difficult to recycle and are economically less favourable. This was particularly relevant in the past where disposal in landfills cost in the United Kingdom was in the range £72 - £80 per tonne in 2013. This normally increases in steps of £8 per tonne, which now cost between £120 and £150 per tonne (Baines and Carruthers, 2013; Halliwell, 2006; Pickering, 2005). Furthermore, the current cost of recycling glass fibre-based thermoset composites is not competitive when compared with the cost of using virgin glass fibres (Thomason *et al.*, 2014b; Lopez *et al.*, 2012a; Lopez *et al.*, 2012b; Yang *et al.*, 2011). Another key factor that needs to be considered is the fact that the mechanical strength of the thermally recycled glass fibres can be lower than the virgin fibres by 90 - 95% (this depends on the temperatures used to oxidise the matrix). This makes these recycled glass fibres inappropriate for use in structural composites where high-strength is required (Jenkins *et al.*, 2015a; Jenkins *et al.*, 2015b).

Therefore, a large proportion of these materials end up in landfills. Considering the existing waste management legislation, for example, EU 1999/31/EC; EU 2000/53/EC; EU 2000/76/EC; EU 2006/12/EC (Chang and Pires, 2015), coupled with the predicted increase of landfill taxes, and the finite landfill capacity, suggests that existing disposal methods will not be an attractive option in the future (Ribeiro *et al.*, 2013). Baines and Carruthers (2013) and Halliwell (2006) were of the view that landfill taxes would need to be increased in order to encourage manufacturers to develop strategies to recycle, reclaim and re-use their composites components at the end of their life, before considering incineration and disposal in landfills as an option. There are various methods for recycling composites. For example, mechanically grinding to produce particulates (regrind), chemical and thermal processes where the matrix is digested or degraded to recover the glass fibres (Hamad *et al.*, 2013; Otheguy *et al.*, 2009; Pickering, 2005). Thermal recycling by pyrolysis is generally carried out using a rotary kiln or equivalent or in a fluidised bed (Chanda and Roy, 2009). However, the glass fibres that are recovered after the thermal degradation of the matrix, in the temperature range 380 - 650 °C, show a 34% - 90% reduction in the tensile strength (Gong *et al.*, 2016; Yang *et al.*, 2015; Thomason *et al.*, 2014b; Feih *et al.*, 2011; Pickering, 2005; Hollaway *et al.*, 2004).

Given the large volumes of waste glass fibre components that are produced annually, there is a need to understand the mechanisms that are responsible for the observed degradation in tensile properties after thermal-based recycling. Key papers that address this subject include the following: Jenkins *et al*. (2015b),Thomason *et al.* (2014a), Lopez *et al*. (2012a), Feih *et al.* (2011), Kao *et al.* (2010), Pico & Bartl (2010), Feih *et al.* (2010), Zainuddin *et al.* (2009), Shrivastava & Hussain (2008), Pickering (2005),Williams *et al.* (2005), DeRosa *et*

al. (2004), Cunliffe *et al.* (2003), Mouritz & Mathys (1999), Kennerley *et al.* (1997) and Sakka (1957).

Research hypotheses that were considered in the current studies were:

(i) Thermal-based techniques for pyrolysing the binder as a means for recovering the E-glass fibres leads to a significant decrease in the tensile strength. There is a need to understand the reasons for this degradation.

(ii) The pyrolysis of the matrix may cause adverse effects which in turn reduce the tensile strength of E-glass, including: (a) the slower cooling rate leading to partial crystallisation; (b) changes to the net stress state where the outer surface assumes a tensile state; (c) pyrolysis of the binder and/or the matrix bringing about a chemical reaction that embrittles the surface; (d) dihydroxylation of the surface as a function of pyrolysis temperature makes subsequent re-hydrolysis, without the protection of the binder (as is the case when the E-glass is manufactured), more detrimental; and (e) phase separation in the glass during the pyrolysis and cooling. Evidence was sought in the current study to progress the above-mentioned hypotheses.

1.2 Aims and Objectives

The aims and objectives of this project are as follows:

(i) To evaluate the tensile properties of as-received and heat-treated E-glass fibre bundles.

The fibre bundle test (FBT) was adopted instead of the single-fibre tensile or fragmented test. The objective here was to conduct the FBT in tandem with surface-mounted acoustic emission (AE) transducers to detect fibre fracture during tensile loading.

(ii) To compare the tensile properties of as-received, spread as-received and lubricated E-glass fibre bundles.

The term "spread" is used here to describe an in-house technique where the filaments in the bundle are spread using a mechanical technique. This results in the width of the bundle increasing along with a concomitant decrease in the thickness. As-received and spread as-received E-glass fibre bundles were prepared and tensile tested using varying gauge lengths (50 mm, 80 mm, 100 mm, 150 mm and 200 mm). This was to quantify the effect of fibre spreading and gauge lengths on the tensile properties of E-glass fibre bundles.

(iii) To analyse the fibre bundle strength distribution of E-glass using the Weibull statistical analysis.

Established Weibull strength distribution models were used to obtain the appropriate slope and modulus parameters. This required 30 samples per batch to be prepared and evaluated. The bundles were end-tabbed and tensile tested to failure. The mechanical and AE data were used to derive the Weibull survival probability parameters.

(iv) To assess the tensile properties of composites manufactured using the treatments mentioned above.

Fibre reinforced composites were manufactured using as-received and specified surface treatments mentioned previously. The samples were impregnated manually, vacuum bagged

and processed in an autoclave. These composites were end-tabbed and tensile tested to failure. Surface-mounted electrical resistance gauges were deployed to log the strain and acoustic emission transducers were used to record the acoustic emissions during tensile testing to failure.

1.3 Structure of the Thesis

The current chapter highlighted the background and motivation for this project where the need to understand the mechanical strength degradation as a function of temperature during the pyrolysis of the matrix was discussed.

Chapter two presents a review of E-glass fibres where the mechanical and thermal properties of E-glass fibre are discussed. The effect of surface treatment, environmental effects, thermal conditioning and Weibull statistical analysis on the strength of E-glass fibre bundle are also reviewed.

Chapter three presents the experimental procedures that were used in studying the effect of the binder removal methods, heat treatment and fibre spreading on the tensile strength of E-glass fibre. Fibre spreading was used as a means, in addition to solvent extraction and heat treatment, to remove or partially remove the binder. Composites were manufactured from these treated fibres. A set of thirty specimens were tested from the samples obtained from the majority of binder removal methods. Surface-mounted strain gauges were used to monitor the strain during tensile loading.

Chapter four presents the research results and discussions based on the experiments carried out in Chapter three.

The final Chapters of the thesis (Chapter 5 and 6) present the conclusions and recommendations for future research.

2 LITERATURE REVIEW

2.1 Introduction

The failure strength of unidirectional composites is linked to the mechanical properties of the reinforcement (Oskouei and Mehdi, 2010; Oskouei, 2009; R'Mili *et al.*, 2008; R'Mili *et al.*, 1996). The single-fibre and single-bundle tensile test (BTT) techniques have been used to obtain the statistical distribution of the tensile strength of the E-glass fibres (Creasy, 2000; R'Mili *et al.*, 1996; R'Mili *et al.*, 2008). The single-fibre test has been reported to be problematic as the sampling method employed can cause damage to the fibres during handling (He and Clarke, 1997; Cowking *et al.*, 1991). This problem is compounded by the fact that the fibres are fragile and the difficulty in handling whilst the sample is being prepared is considerable. On the other hand, the preparation of the single-bundle tensile sample is said to be much easier and less prone to damage caused by handling (He and Clarke, 1997).

Most classes of reinforcing glass fibre is composed of silica with additions of oxides of calcium, boron, aluminium, iron, sodium, potassium and magnesium (Bagherpour, 2012; Hull and Clyne, 1996). Glass fibres are manufactured by melting the raw materials between 1200 and 1600 ºC (Gorowara *et al.*, 2001). The molten glass is then fed into a series of micro-fine platinum/rhodium bushings containing a large number of orifices of diameter between 0.75 and 20 μm (Wallenberger, 2010; Kinsella *et al.*, 2001).

The molten glass flows under gravity and the filaments are quenched rapidly and drawn by mechanical winders operating at linear velocities of approximately 60 meters/second. Prior to the mechanical winding stations, the filaments are traversed over an application roller which coats the fibre within an aqueous mixture of chemicals generally referred to as the binder (Gorowara *et al.*, 2001; Kinsella *et al.*, 2001). This forms a protective layer on the filaments and it minimises fibre-to-fibre abrasion during subsequent handling. Finally, the fibres are wound onto a cardboard mandrel to form what is termed a package. The fibres are thereafter dried for approximately 10 hours at 130 ºC (Gorowara *et al.*, 2001). These filaments are normally drawn together to form a strand or roving.

The term TEX is used to define a roving. The TEX is defined as the mass of fibres (in grams) per 1000 m of roving (Zangenberg and Brondsted, 2015). TEX values for glass rovings range from 100-9,600. The number of filaments of fibres in a roving is called the k-number, and this can be related to the glass fibre TEX using Equation (1) (Zangenberg and Brondsted, 2015):

$$k = \frac{TEX}{\rho_f * d_f} \qquad [1]$$

where ρ_f is the fibre density and d_f is the average filament diameter.

The strength and modulus of glass depends on the atomic structure. In silica-based glasses atoms are primarily bonded by covalent tetrahedral bond angles with silicon at the centre and oxygen at the corners. The oxygen atoms at the edges are shared between the tetrahedral configuration, hence creating a rigid three-dimensional network (Hu and Liu, 2010; Hull and Clyne, 1996). However when elements of low valency, such as Na, Ca, and

K are added, they break up the tetrahedral network by reducing the number of covalent bonds in the matrix. Such functions by these elements lower the stiffness and strength but improve the formability. The properties of glass fibres are isotropic. Hence, the Young's moduli and coefficient of thermal expansion are the same along the axial and transverse axes (Bagherpour, 2012; Hull and Clyne, 1996).

Generally, glass fibres have tensile strengths in the range 1.5 to 4.0 GPa; however, this is influenced by factors such as the exposure time in specified environment (temperature and humidity) and the nature and manner of load application (strain rate) (Maxwell *et al.*, 2005; Jones, 1999). Thomason *et al.* (2014b), reported that when amorphous silica is subjected to thermal treatment above 400 ºC, severe dehydration can occur which may be difficult to reverse. Lezzi *et al.* (2015) found that crystallisation occurred on the surface of glass fibre when heat treated above ~800 ºC. These researchers suggested that this surface crystallisation has been found to lower the tensile strength (Lezzi *et al.*, 2015). The Young's moduli and failure strains are in the range 53 to 87 GPa and 1.8 to 5.4% respectively (Yolken and Matzkanin, 2009; Bunsell and Renard, 2005; Hull and Clyne, 1996; Jones, 1999). Compositions and properties of selected commercial glass fibres are presented in Table 2.1.

Table 2.1 Compositions (in weight %) of typical glasses for fibres, with selected properties (Jones, 2001).

Constituent/ property	**E**	**ECR**	**C**	**A**	**S**	**R**	**Cemfil[11]**	**AR[12]**	**AR**
SiO_2	55.2	58.4	65	71.8	65.0	60	71	60.7	61
Al_2O_3	14.8	11.0	4	1.0	25.0	25	1	-	0.5
B_2O_3	7.3	0.09	5	-	-	-	-	-	-
ZrO_2	-	-	-	-	-	-	16	21.5	13.0
MgO	3.3	2.2	3	3.8	10.0	6	-	-	0.05
CaO	18.7	22.0	14	8.8	-	9	-	-	5.0
ZnO	-	3.0	-	-	-	-	-	-	-
TiO_2	-	2.1	-	-	-	-	-	-	5.5
Na_2O	0.3	-	8.5	13.6	-	-	11	14.5	-
K_2O	0.2	0.9	-	0.6	-	-	-	2.0	14.0
Li_2O	-	-	-	-	-	-	-	1.3	-
Fe_2O_3	0.3	0.26	0.3	0.5	tr	-	tr	tr	-
Fluorides	0.3	-	-	-	-	-	-	-	-
Liquidus temperature [a] (ºC)	1140	-	-	1010	-	-	1201	1172	-
Fiberising temperature [b] (ºC)	1200	-	-	1280	4.7	4.5	1470	1290	-
Single fibre tensile strength at 25 ºC, (GPa)	3.7	3.4	3.4	3.1	-	-	2.9	-	2.5
Single fibre tensile modulus (GPa)	76.0	73.0	-	72.0	86.0	85.0	-	-	80
Density, (g/cm^3)	2.53	2.6	2.49	2.46	2.48	2.55	-	2.74	2.74
Refractive index n_D	1.550	-	-	1.541	1.523	-	-	-	1.561
Coefficient of linear thermal expansion ($10\ K^{-1}$)	5.0	-	7.1	9	2.85	4.10	-	-	-
Volume resistivity (Ω cm)	10^{15}	-	-	10^{10}	10^{16}	-	-	-	-
Dielectric constant at 25 ºC and 10^{10} Hz	6.11	-	-	-	-	6.2[c]	5.21	-	-
Loss tangent at 25 ºC and 10^{10} Hz (10^{-3})	3.9	-	-	-	-	1.5[c]	6.8	-	-

[a] The liquidus temperature is the highest temperature at which a glass, if held there sufficiently long, will develop crystals. The greater the difference between this and fiberizing temperature, the more stable the fibre-forming process.

[b] Indicates temperature at which the viscosity of the glass is 10^3 Pa s.

[11], [12] These were included in the list of references by Jones.

The current study is focused on E-glass and hence, the following section considers aspects of relevance to the aims and objectives of this study.

E-glass is a commercial general-purpose glass, comprising an aluminosilicate glass whose composition is summarised in Table 2.1. According to Wang (2003) and Bunsell and Renard (2005), E-glass fibres are significantly cheaper when compared with most other relatively high-modulus fibres such as carbon and aramid. Hence, they are used extensively in industrial environments such as electrical (printed circuit board), marine (boats), automotive (body panel) and aerospace (pressure vessels).

2.2 Mechanical and Thermal Properties of E-glass Fibres

Based on the first two objectives mentioned in Chapter 1, some of the factors that influence the mechanical and thermal behaviour of E-glass fibre bundle are reviewed.

2.2.1 Mechanical Properties

2.2.1.1 Tensile Strength

Table 2.2 presents a summary of the mechanical properties of the selected organic and inorganic glass fibres. The moduli for the inorganic glasses range from 72 to 87 GPa.

Table 2.2 Specified properties of glass and other classes of reinforcing fibres along with selected materials properties (Jones, 2001)**.**

Fibre types		E (GPa)	σ_u (GPa)	ρ (g/cm^3)	E/ρ (Nm^2/kg)	σ_{fu}/ρ (Nm/kg)	ε_u (%)	d_f (μm)
E-glass fibre		72	1.5-3.0	2.55	2.8-4.8	58,000-117,000	1.8-3.2	10-20
S-glass fibre		87	3.5	2.5	3.5	140,000	4.0	12
Carbon fibre (Type not mentioned)		220-350	2.3-3.7	1.8-2.0	12-18	130,000-190,000	0.7-1.7	7
High-performance polymer fibres:	Aramid	60-80	2.65-3.45	1.44-1.47	4.0-12.2	180,000-235,000	4-1.9	12
	PBT	250	2.4	1.5	17.0	160,000	1.0	20
	PE	60-120	1-3	1.0	6-12	100,000-300,000	-	
Steel		210	0.34-2.1	7.8	2.7	4,300-27,000	-	-
Aluminium		70	0.14-0.62	2.7	2.6	5,000-22,000	-	-
Bulk glass		60	0.05-0.07	2.6	2.3	1,900-2,700	0.08-0.12	-
Resin (epoxy)		2-3.5	0.05-0.09	1.2	0.16-0.29	4,000-7,500	1.5-6	-
High-density ethylene (HDPE)		1.3	0.027	0.96	0.135	2,800	-	-

E=Young's modulus, σ_u=tensile strength, ρ=density, E/ρ= specific modulus, σ_u/ρ=specific strength, ε_u=failure strain, d_f=fibre diameter

Griffith (1921) observed that the strength of brittle materials is influenced by surface flaws, bulk flaws, composition, and temperature. Korwin-Edson *et al.* (2012) reported that surface flaws in fibres could be created within the manufacturing setting by contact-damage with water, sizing applicators, sizing solids, other fibres and collets. These flaws were referred to as physical or chemical in nature and were said to cause significant stress concentrations with depths of a few nano-metres. However, clear evidence was not provided to verify the occurrence or aftermath of the contact-damage.

Griffith (1921) recognised that rapid fracture occurred at a critical flaw size. He found that for glass, as the surface-to-volume ratio is increased, it led to an increase in strength. This was attributed to a reduction in the number of flaws of critical dimensions. It therefore stands to reason that filaments with a low-diameter (for example 10 μm) will exhibit higher tensile strength when compared to its bulk glass counterpart. Furthermore, the strength of a fibre will also be dependent on its gauge length. It is also important to appreciate that a bundle of fibres will exhibit a distribution in the tensile strength (Jones, 2001a).

The theoretical strength of E-glass has been estimated to be 7.0 GPa whilst the strength of a typical E-glass fibre is 3.0 GPa. Schmitz *et al.* (1963) studied flaw growth by corrosion and their incubation period prior to filament fracture in E-glass. Static fatigue and tensile tests were carried out on E-glass at 50 and 100% relative humidity. These researchers found that the initial strength of E-glass fibre did not deteriorate until approximately 95% of its static fatigue life. They suggested that corrosion might have occurred very rapidly within the last phase of the test. It was assumed that chemical processes within the prolonged incubation

during the fatigue test might have reached a critical stage before corrosion could occur. The chemical processes were believed to occur in the vicinity of structural flaws where concentration of terminal cations interrupts the silica network. Water reacts with cations in the glass during hydrolysis which in turn increases the concentration of hydroxyl ions (i.e an increase in the pH). This continues until the pH reaches a critical level for corrosion to set in. The process of corrosion was explained by separating it into two phases: incubation and corrosion. Schmitz *et al.* (1963) said that they were able to identify flaws distribution by analysing the shape parameter of the Weibull strength distribution parameter. The variations in the distributions were mapped with the various gauge length to identify the characteristic flaws distributions. By analysing average filament strength and surface flaws using statistical analysis, Schmitz *et al.* (1963) concluded that three types of flaw population patterns existed:

(i) Severe surface flaws originating from handling and processing which represents the tensile strength of commercial E-glass fibres (3.0 GPa). These surface flaws were said to be spaced at an average of 20 mm.

(ii) Mild surface flaws which were said to represent tensile strengths in the range 3.0–5.0 GPa. These were said to occur at an average spacing of 0.1 mm. They stated that it was likely that this type of flaw originated from etch pits. However, they reported that it was unclear whether this occurs in the absence of stress or during the stress corrosion experiments.

(iii) The third type of flaw was assumed to represent an internal defect that was spaced 10^{-4} mm apart. The tensile strength of this class of fibre was said to be in excess of 5 GPa. They stated that this was representative when the gauge length was below 1 mm.

Bartenev (1968) classified item (ii) above as internal defects. However, despite their differences in opinion, both authors accepted the existence of flaws on E-glass surfaces.

2.2.1.2 Static Fatigue

When glass fibres are subjected to a long-term static tensile stress, they undergo static fatigue (Jones, 2010; Jones, 2001; Jarvela, 1984). Static fatigue is the time-dependent fracture of a material under a constant load as opposed to a conventional fatigue test where a cyclic load is employed (Liu *et al.,* 2009). The factors that influence the static fatigue of glass fibres include: the chemical composition; environmental conditions, (pH, temperature, chemical composition of any applied fluid), magnitude of the applied stress and diameter and length of the fibres. This phenomenon of static fatigue is shown in Figure 2.1 where the failure times of the fibre bundle under stress in distilled water is illustrated (Koike *et al.*, 2007; Harris, 1999; Mattewson and Kurkjian, 1987; Wiederhorn and Bolz, 1970). The same trend was observed on samples tested in air but there was no time-dependent strength observed when the experiments were conducted in a vacuum (Jones, 2001). A number of researchers believe that static fatigue is a corrosion-based mechanism that takes place in the presence of water (Ciccotti, 2009; Khennane and Melchers, 2003; Wiederhorn and Bolz,

1970). Figure 2.2 illustrates generalised reaction schemes showing the degradation of the silica networks in the presence of water:

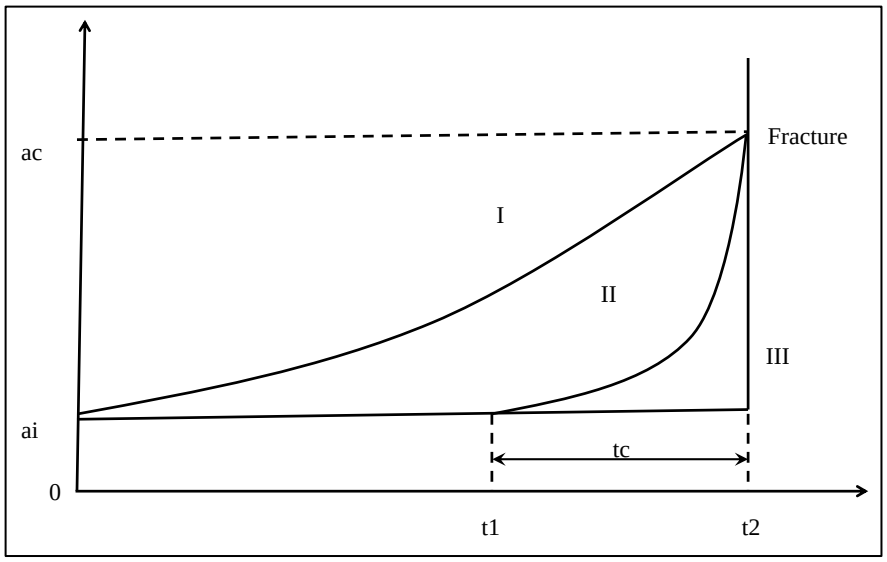

Figure 2.1 Schematic illustration of the failure processes and life for brittle materials under static loading: Stage-I subcritical crack-growth; stage-II: partly subcritical growth; and stage-III: instantaneous fracture (Vikram and Kumar, 2013).

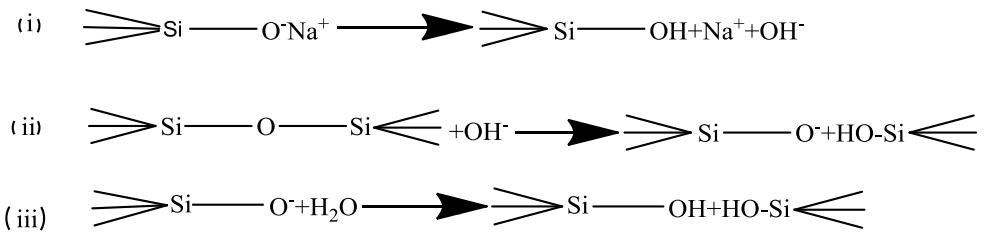

Figure 2.2 Schematic illustration of the failure processes and life description for brittle materials under static loading: Stage-I subcritical crack-growth; stage-II: partly subcritical growth; and stage-III: instantaneous fracture (Vikram and Kumar, 2013).

Liu *et al.* (2009), Jones (Jones, 2001) and Al-Khudairi *et al.* (2014) classified static fatigue into three stages.

Stage-I was defined as the fracture behaviour largely dominated by cracking. Static fatigue phenomenon is determined by the rate of diffusion of sodium ion. Stage-II was referred to as a state where corrosion sets in when interaction between the surface and atmosphere was suspected because the rate of crack growth was found to be equal to the rate of corrosion. Here, the cracks were said to be prominent and advance rapidly into the weakened material. Stage-III was said to occur through the stress-assisted corrosion, where the effect of stress on failure time is less significant. This is because the rate of the hydrolysis of the silica network is higher than the rate of crack growth (Al-Khudairi *et al.*, 2014; Jones, 2010; Jones, 2001; Jones, 1999; Bao and Suo, 1992). According to Ito and Tomozawa (1982) and Charles as reported by Liu *et al.* (2009), the crack tip is blunted by corrosion so that the stress concentration at the tip is reduced (Jones, 1999). Bao *et al.* (1992; 1992) defined the

lifetime as the time of crack growth which is only suitable for stage-I failure. Stage-II failure was referred to as the general type which contains the other two (when t_i=0 becomes stage-I and t_i=t_f becomes stage-III). Then, the lifetime becomes the sum of the time before crack initiation and time of the sub-critical growth as described by Equation [2.2]:

$$t_f = t_i + t_c \qquad [2.2]$$

where t_i, time to crack initiation; t_c, time to reach subcritical crack growth.

According to Jones (Jones, 2001), the chemistry at the crack tip causes a rounding of the crack-tip and a reduction in the potential for cracks to propagate further according to the following equation:

$$\sigma_{\max} = 2\sigma_a \left(\frac{x}{r}\right)^{1/2} \qquad [2.3]$$

where σ_{max}, is stress at the crack tip; σ_a, applied stress; x and r are flaw depth and radius, respectively.

Ghosh *et al.* (2010) studied sub-critical crack growth in E-glass where they measured the static fatigue limit of the threshold stress intensity factor (K_{th}) to be 0.15 ± 0.04 $MNm^{-2/3}$, which they compared with critical stress intensity factor (K_{Ic}) value of 0.93 ± 0.03 $MNm^{-3/2}$ for monotonic loading in stage-I.

In order to calculate the time to failure of a filament, the stress corrosion exponent to K_{th} is required for calculating the crack growth rate. This can be estimated from the strain rate

dependence on the fibre strength for a single filament. However, in the case of the fibre bundle, this has to be combined with Weibull statistical analysis; this is discussed later in this chapter.

2.2.2 Thermal Properties of E-glass

With reference to the research hypotheses stated in the previous chapter, the reasons for the observed thermally-induced degradation in the tensile strength of E-glass is still a subject of significant on-going research.

The thermal history of glass fibres has been used to explain the superiority of the strength of glass fibres when compared to bulk glass. Glass fibre filaments have been reported to have higher tensile strengths and stiffnesses (Tsai and Wu, 1971; Loewenstein, 1962; Griffith, 1921). Lu (1998) detected that there was a relationship between birefringence and tensile strength during annealing. Cherin (1983) reported that the optical properties and the molecular structures of E-glass fibre and the bulk differ. Processing parameters and post-processing operations distort the glass fibre properties in a way that affect the molecular structure. Cherin (1983) studied structural relaxation and sensitivity of glass fibre of different chemical composition by conducting investigation on birefringence, density, shrinkage and heat capacity; this led to the detection of birefringence in drawn silica glass fibre from orifices. Lu (1998) found that glass fibre processing parameters such as temperature and the drawing speed affected the birefringence and the mechanical properties of the fibre. In order to optimise the optical and mechanical properties of glass fibres, the

drawing parameters and post-processing treatment are considered to be important. Birefringence in glass fibres under stress is defined as the optical manifestation of anisotropy in the structure whose relaxation is time and temperature dependent (Lu *et al.*, 1998). Liu (2009), reported that relaxation near the glass transition temperature is similar to viscoelastic strain but despite this, annealing at lower temperature does not provide full relaxation of the birefringence.

Hyper-quenched and highly stretched glasses are reported to make glass fibres attain unique mechanical and physical properties that are substantially different from the materials in their bulk forms (Liu *et al.*, 2009; Ya *et al.*, 2008). Hyper-quenching of glass fibres causes freezing-in of the isotropic liquid structure at a temperature referred to as glass fictive temperature, T_f. It has been proposed that freezing-in of structurally aligned and orientated structure in glass fibre is due to axial stresses exerted by the drawing process (Liu *et al.*, 2009; Mauro *et al.*, 2008; Vieli, 1967; Ya *et al.*, 2008; Hornboll and Yue, 2007; Cherin, 1983). Hyper-quenching refers to a cooling process at a rate of 10^6 to 10^8 K/minute rather than the normal quenching rate of 20 K/minute. These processes are said to influence the solidification process and dictate the outcome of the final structure and bulk properties of glass fibres (Ya *et al.*, 2008; Hornboll and Yue, 2007). The fictive temperature is the temperature at which the structure of a glass melts equilibrium is frozen-in (Yue *et al.*, 2002). The fictive temperature depends on the thermal history and varies with the changes in temperature. T_f of glass fibre is about 200 K above standard T_g (between 783 and 833 K) depending on the cooling rate (Ya *et al.*, 2008). At temperatures above the glass transition

temperature (T_g), the fictive temperature is equal to the physical temperature, T (T_f = T) which, the system needed to be at equilibrium. But as the melt is cooled through the glass transition range, the fictive temperature, T_f lags behind the physical temperature, $(T_f \geq T)$ which indicates an initial departure from equilibrium (Yue *et al.*, 2002). On the other hand, at lower temperatures, the fictive temperature, T_f becomes frozen as some values are clearly seen above physical temperature $(T_f > T)$.

The relationships between several processing parameters used in the fibre drawing with the properties and the structure of glass fibres have been established by previous researchers. These parameters include mass flow, drawing force, drawing pressure, strain, fibre radius and cooling rate (Ya *et al.*, 2008). Yue *et al.* (2004) and Hornboll *et al* (2010; 2007) investigated the release of enthalpy, changes in internal and configurational entropy and the fictive temperature by carrying out calorimetry analysis on as-received and annealed glass fibres. The annealing was carried out by subjecting the glass fibre to heat treatments in air and in an inert gas at different temperatures below T_g for specified durations. Annealing was referred to as physical ageing which affects the mechanical and optical properties of glasses. These researchers also studied the enthalpy and birefringence relaxation of annealed glass fibres.

Yue (2004) also investigated the effect of annealing time and temperature on the excessive heat capacity of silicate fibres whilst Hornboll *et al.* (2010), Smedskjaer *et al.* (2010) and Lu *et al.* (1998) carried out birefringence measurements on annealed borosilicate glass

fibres in order to study the influence of processing and annealing parameters on the anisotropy of the glass. It was discovered that upon annealing the borosilicate glass at $0.9T_g$ the pressure-induced change in the coordination number of atoms remains unchanged, whilst the macroscopic properties such as density, refractive index, and hardness were found to relax.

Ya *et al.* (2008) investigated the dependence of the fictive temperature and the degree of structural orientation on the fibre drawing parameters such as speed and fibre diameter. They also performed annealing experiments in order to find the structural origins and mechanisms for both enthalpy and anisotropy relaxation in the glass fibres. They proposed the following equation to predict the fibre diameter for fibres that were drawn continuously at 1240 ºC at the drawing rates corresponding to 1, 10, 20, 30, 40 and 50 m/s:

$$d = Av^{0.5} \qquad [2.4]$$

where d is the diameter of the fibre, v the drawing speed and A is a constant which was equal to $51.2 \pm 0.7 \times 10^{-6}$ m $1.5^{0.5}$ s for the glass composition used by the authors. Figure 2.3 shows the experimentally derived relationship that they reported between the fibre diameter and the drawing speed. Differential scanning calorimetry (DSC) and optical birefringence measurements were carried out on the fibre drawn at a speed of 20 m/s and diameter of 9.3 µm (Solvang *et al.*, 2014). The DSC was used to carry out two heating cycles on the fibre. The first heating cycle was carried out with the first being made using the pre-annealed fibre and the second using the sample that was heated and cooled previously. The two-fold

heating cycle was used in order to explore the remaining excess energy stored in the hyper-quenched glass which was not released during pre-annealing regime. The glass transition temperature was determined from the C_p curves using the data from the second scan. The T_g was found to be 679 ºC.

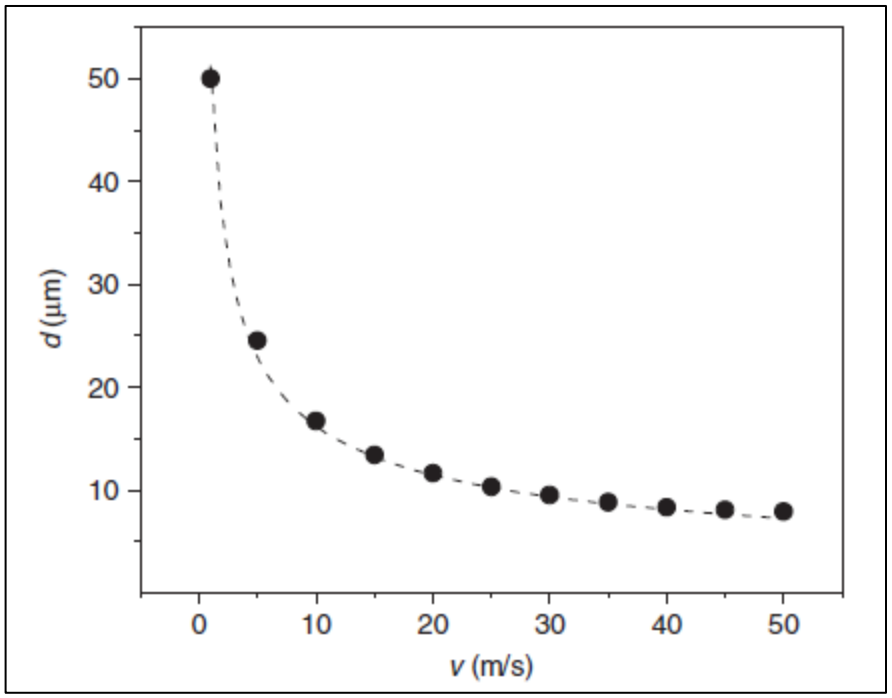

Figure 2.3 Fibre diameter, d as a function of the drawing speed, v of the E-glass fibre. The line corresponds to a fit through the data using Equation [2.4] (Ya *et al.*, 2008).

Yue *et al* (2002) previously proposed an energy-matching method and this was used by Ya *et al.* (2008) to estimate the fictive temperature. They suggested that the energy-matching

technique mentioned indicates that the excess energy stored in the glass fibre as determined from the two DSC scans equalled the increase in the average inherent structure energy when heating from T_g to T_f.

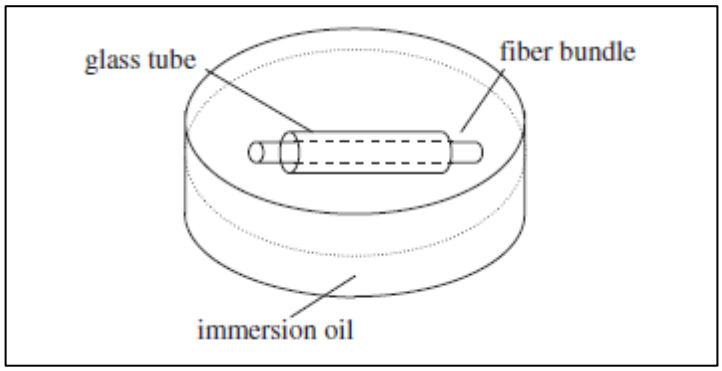

Figure 2.4 Schematic representation of the experimental arrangement for the birefringence measurements carried out by (Ya *et al.*, 2008).

Ya *et al.* (2008) suggested that two kinds of anisotropy are predominantly generated during the fibre drawing processes. One, being a two-dimensional anisotropy, which was said to occur as a result of thermal stress during cooling, whilst the other is a one-dimensional axial anisotropy induced by mechanical stress. Stockhorst and Brukner (1982) reported that mechanically-induced anisotropy overshadowed the thermally-induced anisotropy. The fibre bundle specimen that was used by Ya *et al.* (2008) for optical birefringence is as shown in Figure 2.4. The fibre bundle was inserted into an optically isotropic glass tube with an inner diameter of 0.95 mm. This was claimed to enable the parallel orientation of

the filaments to be maintained. This assembly was then immersed in an oil filled container to reduce light scattering from the fibre surfaces. The refractive index of the liquid was equal to the mean refractive index of the fibres. The birefringence, Δ_n, was calculated using the following equation:

$$\Delta_n = \frac{\Gamma}{d_{bundle}} = \frac{\Gamma_0 Sin(2\theta)}{d_{bundle}} \qquad [2.5]$$

where Γ is the optical path difference of the fibre bundle, Γ_0 is the maximum optical path difference of the compensator, θ is the rotation angle of the compensator and d_{bundle} is the effective diameter of the fibre bundle. The fibre d_{bundle} was computed from the relation:

$$d_{bundle} = 2\left(\frac{G}{l\rho\pi}\right)^{0.5} \qquad [2.6]$$

where G is the mass of the fibre bundle (g), l is the length of the fibre bundle (cm) and ρ is the fibre density (2.54 g/cm^3).

Ya *et al*. (2008) reported that the degree of anisotropy and excess enthalpy increases with an increase in the fibre-drawing speed which led to a decrease in the fibre diameter. They reported a slower decaying of excess enthalpy than with the anisotropy. It was detected that the temperature at which relaxation is the fastest for the excess enthalpy is at around $0.7T_g$ whilst that of birefringence disappeared completely within a shorter period when compared with excess enthalpy. Relaxation of the local structure has been attributed as the cause of

birefringence relaxation whilst structural rearrangement of the frozen-in isotropic network has been suspected to cause excess enthalpy relaxation (Ya *et al.*, 2008).

2.3 Relevant Mechanical Test Methods for E-glass Fibres

The following presents a brief review of techniques that have been used to determine the tensile strength of E-glass fibres.

2.3.1 Test Methods for Determining the Tensile Strength of Filaments and Bundles

It is known that there is variability in the tensile properties of the individual filaments in a bundle (Thomason *et al.*, 2014b). For example, the variability in the tensile strength can be measured using single-fibre test or the bundle tensile test (BTT) technique (R'Mili *et al.*, 2008). In analysing mechanical properties of reinforcing fibres, generally the average properties are used. Given the variability or distribution in the tensile properties, there is need for statistical analyses. The single-fibre and BTT have their advantages and disadvantages. The single-fibre test is time consuming and the risk of damaging the filaments whilst they are separated from the bundle and handling prior to tensile testing is significant. Furthermore, a large number of filaments (minimum of 40) have to be tested for meaningful statistical analyses. The BTT on the other hand is relatively easier and faster to carry out. The BTT gives an overall average tensile property for the filament in the bundle. A fundamental issue with the BTT is that it is difficult to ensure that the individual

filaments are loaded uniformly. This is due to the intrinsic meandering of the filaments. Other problems highlighted in literatures are interaction of filaments (Bar-Sinai *et al.*, 2014) and twisting of the filament which can lead to pre-matured failure (Cornelissen, 2012; Ilankeeran *et al.*, 2012; R'Mili *et al.*, 2008).

2.3.2 Effect of Variable Fibre Diameter Within a Bundle

In a study carried out on specified lengths of single-fibres by Manders and Chou (1983) using laser diffraction fringes, it was found that the fibre diameter varied along the length due to twists and non-circular fibre cross-sections.

In another study by Hillermeier as reported by Kinsella (2001), it was found that the variations in the fibre diameter had an effect on the ultimate tensile strength. It was found that ultimate tensile strength of E-glass fibre increases by a factor of 1.5 when the fibre diameter was reduced from 13 to 3.8 µm. Thomas (1971), Kadogawa and Yamate (1971) and Pahler and Bruckner (1982), also claimed that the tensile strength of E-glass varied inversely with the diameter. Brückel *et al.* (2013), Kinsela *et al.* (2001) and Kim *et al.* (2013) were of the opinion that the tensile strength of fibre is affected by surface flaws. Bedanta *et al.* (2013), Kinsella *et al*. (2001) and Lee (1993) reported that a reduction in the fibre filament diameter led to an increase in the Young's modulus. The general accepted explanation for this phenomenon is that there are fewer imperfections and defects as the fibre diameter is reduced. The data shown in Figure 2.5 illustrated the relationship between fibre ultimate tensile strength and the fibre diameter (Lee, 1993).

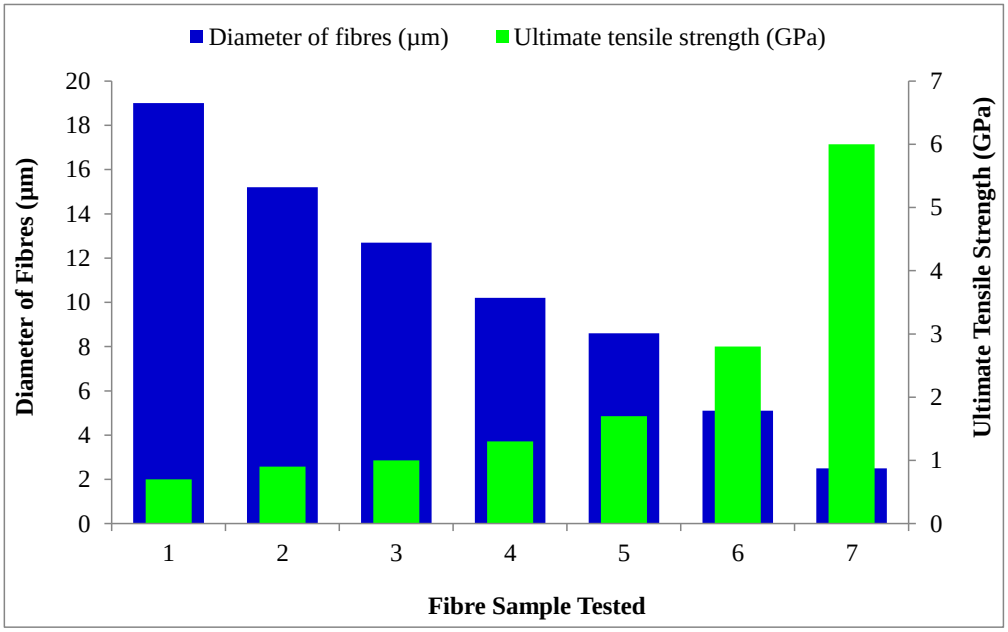

Figure 2.5 Influence of diameter on ultimate tensile strength of glass fibres, fibre length held constant (Lee, 1993).

2.3.3 Effect of the Strain Rate on Tensile Properties of Glass Fibres

A number of researchers have reported that E-glass fibre are sensitive to the loading rate (Shokrieh *et al.*, 2013; Kim *et al.*, 2013a; Dalai and Ray, 2010; Ray, 2005; Welsh and Harding, 1985). Investigation by Taniguchi *et al.*(2012) found that the strain rate had a significant effect on the failure strain and the maximum stress. Figure 2.6 shows a stress-strain curve for E-glass fibre bundles that were subjected to quasi-static tests at strain rates of 8.33×10^{-4} s^{-1} and 250 s^{-1}. The initial slopes for the stress-strain traces for the two strain rates are similar. However, the maximum stress and strain for the 250 s^{-1} strain rate tests are

larger than that observed for the quasi-static tests (See Figure 2.6). Welsh and Harding (1985) reported a similar finding for E-glass fibre composites.

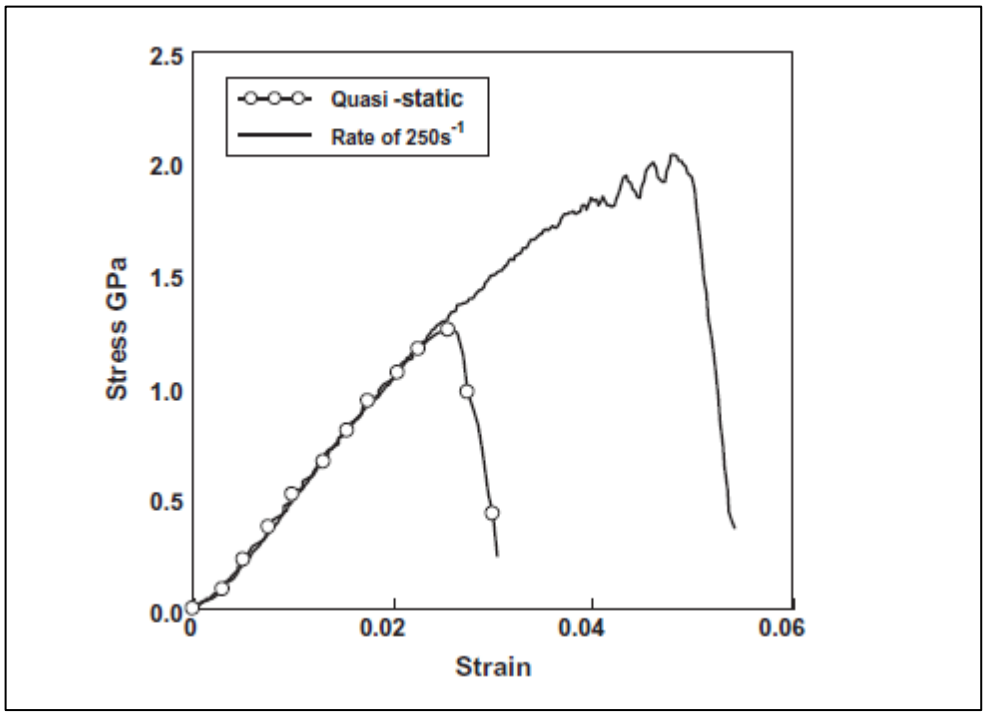

Figure 2.6 Comparison of stress-strain traces for quasi-static and strain rate of 250 s^{-1} for E-glass bundles (Norihiko *et al.*, 2012).

For the intermediate strain rate; the stress-strain curve showed a pronounced "knee" as seen in Figure 2.7. However, when the strain rate was increased above 1000 s^{-1}, an oscillation was observed in the data after the peak stress was reached. The tensile strength was found to increase as a function of strain rate. It was also found that the strain rate dependency on the

tensile strength of E-glass varied according to fibre diameter. Another finding reported was that the fibre glass contributed significantly to the strain rate dependency when compared to the matrix. Kim (2013b) concluded that the fibre diameter was another factor that affected the strain rate dependency of the strength of E-glass. They considered that the strength of glass, σ_f could be represented by the following equation:

$$\sigma_f = \frac{K_{IC}}{Y(a)\sqrt{\pi a(t)}} \qquad [2.7]$$

where K_{IC} is the fracture toughness, a is the crack length and $Y(a)$ is the shape factor. Suratwala and Steele (2003) and Freiman (2012) found that there was slow crack growth behaviour in a glass where the cracks grew slowly at a rate that was dependent on the stress intensity factor before fracturing.

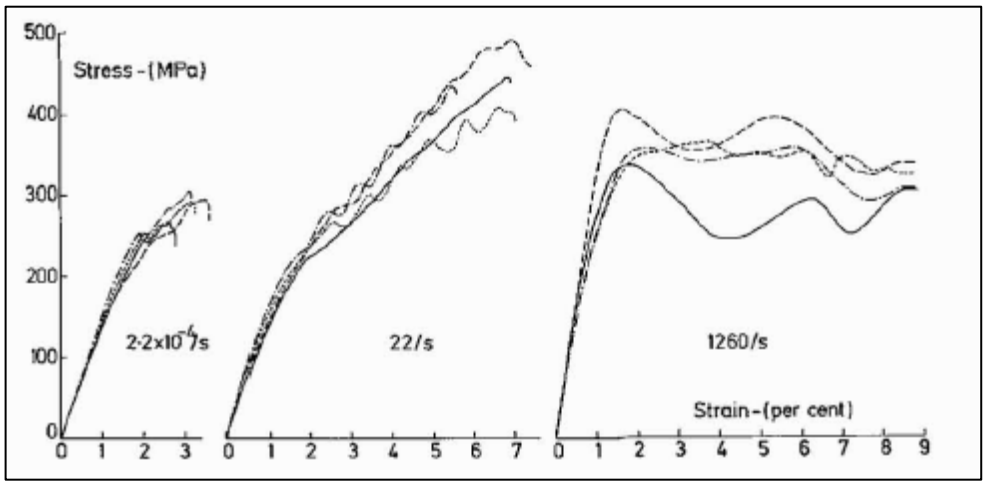

Figure 2.7 Stress-strain traces for a glass fibre reinforced composite as a function of strain rate (Welsh and Harding, 1985).

2.3.4 Significance of the Specimen Gauge Length on Tensile Properties

It has been reported that the tensile strength of glass fibre tends to decrease as the gauge length is increased (Hitchon and Phillips, 1978). Sutherland *et al.* (1998) reviewed the size and scale effects of composites and concluded that larger specimens are likely to contain a larger flaw distribution, thus leading to lower mechanical properties. The decrease in the ultimate tensile strength as a result of the increase in gauge length is generally accepted as being due to an increase in the population of defects. Figures 2.8 and 2.9 show the ultimate tensile strength for single-filaments of E-glass and carbon fibres respectively where 25 samples were tested per set (Pardini and Manhani, 2002). Although a general downward trend is observed for the tensile strength as a function of the gauge length, the scatter in the data suggest that further statistical analyses would be required to draw any conclusion.

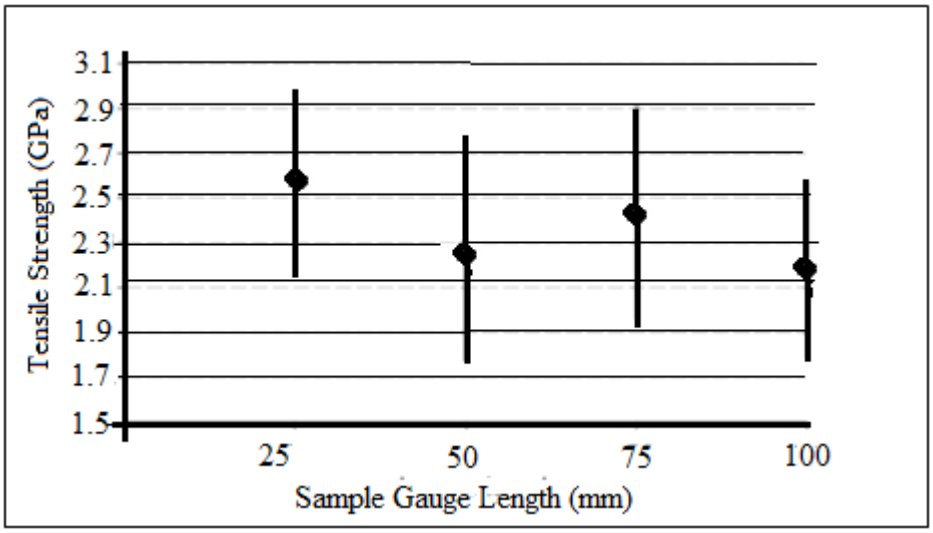

Figure 2.8 Tensile strength as a function of sample gauge length for E-glass fibres (Pardini and Manhani, 2002).

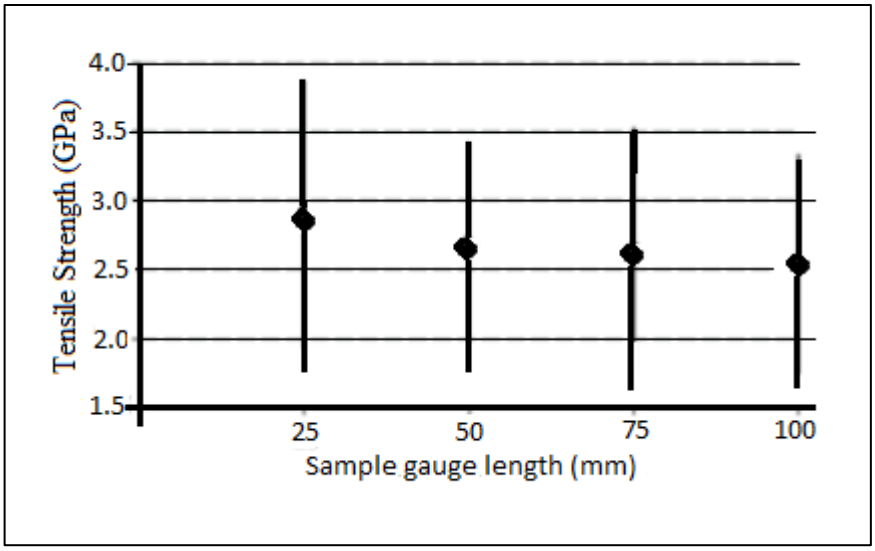

Figure 2.9 Tensile strength as a function of sample gauge length for carbon fibres (Pardini and Manhani, 2002).

Faudree and Nishi (2010) carried out tensile test on three sets of E-glass fibre samples of lengths 0.44 mm, 3.2 mm and 6.4 mm. The results showed that the 0.44 mm length samples exhibited the highest tensile strength (46.0 MPa) whilst 3.2 mm and 6.4 mm length samples had tensile strengths corresponding to 32.5 MPa and 29.0 MPa respectively. A much earlier study by Schmitz *et al*. (1963) reached the same conclusion. Cameron (1960) found that typical flaw densities on virgin glass fibres were spaced at intervals between 0.3-3.0 cm. The observed relationship between the gauge length and tensile strength led Cameron to suggest the presence of two flaw distributions in glass fibres. One was identified as surface flaws. These flaws were reported to be separated by approximately 0.5 cm. The other was identified as mild flaws closely spaced which could not be identified physically. On the basis of Cameron observations regarding flaw density on fibres, Schemitz *et al.* (1963) suggested that surface cracks govern the failure of fibre length above 0.5 cm whilst a more subtle, unidentified flaws govern failure below this length.

2.3.5 Tensile Test Environment

Lund and Yue (2005) reported that thermal and mechanical performance of glass fibre is affected by the interaction between the fibres and the surrounding media (such as humidity, temperature and atmosphere). Kalidass and Balaji (2014) investigated the effect of the environment on glass fibre composite materials. It was found that a “wet” environment, coupled with high or low temperatures was detrimental for composites. McKinnis and Sutton (1959) proposed that physical and chemical adsorption of water reduces the strength of glass fibres through stress corrosion. Carman and Pantano (1990) found that there was an

interaction between adsorbed water and the E-glass fibre surface. Other researchers (Lund and Yue, 2005; Maxwell *et al.*, 2005; Oehler and Tomozawa, 2004; Davis and Tomozawa, 1994; Wakabayashi and Tomozawa, 1989; Tomozawa, 1985) have reported on the influence of atmospheric conditions such as heat, moisture and air-borne pollution as agents that lead to the degradation of E-glass. Therefore, controlling the atmospheric condition during the testing of E-glass was said to contribute to the strength of glass fibres (Lund, 2010).

2.4 Surface Treatment and Coatings on E-glass Fibres

The presence of flaws and their distribution on the surface of a glass fibre has been identified as a factor that controls the strength of E-glass (Jenkins *et al.*, 2015a; Jenkins *et al.*, 2015b; Thomason, 2012b; Feih *et al.*, 2009; Grosse, 2006; Taylor *et al.*, 1999).

As stated previously, the binder is typically an aqueous solution or emulsion of organic materials that is normally applied to the surface of glass filament via a roller-based applicator during the production of E-glass (Brown *et al.*, 2004; Kinsella *et al.*, 2001; Lammon-Hilinski *et al.*, 2001; Hench and Clark, 1978; Ryabov, 1968).

One of its functions is to provide a protective cover on the surface of the filaments. The binder also contains a "size" that enhances the chemical bonding between the fibres and the matrix resin (Kinsela *et al.*, 2001).

2.4.1 Effect of Lubricants on the Tensile Strength of E-glass Fibre Bundle

Lubricants have been used to study their effect on the tensile fracture of E-glass fibre bundles (Brown *et al.*, 2004; R'Mili *et al.*, 2008). The primary hypothesis proposed was that the presence of a lubricant between the filaments in a bundle would reduce interactions between individual filaments in the bundle. In other words, the inter-filament friction that occurs in dry bundles and the subsequent damage would be reduced (Oskouei, 2009; R'Mili *et al.*, 2008; Hamstad, 1986; Phoenix and Wu, 1983). R'Mili *et al.* (2008) attempted to link the fracture behaviour of fibres with the viscosity of the lubricant. They found that the peak tensile load and the corresponding failure strain of the dry fibre bundles were lower when compared to the lubricated ones as illustrated in Figures 2.10 and 2.11. These authors used surface-mounted acoustic emission transducers to record acoustic emissions that were generated when the filaments in the bundle fractured under tensile loading. The use of lubricants was found to aid the coupling efficiency (AE) (Oskouei, 2009; R'Mili *et al.*, 2008). Some of the lubricants reported in literature include: silicone-oil (Hamstad, 1986; Phoenix and Wu, 1983), petrol, Vaseline and light-oil (R'Mili *et al.*, 2008).

The viscosity characteristics of the lubricants investigated by R'Mili *et al.* (2008), is shown in Figure 2.10.

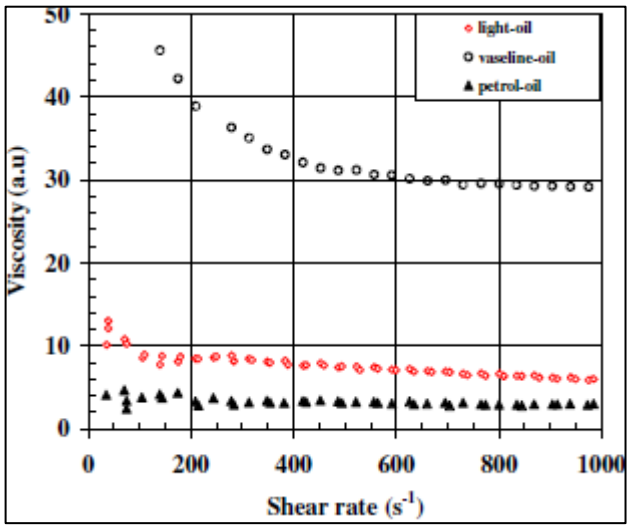

Figure 2.10 Effect of shear rate on viscosity for three types of lubricant oil used (R'Mili *et al.*, 2008).

The researchers undertook bundle tensile tests where the E-glass bundles were tested with and without impregnating the bundles with lubricants. As seen in Figure 2.11, the peak load attained and the failure strain are lower in the dry bundle when compared to the lubricated case. The authors claimed that there was also a marginal increase in the maximum load and the corresponding failure strain for the light-oil lubricant. It was observed that, for the higher viscosity lubricant (Vaseline) there was decrease in the tensile strength. R'Mili *et al.* (2008) suggested that as the viscosity increases, the lateral interaction between the fibres enhances local load sharing which contributes to premature fracture of the neighbouring fibres.

Whilst there is no doubt that inter-filament friction can lead to abrasion-induced damage, it would seem improbable that the relative "stiffness" of the lubricant, Vaseline in this

instance, could enable load-transfer between the filaments. A more plausible explanation, based on the current author's experience, is due to the distribution of the binder in commercial E-glass. The interaction or compatibility between the binder and the lubricant also needs due consideration.

A number of authors, for example, Hill and Okoroafor (1995) and R'Mili *et al.* (1996) reported that a post-tensile tested dry bundle appeared like "cotton-wool" whereas the lubricant samples seemed to maintain their original outstretched appearance after fracture. They concluded that this was an indication that the lubricant reduced the magnitude of inter-filament frictional damage and the premature fracture was due to less interaction between the fibre filaments in the bundle. The efficiency of the lubricant was reported to be dependent on the inter-fibres spacing, the fibre diameters distribution and the wet-ability of the lubricant (R'Mili *et al.*, 2008).

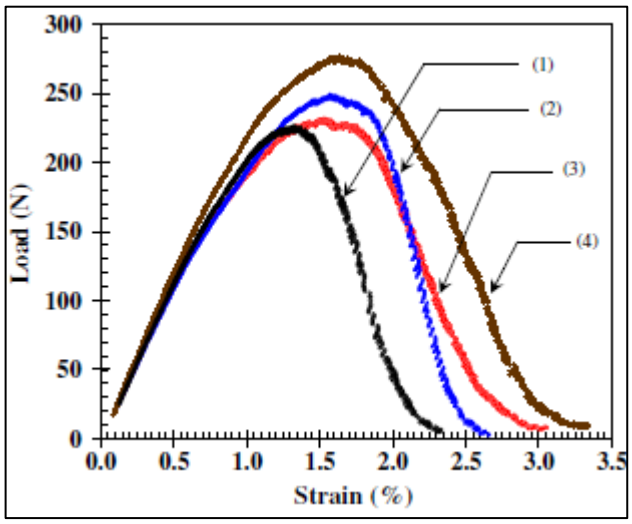

Figure 2.11 Effect of lubricants on the tensile fracture of E-glass bundles with and without lubricants: (1) dry bundle; (2) lubricated with petrol; (3) lubricated with Vaseline; and (4) lubricated with light-oil. The gauge length was 60 mm (R'Mili *et al.*, 2008).

2.4.2 Effect of Solvent Treatment on the Tensile Strength of E-glass Fibre Bundles

Although the binder is important as it serves a number of purposes, including contributing to the interfacial properties of composites, little is known about its chemistry. The exact composition of the binder is generally a proprietary information (Thomason, 2012a). It is known that the binder can contain coupling agents to enhance the interfacial bond strength. Organo-silane coupling agents are used frequently with E-glass (Plonka *et al.*, 2004). Organo-silanes act as a coupling agent whereby one part of the molecule reacts with the hydroxyl groups on the glass fibre and another part enables a reaction with the resin or

hardener. Hence, reactions of this nature enable the creation of covalent bonds between organo-silane, the surface of the glass fibre and the resin system (Ivashchenko *et al.*, 2014; Jones, 2010; Liu *et al.*, 2008). The binder generally includes anti-static agents to prevent the build-up of static charge when the fibres are drawn from the melt and wound onto bobbins McGravey (McGravey, 2008). Examples of such chemicals are LiCl, NH_4Cl, $MgCl_2$ and alkyl-trimethylammonium chlorides which is also acts as a lubricant.

A major component of the binder is reported to be film formers, which represents approximately 79% of the components by mass. The organo-silane was reported to represent 10% by mass (Gorowara *et al.*, 2001). Polyvinyl acetate and polyvinyl alcohols are used frequently as film-formers. Film formers serve to protect the fibres from damage due to fibre-to-fibre interactions within a strand (Zhandarov and Mader, 2015; Cech *et al.*, 2002; Thomason, 2001; Zinck *et al.*, 2001).

Petersen *et al.* (2013) preferred a soxhlet solvent extraction on as-received glass fibres to remove the extractable component of the binder. The fibres were refluxed for 24-hours. The other extraction methods used for removing the binder were treatment of as-received glass fibre in solvent for twenty four hours, followed by drying in oven at 0.2 bar, 80 ºC for 2 hours before being pyrolysed at 565 ºC for 3-hours. Five samples each were used in this experiment. Each fibre was weighed prior to the experiment and the mass-loss was determined after pyrolysis. Petersen *et al.* (2013) observed that the fibre appeared to be electrostatically charged after solvent extraction. However, they were fragile and brittle after heat treatment. It was estimated that about 25 wt% of the binder could not be removed

by solvent extraction and heat treatment at 565 ºC. They reported that the extractable amount of binder that could be removed from fibre surface was in range 80-90% of the total binder which was estimated to be in the range 0.2-1.0 wt%. Chung (2001) and Thomason (2007) reported that the mass of the binder present on E-glass fibres is between 0.2 and 2.0 wt%. Thomason (2001) reported that binder layer is unevenly distributed along the bundle with thickness in the range 1.0 nm - 1 µm.

Attenuated total reflectance Fourier transform infrared (ATR-FTIR) spectroscopy was used by a number of researchers to study the nature of the surface of glass fibres (Chan and Kazarian, 2016; Liu *et al.*, 2009; Ishida and Koenig, 1978). With reference to the reports by Petersen *et al.* (2013), Figure 2.12 illustrates spectra obtained from E-glass fibre bundles after specified types of surface treatments were identified by using two pure organo-silanes as reference materials.

The observation of Petersen *et al.* (2013) was that acetone extraction removed the physisorbed organo-silanes and the film former whilst burn-off removed all the organic materials and organic functional groups, leaving the strong chemically bonded binder at the fibre surface.

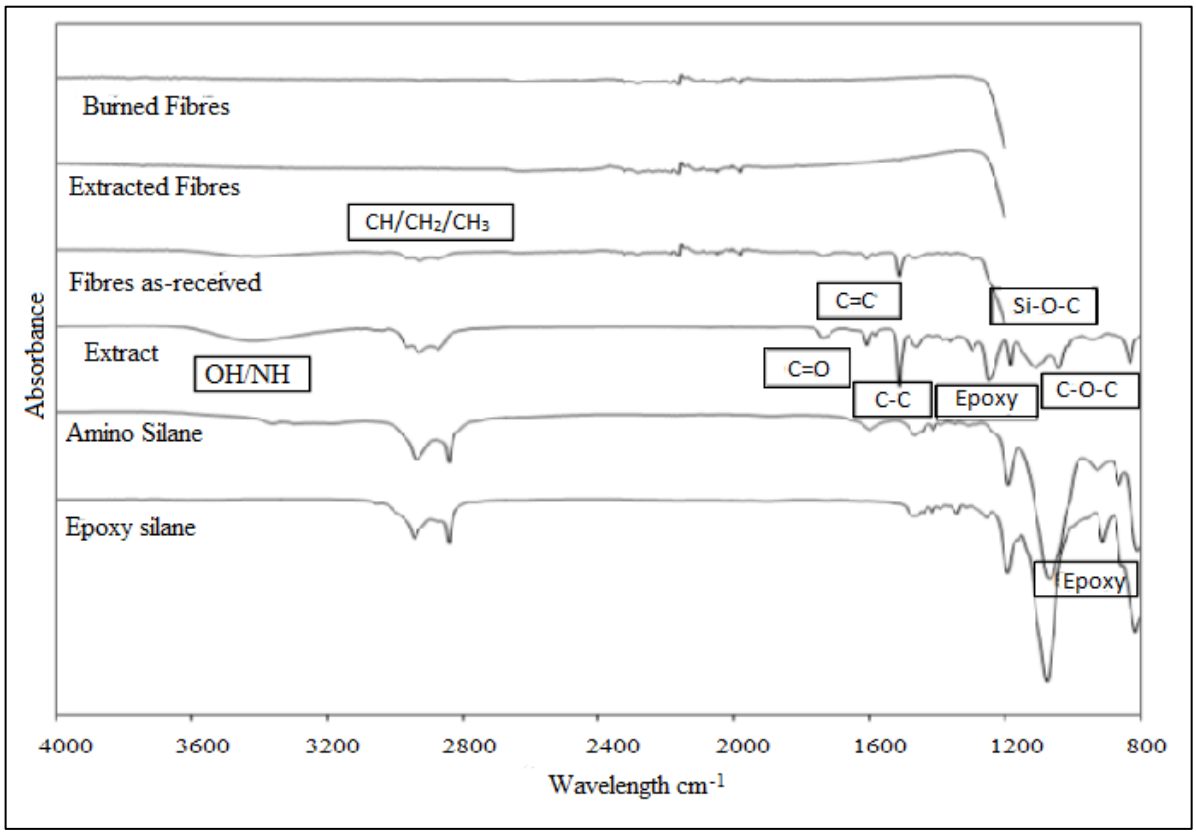

Figure 2.12 ATR-FTIR spectra of as-received, acetone-treated, heat treated two reference organo-silane as reported by (Petersen *et al.*, 2013).

The spectra below 1200 cm^{-1} were not shown for the as-received, heat-treated and solvent treated fibres because the bands were dominated by strong absorption from Si-O-Si bonds in the glass fibre which is in the region of 900-1100 cm^{-1} (Petersen *et al.*, 2013). By comparing the sizing content with that given by the manufacturer, the researcher concluded that about 25 wt% of the sizing is not removable and was regarded as strongly, chemically bonded to the glass surface. Also, the bands found in ATR-FTIR spectra of the as-received and extracted fibre bundle correspond reasonably with the presence of an epoxy-resin

containing film former and polyethylene oxide lubricant/surfactant compared to absorbance bands published in the literature for these substances.

2.5 Effect of Thermal Conditioning on Heat-Treated E-glass Fibres

It has been suggested that the weakening of pristine glass fibre is caused by surface degradation (Yang *et al.*, 2015; Thomason, 2012b; Petersen *et al.*, 2013; Liu *et al.*, 2008; Plonka *et al.*, 2004; Agrawal and Broutman, 1990; Sakka, 1957). Cameron suggested that acid treatment of re-heated glass fibre removes surface contamination (Cameron, 1968). Feih *et al.* (2011) and Thomas (1960) had demonstrated that a given glass fibre would reach a steady state minimum tensile strength, at a finite time, whilst the time taken to attain this steady-state decreases as the temperature is increased. Although the two researcher teams used different materials and thermal methods, they reached the same conclusions. Fibres treated at 450 °C required 30-minutes to reach the steady-state with regard to the tensile strength of E-glass fibres; however, it required approximately two and eight hours at 350 °C and 150 °C respectively.

Ya *et al*. (2008) and Kennerley *et al.* (1998; 1997) attributed the weakening of heat-treated fibre to the formation of flaws and cracks due to molecular and structural rearrangements in the glass. It was reported that electron microscopy could not reveal any features on heat-treated E-glass rods until the temperature exceeded 800 ^{0}C (Mallick and Holland, 2013;

Brearley and Holloway, 1963). However, this is in contrary to that reported by Bott and Barker (1968) where E-glass was exposed to a moderately moist air atmosphere without any additional treatment. They found that the surface topology was uniformly smooth. When a sample was exposed to elevated temperatures in combination with moisture, typical cracks appeared on the micrographs. These features resembled chapping (scaling) or blistering of the glass skin. They reported that the near-smooth surface of glass fibre coated with organic polymers could be removed by brief treatment with hot water. A correlation was drawn between the mechanical strength and the changes caused by cracks and blisters. It was concluded that the smoother the surface, the higher the tensile strength of the glass fibre.

Feih *et al.* (2011) investigated the effects of temperature, heating time and atmosphere on the tensile modulus, strength and the failure mechanisms in E-glass fibres. The tensile properties of E-glass were investigated following heat treatments ranging from 150 to 650 ^{0}C for up to two hours. The atmosphere within the furnace was air, dry-air or nitrogen gas. The study by Feih *et al.* (2011) was carried out in the absence of a polymer matrix. They reasoned that this was necessary to avoid the possible fibre-matrix interactions.

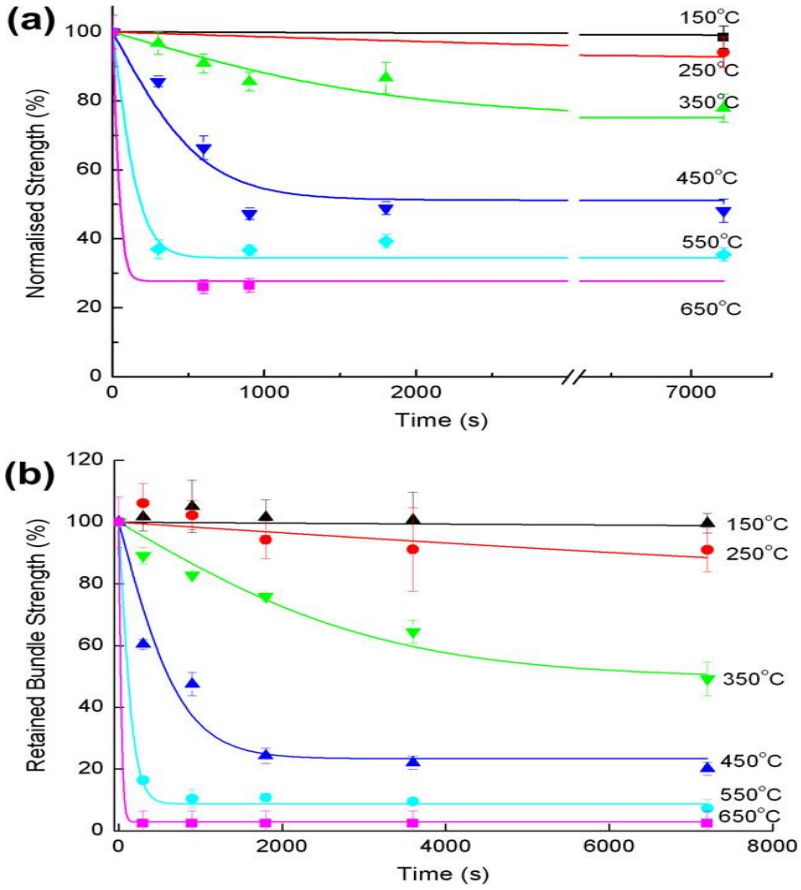

Figure 2.13 Effects of temperature and heating time on the tensile strength of: (a) single fibres (σf,av = 2248 MPa) and (b) fibre bundles (σav,fb = 1058 MPa) after heating in air (Feih *et al.*, 2011).

Figure 2.13 shows the effects of temperature and heating time on the tensile strength of the single-glass fibre and BTT. The bundles tensile strength showed a decrease of about 50% or more which has been attributed to inter-filament friction between the fibres, uneven straining of fibres under tension and the longer specimen length of 150 mm compared to 20 mm for the single-fibres. Reynaud *et al.* (2007; 2007) had also reported differences in the

tensile strengths between the single-fibre and bundle tensile test in the as-received condition.

Figure 2.13 shows a rapid drop in the tensile strengths for the single-fibre and fibre bundle samples between 250 °C and 550 °C. Initially, it drops with heat treatment time until it reaches a steady-state, which is determined by the conditioning temperature. The time taken to reach a steady-state tensile strength decreased with increasing temperature. Although the single-fibre and fibre bundle samples showed a similar trend, the reduction in the tensile strength for the fibre bundle samples was higher than the single by about 30% at the same temperature. Kennerley *et al.* (1998; 1997) reported a 90% decrease in fibre tensile strength after heating a glass fibre composite at 650 °C. Loewenstein (1962) reported that the surfaces of glass are covered with layer of water of approximately 20 molecules thick when they are manufactured. He stated that this layer could be removed by heating above 250 °C. He suggested that this dehydration led to the formation of cracks and thus was responsible for weakening the fibres.

2.6 Effect of Water Vapour on Heat-Treated Glass Fibres

Glasses are known to exhibit slow-crack growth in environments containing water or water-vapour below 200 °C. The effect of water-vapour on the tensile strength of glass has been studied and reported extensively (Li and Tomozawa, 1995; Tomozawa and Han, 1991; Piggott and Yokom, 1968). Slow-crack growth is likened to stress corrosion. Haldimann *et*

al. (2008) and Francois *et al.* (2013) reported stress-corrosion as a slow flaw growth that occurs in glass when they are exposed to the reactions between the silica network and water as discussed previously (see Figure 2.2).

François *et al.* (2013) explained that glass fibres are sensitive to the atmospheric environment below the bushing, when they are manufactured. They considered the stress-induced corrosion that took place as the molten glass was being drawn during production. They found that the tensile stresses experienced by the hot glass fibres during drawing could be as high as 300 MPa. Although, the duration of this stress is short, they proposed that it was sufficient for stress-corrosion to take place between the bushing and the roller where the binder is applied.

Other investigators believe that the stress-corrosion reaction is limited to the surface of the glass fibre. For instance, Michalske and Freiman (1983) suggested that slow-crack growth is caused by the reaction between strained Si-O bonds on the glass surface and water molecules on the glass. Others have suggested that water may be causing weakening of glasses as it diffuses into the glass.

2.7 Restoring the Tensile Strength of Weakened E-glass Fibres

Thomason *et al*. (Thomason, 2012a; Thomason, 2012b), Feih *et al.* (2011), Pico (2010), Pickering *et al.* (2000), and Kennerley *et al.* (1998) have demonstrated in recent years that reinforced composites can be recycled, using thermal methods, whereby the bulk of the

matrix is removed. However, thermal-based removal of the matrix has been noted to lead to a significant reduction in the tensile strength of the recovered fibres when compared with pristine fibres. For example, degradation in the tensile strengths by up to 50% and 90% has been reported for composites treated in a fluidized-bed at 450 ^{o}C and 650 ^{o}C (Thomason *et al.*, 2012; Feih *et al.*, 2011; Pickering *et al.*, 2000; Kennerley *et al.*, 1997). Due to this reduction in strength of the recovered fibres, Thomason *et al.* (2012) and Cunliffe *et al.* (2003) reported that the re-use of the recovered fibre has been limited to a small replacement of virgin glass or used as filler materials in composites.

Karlsson *et al.* (2010a) and Hogan (1981) have reported that it is possible to "reinstate" some of the original strength of glass fibres and a number of techniques had been identified and published. Donald (1989) classified these into surface and bulk techniques, stressing that the surface compressive method worked better as it is capable of limiting the deleterious effect of static fatigue.

2.7.1 Surface Modifications

The effect of permanent bending of glass fibre at temperatures lower than the transition temperatures for selected glasses in an atmosphere containing water, has been attributed to and analysed in terms of surface stress relaxation and the resulting residual stress (Karlsson *et al.*, 2010b; Karlsson *et al.*, 2010a).

Chemical tempering is a method that is used to form a layer of compressive stress on the surface of a glass article. Since fracture predominately originates from the surface of the

glass, tempering can be used to increase the fracture strength of the glass by forming a compressive stress field on the glass fibre surface (Karlsson *et al.*, 2010a; Hogan, 1981). The magnitude of the tensile strength that will be apparent in the glass will depend on the compressive stress field achieved. This is primarily due to the fact that tensile stress will not be established until a sufficient strain is firstly applied to overcome the compressive stress (Naimeh, 2004).

Donald (1989) reported that glass strength can be increased by removing or minimising such defects or by placing the surface of the glass in compression.

2.7.1.1 Thin Coatings and Cladding

Thomason *et al.* (2012) thought that the lower mechanical performance of recovered glass fibres may be attributed to the removal of the silane coating from the surface of glass fibre during pyrolysis of the matrix at elevated temperatures 600 °C). It has also been reported that silane coatings can provide a protective layer on glass fibre as well as increasing the interfacial properties with polymeric resin. Silanes are also known to offer resistance to interfacial degradation caused by moisture ingress. It has been suggested that silane coupling agents, to a certain degree, have the ability to heal flaws on the surface of glass fibres. With this in mind, Thomason *et al.* (2012) was of the opinion that re-silanisation may increase the mechanical properties of recovered glass fibres.

2.7.1.2 Thermal Treatments

One of the methods recommended for establishing a surface compressive stress in glass is thermal "strengthening". This is a method whereby the glass is cooled (quenching the glass with air or liquid) within a few tenth of seconds from a temperature above the T_g, at a controlled constant rate beyond its strain point (Karlsson *et al.*, 2010; Daudeville and Carre, 1998; Carre and Daudeville, 1996). The strain point is the temperature where the internal stresses within is relieved when the glass is being cooled. It is the temperature at which the viscosity of a typical glass is 10^{12} Pa.s. As the cooling regime is being experienced by the glass, the surface layer goes beyond the strain point of the glass and this causes it to solidify before the core (inner layer). Since the core, still in a liquid state, it continues to cool and contract; a stage is reached when the interior also solidifies. At this point, the internal temperature is still higher than that of the surface, causing contraction of the interior which is opposed by the surface; consequently, the surface is put in compression whilst the core is in tension. After tens of seconds, an equilibrium is reached as shown in Figures 2.14 to 2.16 (Karlsson *et al.*, 2010; Daudeville and Carre, 1998; Donald, 1989; Hogan, 1981).

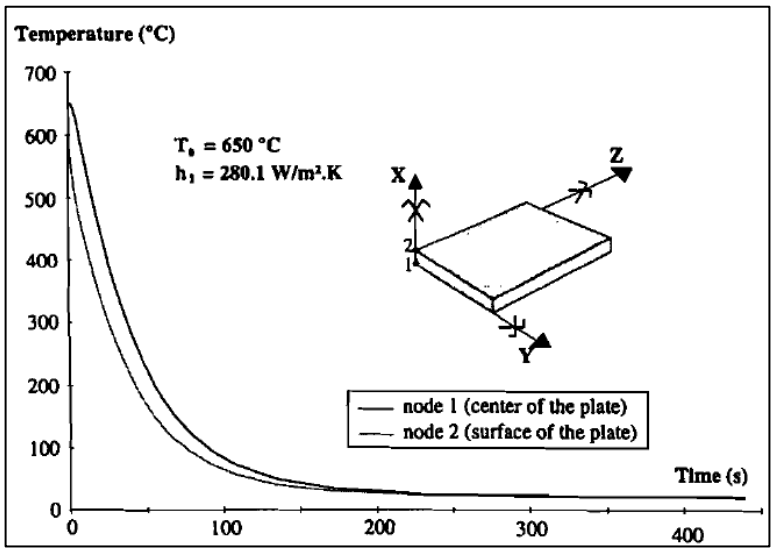

Figure 2.14 Effects of temperature and heating time on the tensile strength of: (a) single fibres (σf,av = 2248 MPa) and (b) fibre bundles (σav,fb = 1058 MPa) after heating in air (Feih *et al.*, 2011).

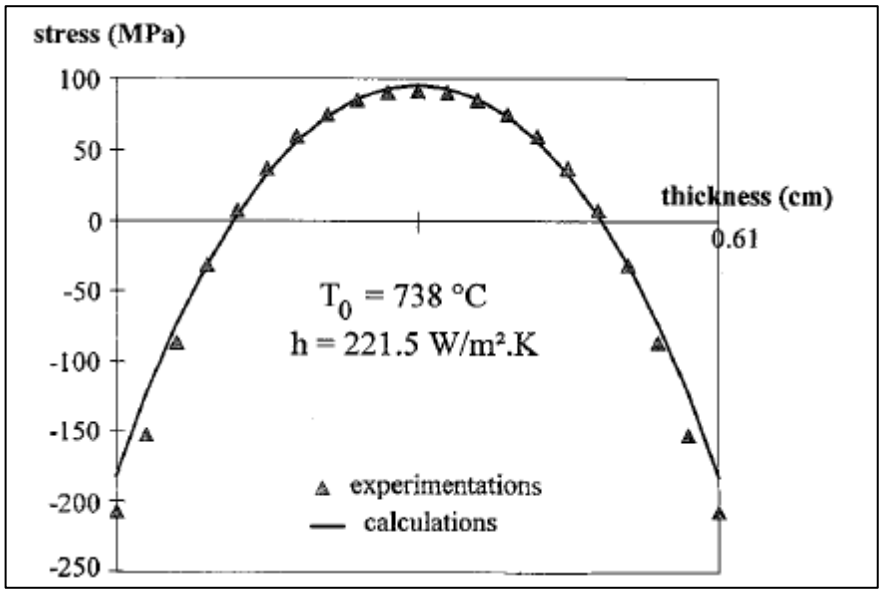

Figure 2.15 Variation of the residual stresses in the thickness of the plate (Daudeville and Carre, 1998)

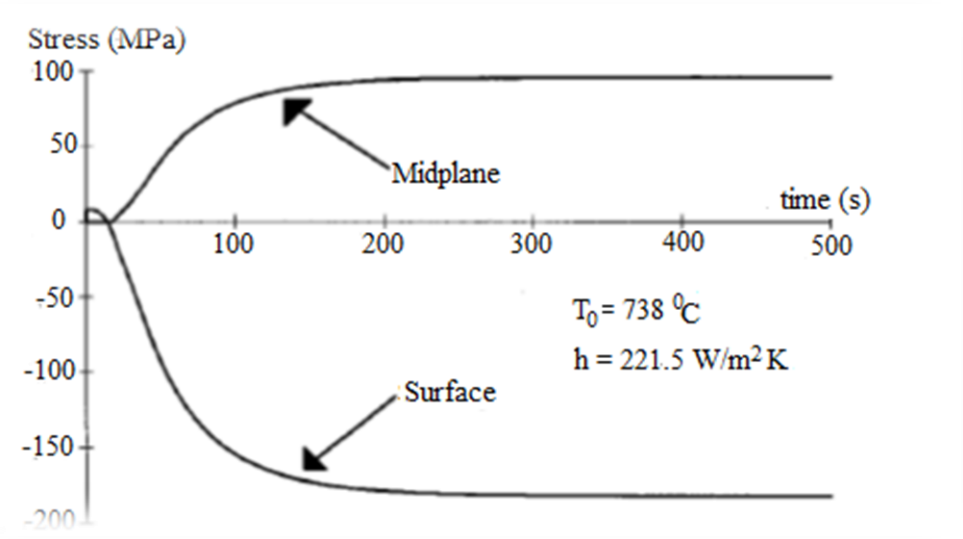

Figure 2.16 Variation with time of the longitudinal stresses at the surface and in the mid-plane of the plate (Carre and Daudeville, 1996; Daudeville and Carre, 1998)

2.7.1.3 The Ion Exchange Processes

This is a method of exchanging ions present in the glass with ions of different sizes. Glass strengthening by this technique is a process where the original glasses are submerged into a molten alkali salt at a temperature below the glass transition. During the time of immersion, the alkali ions from the glass that are close enough to the surface are exchanged with those from the molten salt. This simply means replacing a smaller ion in the glass with a larger ion in a solution to provoke surface compression with balancing tensile strength in the core (see Figure 2.17) (Karlsson *et al.*, 2010; Calvez *et al.*, 2009; Gy, 2007; Nordberg *et al.*, 1964). Introduction of any ion whose size is different from the original ion in a material changes its structure. This procedure increases the strength, thermal shock resistance and

sealing of the surface micro-cracks of the glass (Karlsson *et al.*, 2010; Calvez *et al.*, 2009; Nordberg *et al.*, 1964). There is no risk of surface deformation since the ion exchange process was carried out at the temperature below the T_g (Karlsson, 2012; Karlsson *et al.*, 2010; Shen and Green, 2004; Kadogawa and Yamate, 1971; Nordberg *et al.*, 1964).

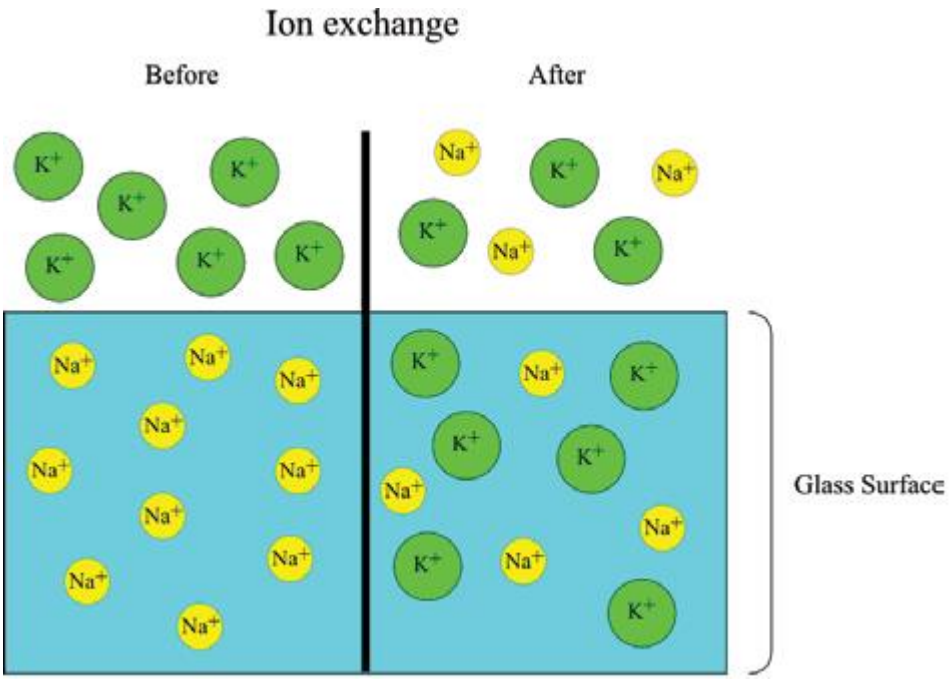

Figure 2.17 Schematic illustration of an ion exchange process (Karlsson, 2012)

Within the periodic table, Sodium ionic radius is 190 picometer which is lower when compared to potassium with atomic radius of 243 picometer whilst lithium has ionic radius of 152 picometer (Strickland, 2011; Calvez *et al.*, 2009; Gy, 2008; Wierzhowski, 1995; Hogan, 1981). The most commonly investigated ion exchange systems are soda-silica

where Na^+ ions are replaced by K^+ ions and lithia-silica where Li^+ ions are replaced by Na^+ ions (Karlsson *et al.*, 2010). A number of researchers have replaced sodium ions with potassium ion in order to create compressive stress on the surface of the glass particle. The process was carried out at higher temperature to break down ionic bond that sodium has with the glass (Sglavo, 2015; Strickland, 2011; Calvez *et al.*, 2009; Gy, 2008; Karlsson *et al.*, 2010a; VArshneya, 2010; Wierzhowski, 1995; Donald, 1989; Cooper and Krohn, 1969; Nordberg *et al.*, 1964).

2.8 Tensile Strength Distribution using Weibull Statistical Models

2.8.1 Theoretical Bundle Strength Model

Theoretical models of dry fibre bundles generally consider a set of parallel number (N_o) of fibres with a statistically fibre strength distribution. With regard to the tensile test method, the sample is loaded in tension parallel to the fibre direction and the fibres fail when the load exerted exceeds a critical value. When any of the fibres fail, the load carried by that fibre is re-distributed equally on the surviving ones; this is generally referred to as the equal load sharing rule. The assumption here is that there are no interactions between the fractured fibres and their neighbours. It is generally accepted that brittle materials such as glass fibres have a distribution with regard to the tensile strength. The variability is due to

the randomly distributed flaws in the fibres. The other assumptions generally used in this analysis are referred to as the Coleman conditions. These are:

(i) the filament length is constant within the bundle;

(ii) the stress-strain relationship for a single-fibre follows Hooke's law up to failure;

(iii) the load released from a fractured fibre is evenly distributed to the surviving fibres; and

(iv) the assumption is that there is no reaction between the fibres which could lead to a premature failure of the fibres.

Alternatively, if the fibre bundle exhibits catastrophic failure and a load-drop or progressive failure is observed after the peak load has been achieved on the load-strain curve, this behaviour is not predicted by the theoretical model. This non-catastrophic failure mode can be explained by the interactions between the fractured and intact filament in the bundle

The Weibull distribution is a versatile statistical tool for analysing materials that exhibit a significant scatter or variability in properties. The following section presents a brief review of the Weibull strength distribution function.

2.8.2 Statistical Distribution of Fibre Strength

In general, the observed scatter in the properties of materials is attributed to defects and flaws existing in varying sizes, shapes and orientations. In order to analyse the strength of a material, a finite number of specimens have to be tested under the same conditions to

establish the statistical distribution in properties; for example, the tensile strength. The fracture strength distribution of brittle materials is commonly described using the Weibull distribution function (R'Mili *et al.*, 2008; Andersons *et al.*, 2002; Jayatilaka and Trustrum, 1977; Trustrum and Jayatilaka, 1983). The general Weibull distribution function is:

$$P_f = 1 - \exp\left[-\left(\frac{\sigma_f - \sigma_u}{\sigma_o} \right)^m \right] \qquad [2.8]$$

where,

P_f = fracture probability, σ_f = fracture strength, σ_u = threshold strength below which fracture cannot occur, σ_o = scale parameter, m = Weibull modulus (shape parameter)

The scale parameter is also known as the characteristic strength and it corresponds to the fracture stress with a failure probability of 63.2% on the Weibull failure probability plot. The Weibull modulus, m, otherwise referred to as shape parameter, describes the degree of scatter in the fracture strength. The Weibull modulus and the characteristic strength have positive values.

The distribution function (Equation [2.8]) is referred to as the three parameter Weibull distribution. The problem in using Equation [2.8] is the complexity of determining the relevant parameters from experimental data. Hence, for a set of nominally similar fibres, the strength distribution is represented by a two parameter Weibull function (which mean that $\sigma_u = 0$). The two-parameter Weibull distribution function is reduced to:

$$P_f = 1 - \exp\left[-\left(\frac{\sigma_f}{\sigma_0} \right)^m \right] \qquad [2.9]$$

The values for 'm' and 'σ_o' can be estimated directly from the measured strength by taking the logarithms of Equation [2.9] twice and then rearranging it:

$$\ln\left(\ln\left(1/\left(1-P_f\right)\right)\right) = m\ln\sigma_f - m\ln\sigma_o \qquad [2.10]$$

A plot of ln(ln(1/(1 – P_f))) versus ln (σ_f) will yield a straight line with slope giving the Weibull modulus, 'm' and the characteristic strength is estimated from the intercept.

When estimating Weibull parameters, a number of manipulations are required prior to plotting Weibull plot to eliminate parameters of interest. This is done by ranking the strength of individual fibres or bundle tested in an increasing order of their strength. The cumulative failure probability of the i^{th} measured strength is calculated. To do this, several recommendations have been proposed and evaluated in literature (Wu and Ni, 2006; Khalili and Kromp, 1991; Bergman, 1984; Jayatilaka and Trustrum, 1977). A typical example, when the sample sizes (N) is up to 50, Equation [2.11] should be used. Alternatively, for better accuracy Benard's proposed Equation [2.12] should be used (Bergman, 1984).

$$P_i = \frac{i - 0.5}{N} \qquad [2.11]$$

$$P_i = \frac{i - 0.3}{N + 0.4} \qquad [2.12]$$

The value of ‘m’ can be estimated from Equation [2.10] but several other methods have been used in literature (Khalili and Kromp, 1991; Phoenix and Wu, 1983; Jayatilaka and Trustrum, 1977). For example, the method of least square was used to estimate the Weibull modulus using Equation [2.10].

The relevance and reliability of the Weibull parameters determined experimentally is dictated by the number of specimens that are tested. Generally, the number of specimens suggested and used for the characterisation of the strength of brittle material is 30 (Faucher and Tyson, 1988). Comparison of the Weibull parameters stated in the literature is difficult because the number of specimens used vary between 12 to 40 (R'Mili and Lamon, 2011; Lund, 2010).

2.9 Summary

A detailed review was undertaken on the parameters that influence the tensile strength of E-glass fibre. In particular, attention was given to the effect of the binder remover methods on the tensile properties of E-glass. A large volume of literature was studied and it was established that heat treatment and/or humid environment tended to have a detrimental effect on the tensile properties of E-glass. Previous researchers have proposed a number of hypotheses to account for the degradation in properties when E-glass fibres are subjected to elevating temperatures. However, it was concluded that no direct evidence has been provided to-date to explain the degradation of E-glass when it has been subjected to temperature in excess of 250 °C. Subjecting composites to these elevated temperatures is of

importance commercially, because pyrolysis-based recycling, where the matrix is oxidised to recover the fibre is common practice with carbon fibre reinforced composite. Unfortunately, this is not possible with glass fibre composites. Hence, one of the motivations for undertaking this current study was to try and obtain evidence for the degradation mechanisms when E-glass is subjected to elevated temperatures.

3 EXPERIMENTAL

3.1 Introduction

The primary aim of this study as highlighted in Section 1.2 was to assess the effect of the binder removal methods and heat-treatment on the tensile properties of E-glass fibre bundles. In addition, an investigation was carried out to investigate the effect of fibre spreading (as a means of breaking up the binder) on the tensile properties of E-glass fibre bundles. The tensile failure loads of spread fibre bundles at specified gauge lengths (50 mm, 80 mm, 100 mm, 150 mm and 200 mm) were compared with the as-received bundles. The effect of lubricating the filaments and the resulting effect on the tensile strength was also investigated.

Creels of 2400 Tex E-glass fibres were donated by a commercial source in the UK. The as-received and spread E-glass fibre bundles of approximately 500 mm were obtained from the creel and a fibre spreading rig (discussed later) and then prepared into 100 mm gauge length tensile test specimens. Thirty bundles each of the as-received and spread fibre bundles were end-tabbed and tensile tested to failure. A pair of piezo-electric acoustic emission transducers were surface bonded to the end-tabs.

3.2 Materials and Equipment

3.2.1 As-received E-glass Fibre Bundles

The 2400 Tex E-glass fibre bundles used in the current study consisted of approximately 4000 filaments with a mean diameter of 17 ± 2 μm and a binder that was compatible with epoxy and vinylester resin systems.

3.2.2 Resin and Adhesive Systems

The resin systems used for this study were: (i) an epoxy resin LY3505 and hardener XB3403 (supplied by Huntsman, UK) for manufacturing composites; (ii) Epo-fix (supplied by Struers Ltd. UK) for preparing samples for optical microscopy; (iii) Scotch Weld adhesive (supplied by 3M UK) for attaching the end-tabs; and cynoacrylate adhesive (supplied by Tokyo Sokki Kenkyujo Co., Ltd. Japan) for bonding the electrical resistance strain gauges.

3.2.3 Other Materials Used

Aluminium sheets were used to fabricate the end-tabs. A rig built from medium density fibreboard (MDF) was used for aligning the fibre bundles and composites for end-tabbing. A clamping fixture was fabricated from steel to polish the edges of the composites prior to tensile testing. A custom-made jig was manufactured from steel to mount fibre bundles for

heat treatment in a tubular furnace. A custom designed glass apparatus was used for soaking the as-received E-glass bundles in acetone to remove the binder.

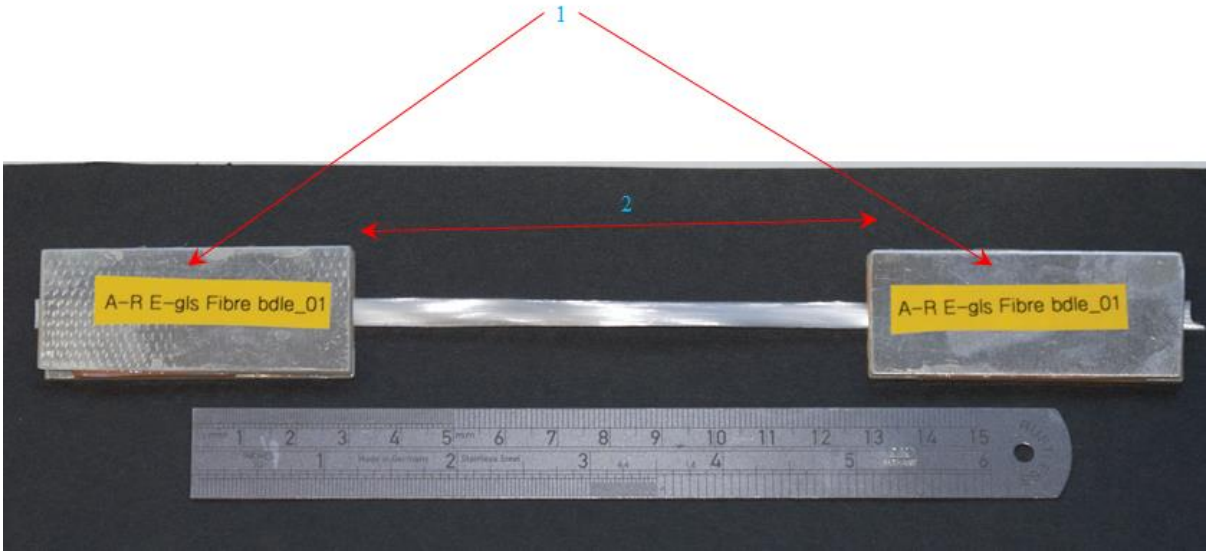

Figure 3.1 A photograph showing an end-tabbed fibre bundle. (1) and (2) refer to the end-tabs and gauge length respectively.

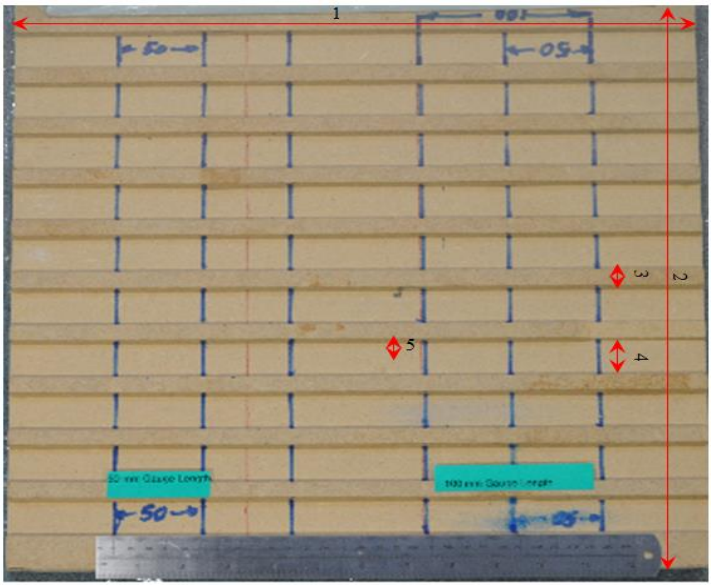

Figure 3.2 Photograph showing the MDF rig that was used to align the specimens during end-tabbing. (1) Length of rig, 400 mm; (2) Width of rig, 400 mm; (3) Grooves separator, 5 mm; (4) width of groove, 25mm; and (5) Depth of groove, 5 mm.

3.2.4 End-tabs Rig

With reference to Figure 3.2, a custom-designed rig fabricated from an MDF board of 400 mm x 400 mm (supplied by Homebase, UK), was used to prepare the end-tabbed samples. The rig consisted of ten grooves (25 mm) that were milled along the breadth (400 mm) of the board and this made it possible to fabricate 10 samples at a time.

3.2.5 End-tabs

It was necessary to bond end-tabs to each end of the fibre bundle to prevent them from being crushed in the jaws of the tensile test machine. Since 30 test specimens were used for each batch of specimens (as-received, solvent-treated, lubricated and heat-treated), it was necessary to prepare 60-pairs of end-tabs for each sample batch. The dimensions of the end-tabs were 60 x 25 x 1.5 mm as illustrated in Figure 3.3. End-tabs were cut from a large sheet of 1.5 mm thick aluminium sheet by means of a guillotine. The edges of the cut end-tabs were dressed to remove sharp edges. End-tabs used for fibre bundles were solvent-cleaned, dried then primed by applying and curing a very thin layer of adhesive. With regard to the end-tabs used for tensile testing of composites, a different procedure was used. The end-tabs were sand-blasted on one face using medium grit abrasive. The end-tabs were transferred to a beaker with acetone and cleaned using an ultrasonic bath for 10 minutes.

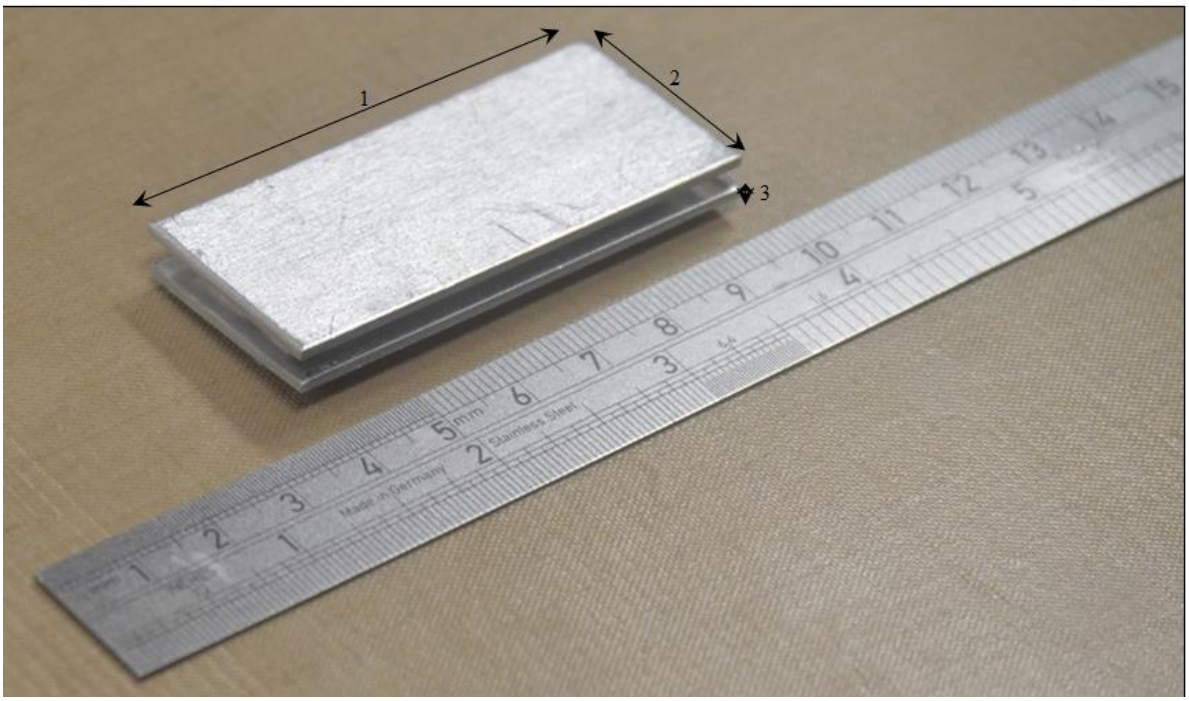

Figure 3.3 Dimensions of the aluminium end-tabs used in this study. (1) Length, 60 mm; (2) width, 25 mm; and (3) Thickness, 1.5 mm.

They were removed, dried on an absorbent tissue and transferred to an air-circulating oven at 40 °C for half an hour. Upon cooling to ambient temperature, the end-tabs were stored in a desiccator until required. The priming and sandblasting were carried out to ensure there was no premature failure of bond interface during tensile loading.

3.2.6 Heat Treatment Jig

A photograph of the jig that was used for heat-treating the E-glass bundles is shown in Figure 3.4. The jig was composed of a threaded steel rod, a circular plate at each end with

five (5 mm diameter) holes located around its circumference. The two plates were positioned as required using pairs of nuts for each plate. In the current series of experiments, the end-to-end distance of the plates was 450 mm. Individual as-received E-glass fibre bundles were inserted in each hole and held in position with stainless steel foil (0.5 mm thick RS Pro supplied by RS Components, UK) as shown in Figure 3.5. The dimensions of the jig was limited by the bore diameter and length of the furnace.

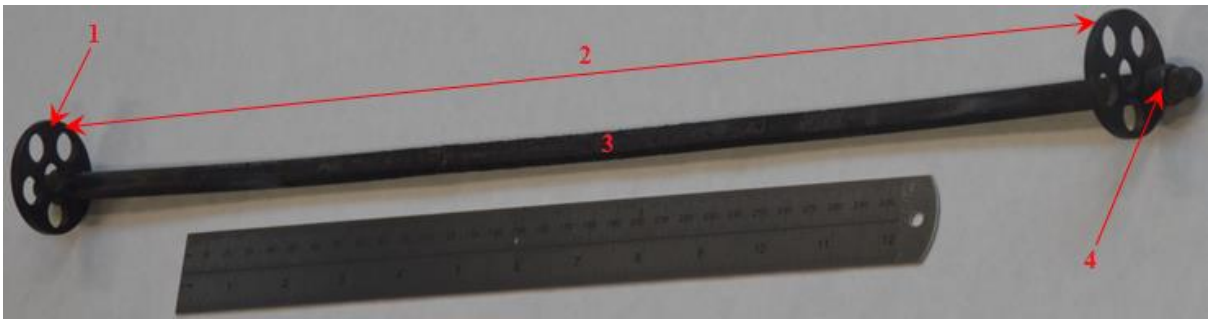

Figure 3.4 Customised heat treatment jig: (1) Circular plate with five holes of diameter 5 mm; (2) Jig length of 450 mm; (3) Threaded steel rod; and (4) Nut used for tightening the circular plate and threaded rod.

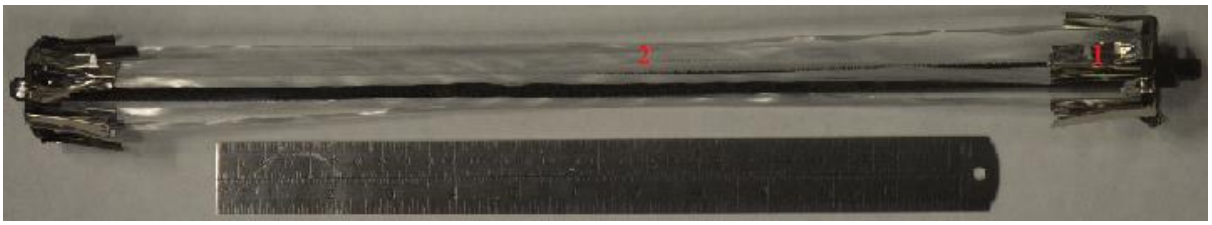

Figure 3.5 Heat treatment jig with as-received E-glass bundles fitted: (1) Stainless steel foil; and (2) As-received E-glass fibre bundles.

3.2.7 Lubricant

A commercially available vegetable oil (Sunflower Oil supplied by Co-operative Group Ltd., UK) was used as a lubricant for one batch of the 30 individual E-glass fibre bundles tensile tested.

3.2.8 Sample Holder for Polishing the Edges of the Composites

This device comprised two customised fabricated metal plates (260 mm x 30 mm x 50 mm) which when fitted together provided a housing to securely clamp the samples as shown in Figure 3.6. Two housing bolts clamp the two halves together allowing a 220 mm sample length. A further five plastic sample clamp screws were equally spaced along the length to secure the sample. The weight of the plates provides sufficient force on the composite whilst grinding to ensure there is no need to exert manual force.

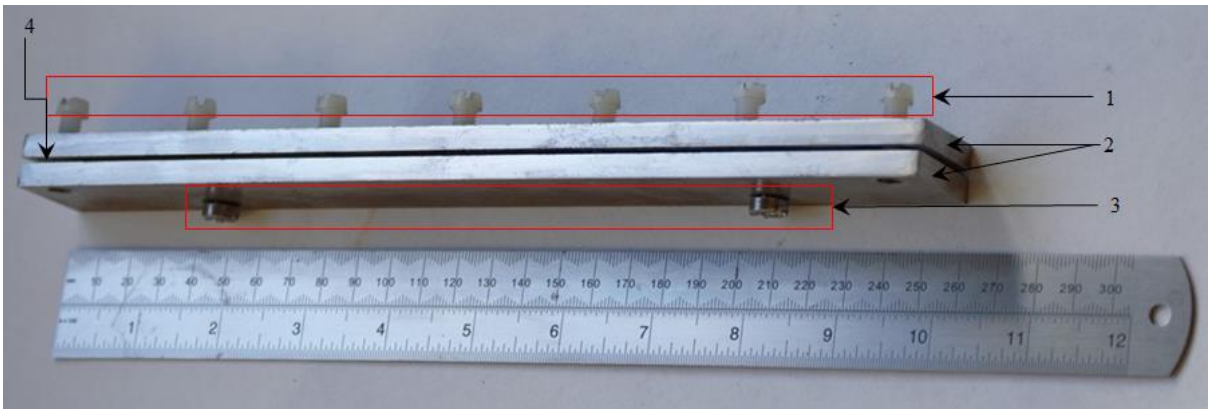

Figure 3.6 Sample holder showing two metal plates with sample secured in between: (1) Five plastic sample clamp screws; (2) Two customised fabricate metal plates; and (3) Two housing bolt clamp.

3.3 E-glass Fibre Bundle Preparation

3.3.1 As-received E-glass Fibre Bundle

Ten as-received E-glass fibre bundles of 500 mm length were taken from the creel. Ten samples at a time could be produced using the MDF end-tab rig shown in Figure 3.3.

3.3.2 As-received E-glass Bundle Spreading

A custom-built in-house fibre spreading rig was used to optimise the processing parameters. The initial design and implementation of the fibre spreading rig was reported previously by Irfan *et al* (2012). This was improved and optimised by Murray (2016), using Hybon® 2026 2400 Tex E-glass. As-received fibre bundles were spread using the rig below for tensile testing.

A photograph of the original fibre spreading rig can be seen in Figure 3.7. With reference to the coding system used in Figure 3.7, an as-received fibre bundle was fed from the central bore of a fibre creel (i) into a pair of serpentine pinch rollers (ii). These rollers fed the fibre bundle into a pre-tension rig (iii) consisting of three rods (iv), with a diameter of 15 mm and a length of 300 mm, positioned in a 'V' shape. The bundle then entered the spreading rig which consisted of a Perspex chassis (v) containing three pairs of roller carrier-hubs (vi). Each carrier-hub consisted of an acetal drive shaft (dimeter and length of 30 mm and 300 mm respectively) the opposing ends of which were located in Perspex bearing housings (discs with a diameter of 150 mm). On each Perspex bearing housing, a series of recesses

were machined around the circumference to enable ball bearings to be mounted. The ball bearings served to secure an acetal rod (vii), supplied by Direct Plastics UK, with a diameter of 30 mm and a length of 300 mm, between a pair of the bearing housings (vi). These were designed to accommodate a single or multiple acetal rods around the circumference. These acetal rods were able to be used as pins or freely rotating rollers.

Each roller carrier-hub (vi) was powered by an individual 12-Volt DC direct-drive motor and gearbox. The motors were connected to one of the individual channels on a pair of dual-channel power supply units (viii); TT*i* CPX200 Dual 35V 10A PSU. This allowed independent control of the revolutions per minute (rpm) of the three roller carrier-hubs (vi), in the clockwise or anti-clockwise direction. The rotation rates of the individual roller carrier-hubs were measured using a digital photo tachometer (Model RM1501, RS Calibration, UK). At the end of the fibre spreading rig was a larger diameter roller (ix) in order to preserve the degree of spreading achieved as the spread fibre bundle traversed towards the haul-off unit (x) (Pultrex, UK Ltd). It also served to minimise the cyclic loading on the fibre due to the intermittent "tension-on/tension-off" action caused by the acetal rods on the roller carrier-hubs. The fibre bundle was wound onto a cardboard mandrel (xi). The spread fibre bundle was then unspooled from the cardboard mandrel and sections were cut for preparation of tensile test samples.

The parameters used for spreading the fibre bundles can be seen in Table 3.1. The winding speed was set at 1 m/min, the pre-tension was set at 10 N and the rotation speed of the roller carrier-hubs was set to 100 r.p.m. With reference to the roller carrier-hubs the configuration

consisted of three acetal rods evenly spaced around the bearings housings and set as roller i.e. they were allowed to rotate freely.

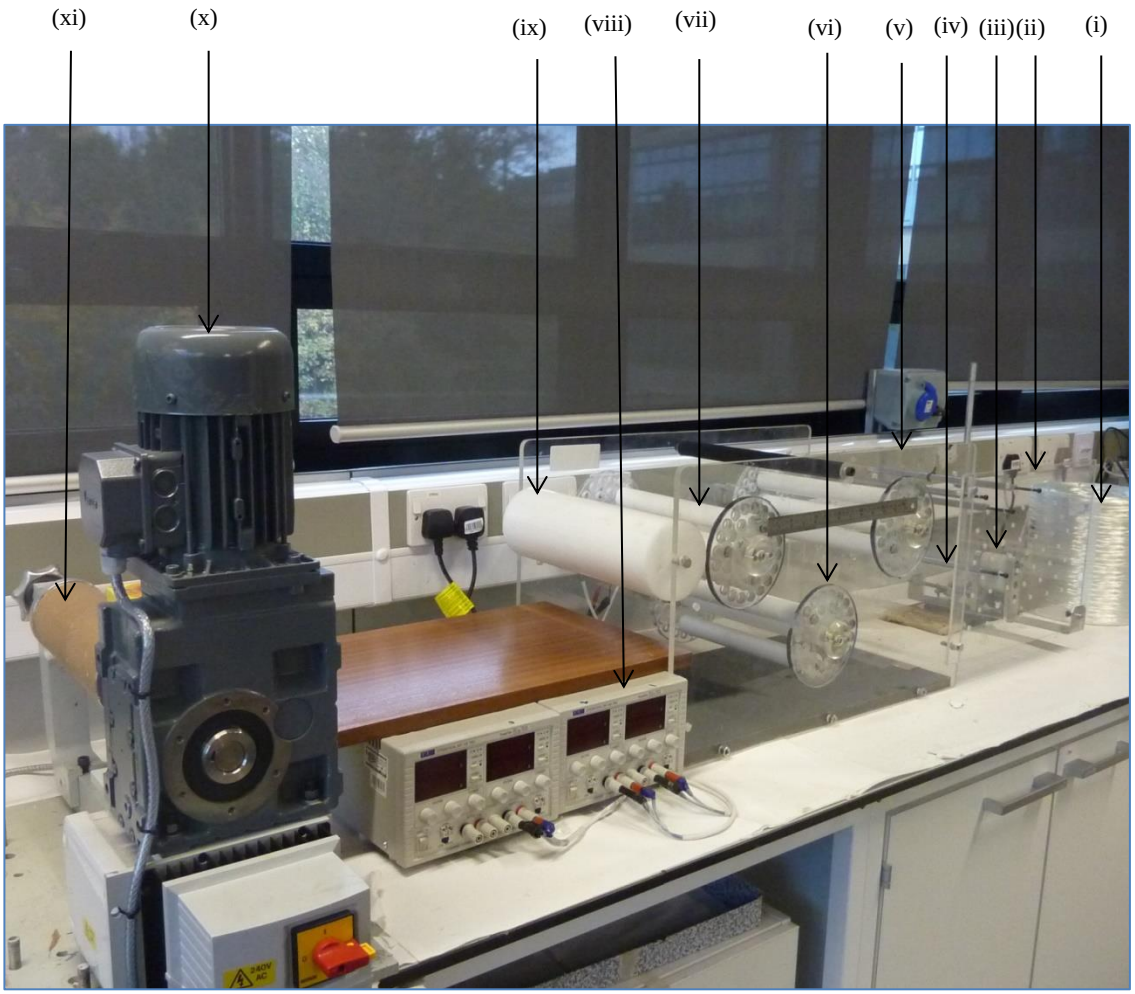

Figure 3.7 A photograph of the fibre spreading rig that was used in this study: (i) Serpentine pinch rollers (ii) Pre-tension roller (iii) 3 rods (iv) perspex chassis (v) Roller carrier hobs (vi) Carrier hub (vii) Acetal drive shaft (viii) TTi CPX200 Dual 35V 10A P PSU (ix) Larger diameter roller (x) Haul-off unit (xi) Cardboard mandrel.

Table 3.1 Fibre spreading parameter.

Parameter	Value
Roller Carrier-hub Configuration	Three rollers equally spaced
Rotating Hub Speed	100 r.p.m
Winding Speed	1 m/min
Pre-Tension	10 N

3.3.3 Lubrication of As-received E-glass Bundle

Thirty end-tabbed, as-received E-glass fibre bundle samples were immersed in vegetable oil (Sunlife oil supplied by Co-operative Group, UK) to ensure fibre filaments were lubricated as shown in Figure 3.8. This was achieved by forming a container from aluminium foil where the oil reservoir measured 100 mm x 200 mm by 10 mm deep as shown in Figure 3.9. Raised platforms on either side of the reservoir supported the end-tabs region above the oil level. Fibre bundles were left to absorb oil for 5 minute duration, then transferred to a platform to allow excess oil to drain for 10 minutes. Due care was taken to prevent the aluminium end-tab region from being contaminated; this was to avoid slippage within the jaws of the Instron test machine.

Figure 3.8 End-tabbed as-received E-glass fibre bundle in lubricant.

Figure 3.9 Oil bath for fibre bundle lubrication: (1) Raised part of the oil reservoir to provide platform upon which end-tab rested whilst fibre bundle is being lubricated; and (2) Oil Reservoir.

3.3.4 Heat Treatment of E-glass Fibre Bundle

The fibre bundles were carefully attached individually to each hole on the heat treatment rig described in Section 3.2.5. Five bundles could be treated at once due to the number of fibre bundles attachment points of the jig. Once these samples were prepared, the jig was carefully inserted into the tubular furnace and covered with a purpose made steel tube neatly lined with rock wool to prevent heat loss. The oven temperature setting dependant on the heating regime needed. This is due to three different heat levels being chosen to subject the samples to (450 °C, 550 °C and 650 °C). The increment rate for the temperature was set at 10 °C/min and a dwell time of 2 hrs was programmed once target temperature was achieved. Once the heat cycle was complete, the furnace was allowed to cool to ambient temperature. After 24 hrs, the sample was removed, detached from the jig and stored away in a desiccator until they were needed for the experiment.

3.3.5 As-received E-glass Fibre Bundle in Vacuum

Each E-glass fibre bundle sample was inserted into a glass tube with an internal diameter of 5 mm. The 5 mm tube was sealed. One end of the sample was wetted using acetone to assist in threading fibres into the tube. Upon producing 8 samples, they were inserted into a larger 45 mm diameter tube. This tube then had a vacuum drawn, then sealed (see Figure 3.10). The glass used for these samples was fused quartz. Quartz was chosen due to its ability to withstand a temperature of 1200 °C which was far above 650 °C needed for the heat

treatment. A photograph of a vacuumed as-received E-glass fibre bundles is shown in Figure 3.11.

Figure 3.10 Pre-vacuumed E-glass fibre bundles sample: (1) Vacuumed glass tube length, 380 mm; (2) Stop cock; and (3) vacuumed quartz glass tube.

Figure 3.11 Vacuumed E-glass fibre bundles sample.

3.3.6 Heat Treatment of As-received E-glass Fibre Bundle in Vacuum

The vacuum tube containing as-received E-glass fibre samples shown in Figure 3.11 was then inserted into a steel pipe of 50 mm internal diameter. This steel pipe was sealed with rock wool at both ends. The pipe was then inserted inside a muffle furnace (Elite Thermal Systems Limited, UK). The heating and cooling rates were set to 10 °C/min, the temperature was set to 650 °C and 2 hrs dwell time was selected. At the end of the cycle, the

furnace was allowed to cool to ambient and, after 24 hrs the sample was removed. The vacuumed glass tube was removed from the steel and stored until required.

3.3.7 Solvent Treatment of As-received E-glass Fibre Bundle

Five fibre bundles each of 500 mm length were attached to the heat treatment jig described in Section 3.2.7 with the aid of aluminium foil at both ends. The fibre bundle was carefully pulled straight without applying undue tension. The jig was then immersed gently into the solvent treatment cylinder filled with acetone, and was then covered and left in a fume cabinet for 72 hrs. Due to evaporation, the solvent was topped up every 24 hrs. A photograph of the E-glass fibre bundles being soaked in solvent is shown in Figure 3.12. After 72 hrs, the samples were removed and then dried in an air-circulated oven for 2 hrs at 80 °C. They were stored in a desiccator until required.

Figure 3.12 Photograph of solvent treatment cylinder with a batch of samples undergoing treatment.

3.3.8 Heat Treatment of Solvent-treated As-received E-glass Fibre Bundle

The fibre bundles obtained from the solvent treatment process described in Section 3.3.6 were transferred into a tubular furnace. The furnace was set to 650 °C with a heating rate of 10 °C/min and a dwelling time of 2 hrs. At the end of the cycle, the furnace was allowed to

cool to ambient temperature and after 24 hrs, the jig was removed. The samples were gently detached from the jig and stored in desiccator until it is needed.

3.3.9 Fibre Bundles Recovery from Composite

Ceramic tubes of 300 mm length and 30 mm diameter were used to contain these composites in a muffle furnace during pyrolysis. Each composite sample was inserted into the ceramic tube and both sides left opened. The ceramic tubes were placed inside the muffle furnace and a temperature of 650 °C was set at a rate of 10 °C/hr. As described in Section 3.3.6 for pyrolysing vacuumed as-received E-glass fibre bundles. Once the heat treatment was completed, the furnace cooled to ambient and the sample was collected.

3.3.10 End-tabbing E-glass Fibre Bundle

The end-tabs rig and the end-tabs described in Sections 3.2.4 and 3.2.5 respectively were used for this process. The gauge length needed for the samples was precisely marked in position on the rig. The adhesive that was used for bonding the end-tabs to the fibre bundle was Scotch Weld 9323 (3M, UK). A thin layer of the adhesive was applied to the intended bonding face of the end-tab. The end-tabs were positioned to align with the measured gauge length. The fibre bundles were secured in position by holding each end down using a bulldog type clip to maintain an equal tension of individual filaments as shown in Figure 3.13. However, this could not always be guaranteed considering the number of filaments in the bundle (approximately 4,000). A photograph of a sample of end-tabbed E-glass fibre bundle is as shown in Figure 3.2.

Adhesive penetration into the fibre bundle was achieved by means of manipulation using a wooden spatula at which time the upper adhesive coated end-tab was carefully positioned and pressed into place to align with the lower end-tab. The entire rig was covered with a thin sheet of Clear Melinex (1016/75M/Clear, supplied by Pennine drawing office supplies, UK), this acted as a release material to avoid unwanted bonding of excess adhesive. A flat MDF board was placed on top of the samples and a 4 kg load placed on top to apply lateral pressure.

Figure 3.13 Finished end-tabbed as-received E-glass fibre bundle in the end-tabbed rig lined with aluminium foil ready to be removed for tensile testing/storing in deciccator: (1) End-tabs; (2) Fibre bundle; and (3) Bulldog clips.

3.4 E-glass Fibre Reinforced Composite

3.4.1 Production of E-glass Fibre Reinforced Composite Manufacturing

E-glass/epoxy composites from each of the different processed sample types, as described in Section 3.3, were manufactured using 30 as-received, 30 heat-treated, 30 solvent extracted, 30 solvent extracted and then heat-treated, 20 solvent extracted then vacuumed & heat-treated, 20 vacuumed and then heat-treated, and 20 recycled (recovered fibre from composites); whilst the epoxy used was LY3505/XB3403 (Huntsman, UK). The heat-treated samples were thermally treated at temperatures of 650 ºC whilst the composites were pyrolised at 650 ºC in order to extract the reinforced fibre bundle (recycled) for re-use.

3.4.1.1 Preparation of the Tooling

The tooling plate was an aluminium plate with a flat polished surface, upon which the composites were formed and then cured in the autoclave. A release agent (PAT-656/B3R, supplied by E. und P. Würtz GmbH & Co. KG, Deutschland), was applied by cloth, impregnated with the release liquid; this was allowed to dry for approximately 1 minute and then buffed with a clean fresh cloth. This process was repeated 5 times to aid easy demoulding of composites from the tooling. The same process was carried out on the surface and the sides of the caul plate which was another flat aluminium plate positioned on top of the composite to aid compression of the materials sandwiched between the two surfaces.

3.4.1.2 Lay-up of E-glass Fibre Bundles

As can be seen in Figure 3.14 (a,b,c), fourteen fibre bundles from each of the processed sets, described in Section 3.3, were individually laid across the surface of the tooling plate at 25 mm intervals. One end of each bundle was secured to the plate using flash tape as shown in Figure 3.14a. A 2 kg weight was used for the as-received and solvent extracted [A-R and S-X], whereas a 1 kg weight, was used for the heat-treated (H-T) bundles. The 2 kg weight was attached to the other end of the fibre bundle, using flash tape and the weight was allowed to hang freely thus introducing an equal tension for each bundle. Once under tension, the fibre bundle was securely attached to the tooling plate using flash tape. The weight was removed and excess length cut from the fibre bundle. In the preparation of heat-treated fibre bundles a 1 kg weight was attached but was manually supported to uni-directionally tension the fibre bundle without causing damage due to the fragility of the fibre bundles.

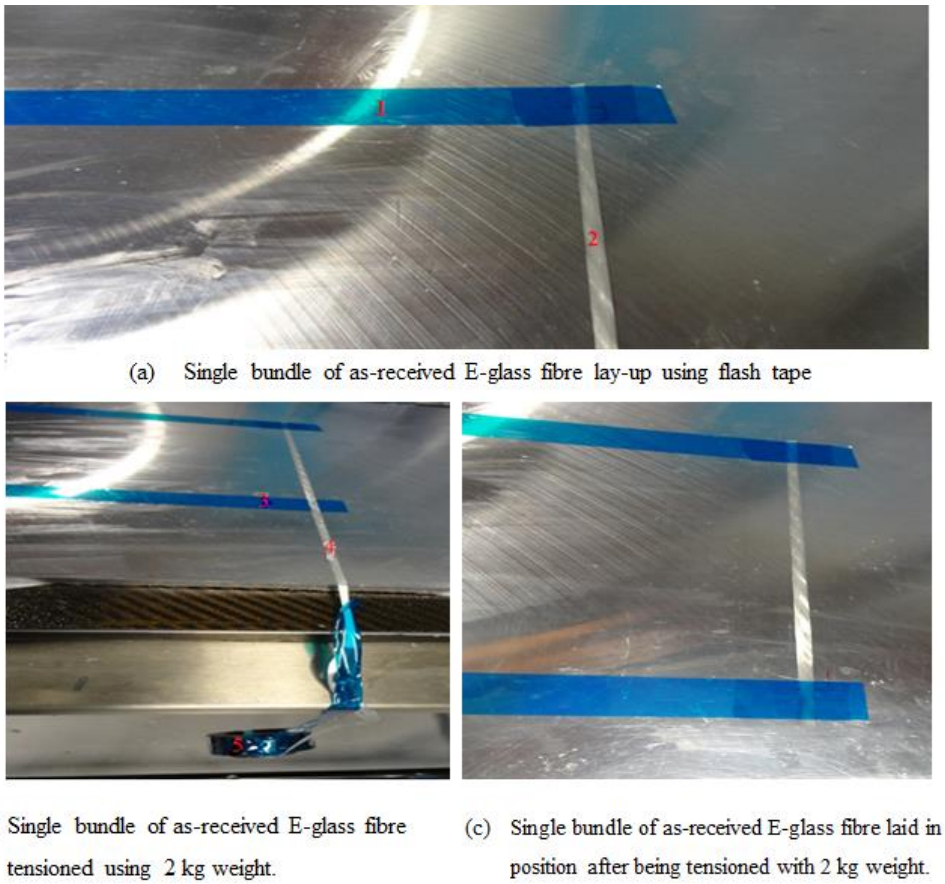

(a) Single bundle of as-received E-glass fibre lay-up using flash tape

(b) Single bundle of as-received E-glass fibre tensioned using 2 kg weight.

(c) Single bundle of as-received E-glass fibre laid in position after being tensioned with 2 kg weight.

Figure 3.14 Lay-up of E-glass fibre bundles using 2 kg weight for tensioning: (1) Flash tape; (2) E-glass fibre bundle; (3) Flash tape; (4) E-glass fibre bundle under tension; and (5) 2 kg weight.

3.4.1.3 Resin Impregnation

The amount of resin required was mixed using a stoichiometric ratio of 100:35 by weight of resin and hardener. Mixing of the resin system was carried out under extraction to safely remove fumes created by chemical reactions. The resin was placed in a vacuum assisted desiccator for 40 minutes to remove entrapped air bubbles formed whilst being mixed. A

moat/dam was prepared around the laid-up samples on the tooling plate to contain the liquid resin. This was carried out by creating a border of vacuum sealing tape (supplied by Easy Composites Ltd., UK) around the laid-up samples beyond the perimeter area of the caul plate as shown in Figure 3.15.

One side of the tooling plate was then raised to allow resin flow along the length of the laid-up fibre bundles. The degassed resin was removed from the vacuum desiccator and one-third of it was poured on to the raised ends of the fibre bundles. The resin was allowed to flow along the length of the samples to the opposite end (lowered position). More resin was added until all samples were wetted out. The raised end of the tooling plate was then lowered and the opposite end raised to allow the resin to flow in the opposite direction. The plate was returned to its flat position once satisfied that the fibre bundles had been fully impregnated.

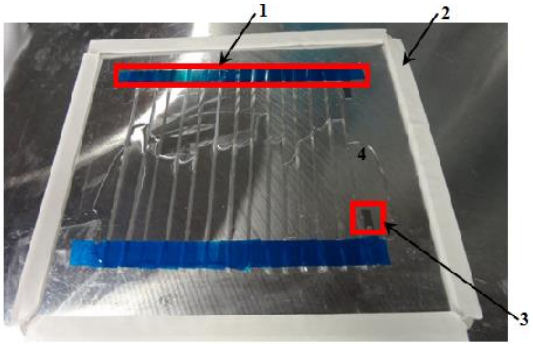

Figure 3.15 Photograph showing fibre bundles being impregnated: (1) Flash tape; (2) Tacky tape; (3) Spacer; and (4) Epoxy resin.

3.4.1.4 Caul Plate

Four spacers measuring 0.25 mm thickness were placed within the four corners of the sample area (see Figure 3.15). The polished surface of the caul plate was placed on top of the samples, ensuring all spacers were underneath the plate. Flash tape was used to secure the caul plate in position, as shown in Figure 3.16, to prevent slippage.

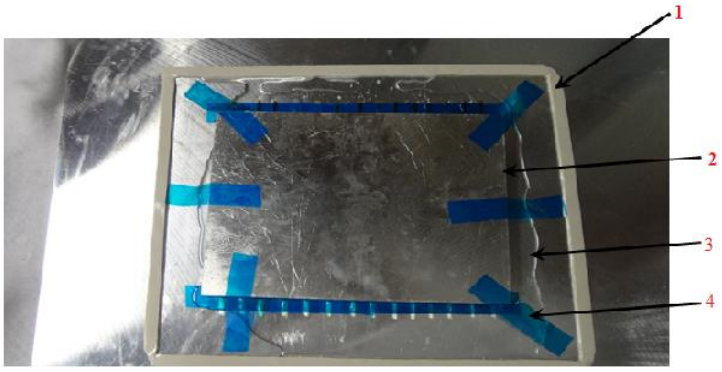

Figure 3.16 Photograph of caul plate secured in position with flash tape: (1) Tacky tape; (2) Caul plate; (3) Excess epoxy resin flow; and (4) Flash tape for securing the sample between the platform and the caul plate.

3.4.1.5 Vacuum Bagging

A sheet of non-perforated release film (R250, supplied by Easy Composites Ltd., UK) was spread carefully over the caul plate, ensuring all edges attached to the vacuum sealing tape of the moat. This was done to prevent resin seepage. A bleeder/breather cloth (BR180, supplied by Easy Composites Ltd., UK) was spread over the entire sample area. A border of vacuum sealing tape was positioned around the edges of the tooling plate (about 25 mm

from the edge) as shown in Figure 3.17. A sheet of vacuum bagging material (R250, supplied by Easy Composites Ltd., UK) was carefully stuck to the sealing tape along one of the long edges (see Figure 3.18b), having made sure that there were no wrinkles or gaps in the joint. After the breach valves were fitted into position through the vacuum bagging sheet, the bagging materials were tensioned by hand prior to attaching to the sealant along the remaining edges. Flash tape was applied to the edges of the vacuum bagging sheet and the tooling plate to secure all four sides.

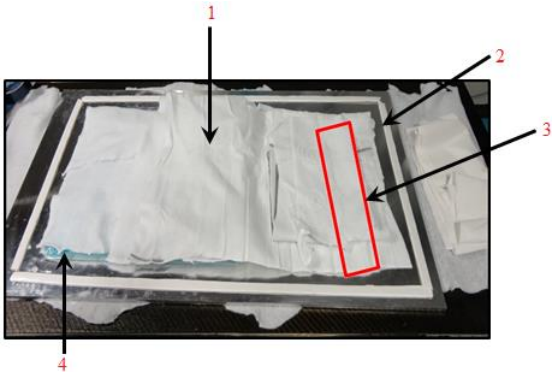

Figure 3.17 Showing photograph of tacky tape round the sample area with bleeder/breather cloth used for covering the sample with extension to where the breach valves were to be located (red triangle): (1) Breather cloth; (2) Bordered tacky tape; (3) Breach valves position; and (4) Non-perforated release film.

(a) Vacuum bag assembly.

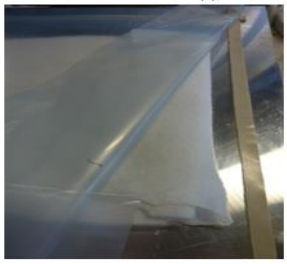

(b) Attaching the vacuum bag to one of the edges using vacuum tape.

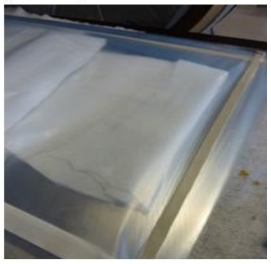

(c) An assembled vacuum bag.

Figure 3.18 Photographs showing the stages involved in vacuum bagging.

(a) Tacking the vacuum bag to the second short edge.

(b) Breach valve location preparation.

(c) Breach valve screwed in place.

Figure 3.19 Photographs showing tacking of vacuum bag to the tacky tape and screwing of breach valves to its location: (1) Vacuum bag peeled; Breach valve bottom half; (3) Vacuum bag top; and (4) bottom part of the breach valve.

(a) Tacking the vacuum bag to tacky tape along the second longest edge.

(b) The excess vacuum bag and protruding tacky tape to seal it up.

Figure 3.20 Photographs showing the last step of sticking the vacuum bag to the tacky tape by taking care of the excess vacuum bag and usage of extra tacky tape to seal it tight: (1) Breathing cloth; (2) Vacuum bag; (3) Tacky tape; (4) Extra tacky tape to seal excess vacuum bag; and (5) Excess vacuum bag.

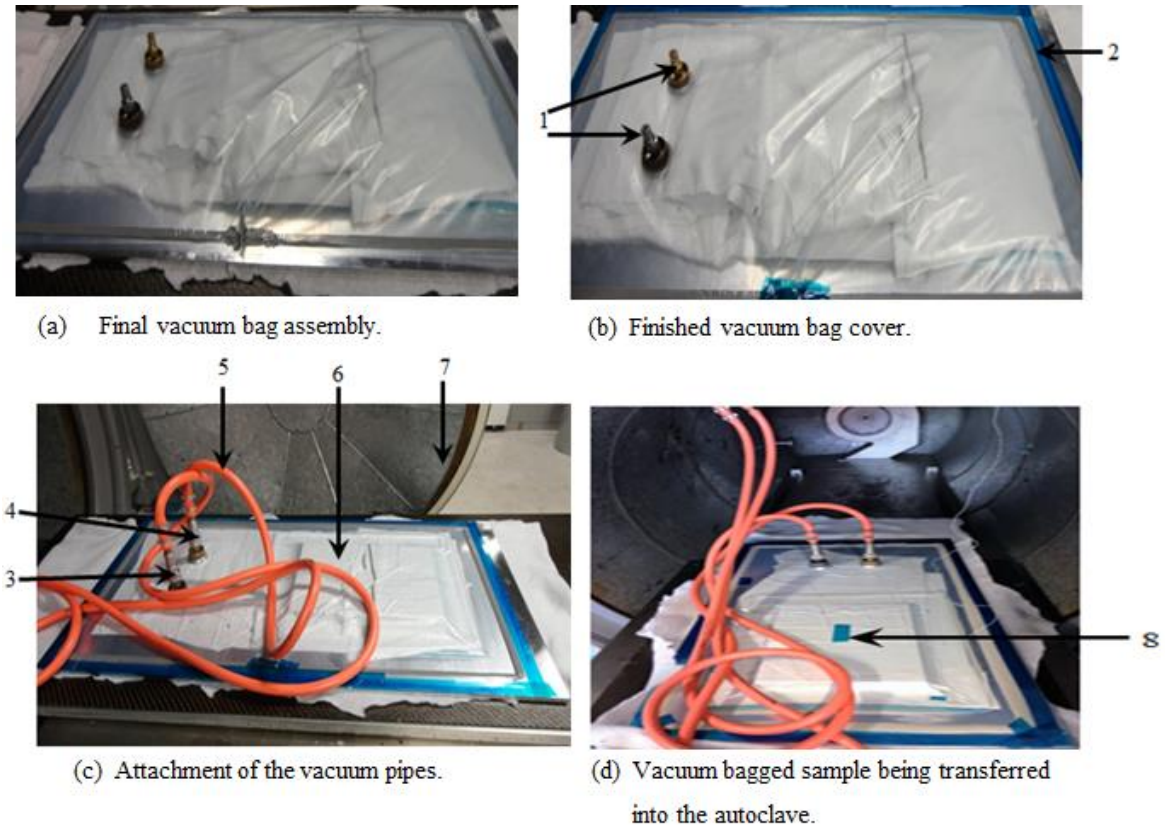

Figure 3.21 Photographs showing finished sample preparation ready for curing in the autoclave: (1) Breach vacuum valves; (2) Flash tape; (3) Breach vacuum valve fitted with hose; (4) Breach vacuum testing valve fitted with hose; (ISO 527-5:2009) hose pipe; (6) vacuumed sample; (7) Autoclave door; and (8) Thermocouple.

3.4.1.6 Autoclave Settings and Processing

The tooling plate was inserted into the autoclave and a thermocouple was carefully attached to the surface using flash tape. A vacuum hose from inside of the autoclave was attached to one breach valve (see Figure 3.21c) and a vacuum pressure gauge was fitted to the second breach valve to test for leaks in vacuum bag.

After ensuring that the vacuum was strong and secured, the vacuum gauge was removed from the second breach valve and a monitor hose from inside of the autoclave was fitted to the breach valve. The autoclave door was closed and locked.

Figure 3.22 Photograph of graph showing autoclave programs available in the system where the curing regime for L3505/XB3403 resin was selected/defined.

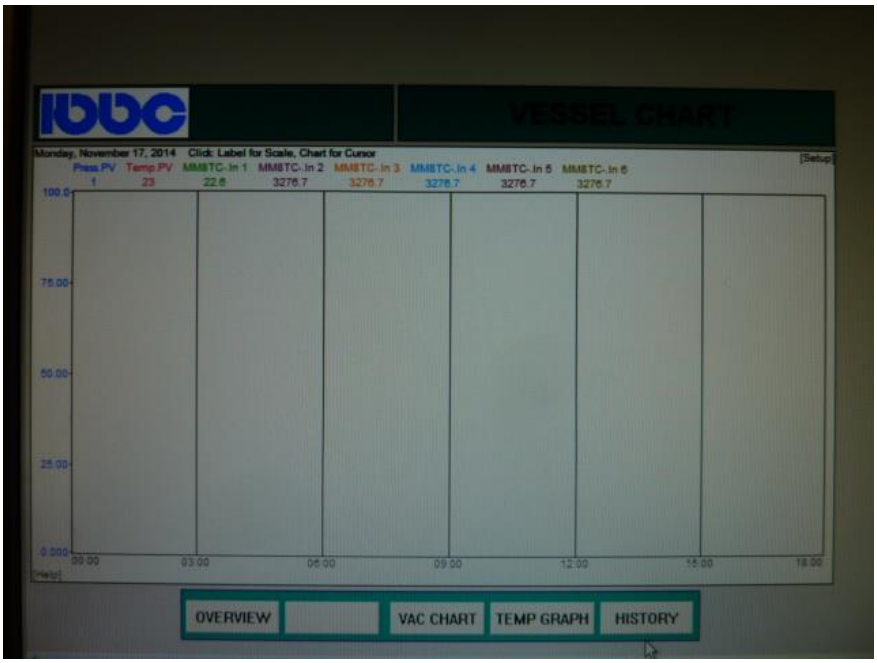

Figure 3.23 Photograph of graph where thermocouple reading was checked.

The program for epoxy/amine (LY3505/XB3404) was selected (i.e. cure cycle: 80 ºC and 80 Pci for 6 hrs) from the program shown in Figure 3.22. Figure 3.23 shows the program chart where air temperature, pressure and 3 individual thermocouple readings are shown as a function of time. Figure 3.24 shows a program overview. The screen shows the program status of vacuum, pressure and temperature throughout the duration of the cured cycle. The autoclave was switched on by consecutively pressing the buttons indicated by red rectangles in Figure 3.25 in order to begin the curing cycle. Once the programmed cure cycle was completed, the autoclave was allowed to cool to ambient before opening the door to remove the sample. By selecting the chart program a chart of the actual cure cycle of this sample could be examined to ensure a full cure of the resin system had taken place.

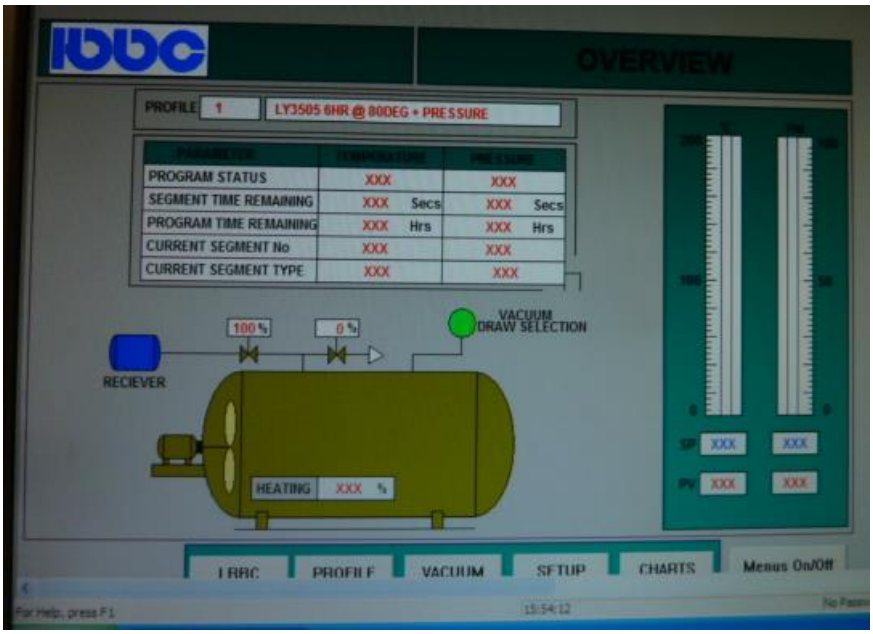

Figure 3.24 Photograph showing temperature and pressure gauge reading.

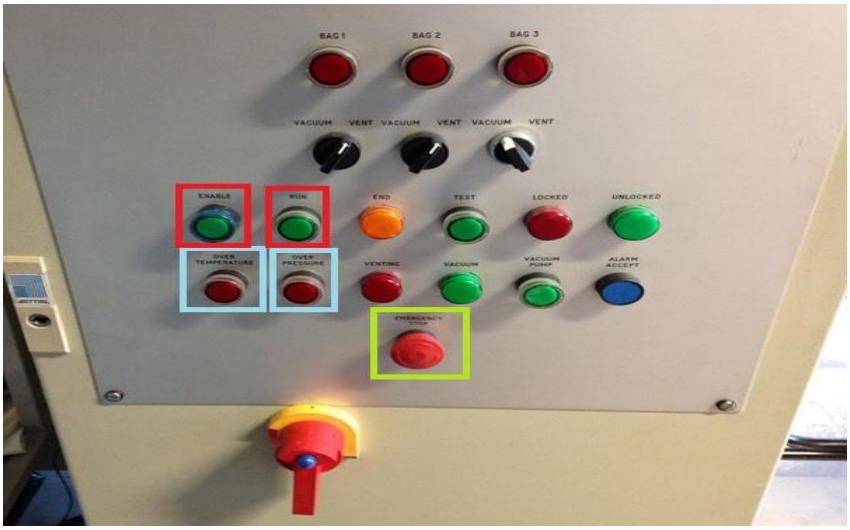

Figure 3.25 Photograph showing manual control panel for the autoclave.

The vacuum bag and composites were removed with great care from the tooling plate.

3.4.2 Polishing the Edges of the Composites

The equipment used for this procedure was a linisher/belt sander and the composites sample holder shown in Figure 3.6, which was described in Section 3.2.8. The grade of the polishing belt used was 400 micron. Grinding/polishing was carried out to remove excess cured resins along the longitudinal edges of the composites.

The samples were prepared by cutting them to a length of 220 mm, which is the maximum length that can be accommodated by the sample holder. In addition to this, the strip needed to be ground/polished off to ensure that approximately 2 mm of excess resin was left on each edge of the impregnated fibre bundle. This was to avoid damage of the fibre within the composite. The sample was slid in between the two metal plates of the sample holder, by aligning the marked area of the sample with the surface of the metal plates. The two primary metal screws at both ends were tightened to secure the two halves and then the five plastic clamp screws were tightened to secure the sample along its length.

The grinding/polishing was carried out by lowering the protruded portion of the sample on to the linisher belt as the belt was moving. No pressure was exerted on the sample holder, as its weight was adequate to remove excess materials to the marked level. The level of polishing achieved was checked periodically throughout the process and again after the targeted level was achieved. This process was repeated for all samples.

3.4.3 End-tabbing Fibre Reinforced Composites

The thickness of the composites manufactured from single fibre bundles were thin enough to allow a similar method used for end-tabbing fibre bundle described in Section 3.3.9. The end-tabs used for the composite samples needed to be sand-blasted to increase surface bonding between the composite/adhesive and end-tabs/adhesive interface. The adhesive used was Scotch Weld 9323 supplied by 3M, UK. Prior to end-tabbing the samples, the thickness and width of the samples were measured and recorded and a gauge length of 100 mm was marked out. The end-tabs area of the sample was lightly abraded using 120 grade sand paper (GXK51-P-P 80, supplied by Screwfix Direct Ltd., UK) to increase surface bond of composite/adhesive.

A thin, even layer of adhesive was applied to the sandblasted face of the end-tabs and the end-tabs were positioned to align with the 100 mm gauge length marked on the end-tabbing rig. The samples were aligned with their gauge length markings to the edges of the end-tabs and then embedded into the adhesive. Further adhesive was applied on to the sample and spread evenly. A second end-tab was positioned to align with the previous end-tab and lightly compressed into position. After a period of 30 minutes, a sheet of Melinex (1016/75M/Clear, supplied by Pennine Drawing Office Supplies, UK) was laid over the samples and the MDF plate was put on top with 4 kg weight.

3.4.4 Bonding Strain Gauges on Composites

To obtain accurate load/strain data during tensile testing using the Instron machine, strain gauges (FLA-6-11 type, with gauge length and factor of 6 mm and 2.10 Supplied by Tokyo Sokki Kenkyujo Co, Ltd.) were used respectively. The centre of the sample was marked and strain gauges were carefully attached to be central and parallel to the edge of the sample.

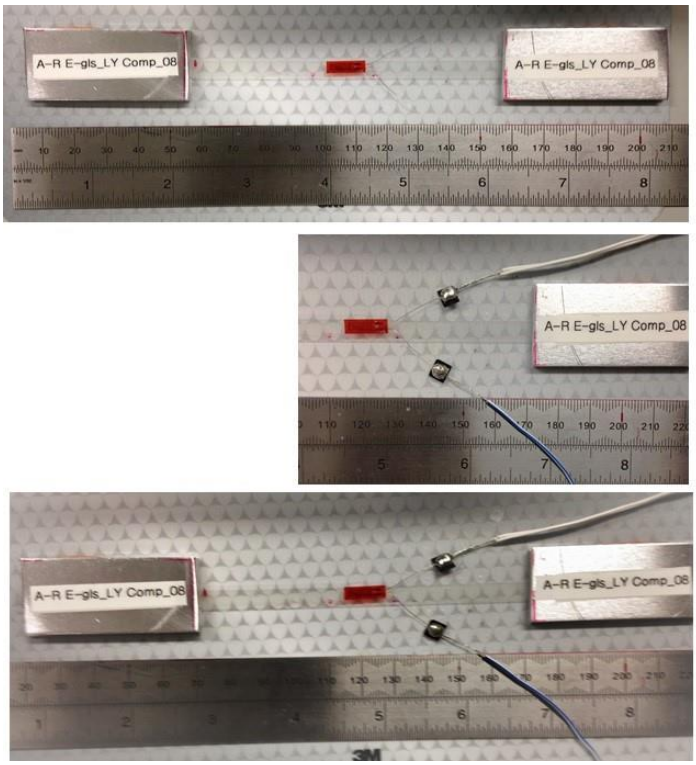

Figure 3.26 Photograph showing strain gauge bonded to one of the S-X & H-T reinforced E-glass (single bundle)/epoxy composite samples.

Cyanocrylate adhesive (Supplied by Tokyo Sokki Kenkyujo Co, Ltd.) was used for this purpose. The two strain gauge legs (see Figure 3.26a) were separated whilst the wire leads were stripped and 2 ports were used. Two white wires were twisted together whilst the blue one was isolated. The twisted white wires which were soldered to one leg of the strain gauge were to compensate for temperature and the blue wire soldered to the other leg over each gauge port (see Figure 3.26b). The integrity and quality of the strain gauge was then tested, using an electronic meter.

3.4.5 Composites Re-manufactured from Recovered Glass Fibre Bundles

All techniques used for manufacturing composites from recovered glass fibre bundles were identical to the processes outlined in Section 3.4.1 but had to be carried with extra care due to their fragility.

3.5 Test Methods

3.5.1 Tensile Testing

The tensile tests were performed using an Instron 5566 mechanical test machine. Cross-head displacement rates of 0.1 mm/minute, 1 mm/minute and 2 mm/minute were used for various samples. The fibre bundles and composites were tested at room temperature (20 °C - 21 °C); the relative humidity was measured to be 50 ± 7%. A pair of piezo-electric acoustic

emission transducers were surface-bonded to the protruding section of the end-tabs. Figure 3.27 shows a schematic illustration of the fibre bundle tensile test set up.

3.5.1.1 Tensile Testing of E-glass Fibre Bundle

A set of five batches of thirty as-received and spread E-glass fibre bundles of gauge lengths 50, 80, 100, 150 and 200 mm were end-tabbed as described in Section 3.3.9 for tensile testing. The cross-head displacement used for these batches was 2 mm/minute.

A second set of samples comprised five batches of thirty as-received, lubricated, heat-treated, solvent-treated, and solvent & heat-treated E-glass fibre bundles. And a third set comprises two batches of twenty vacuumed & heat-treated and solvent, vacuumed & heat-treated E-glass fibre bundles. These sets were all end-tabbed with a gauge length of 100 mm for tensile testing whilst the cross-head displacement used for the batches was 0.1 mm/minute.

3.5.1.2 Tensile Testing of E-glass/Epoxy Composites

One set of four batches of thirty as-received, heat-treated, solvent-treated and solvent & heat-treated E-glass fibre reinforced/epoxy composites were end-tabbed as described in Section 3.4.3. Eight of the thirty end-tabbed composites from each of these four batches were attached with strain gauges as described in Section 3.4.4. The second set of three batches of twenty vacuumed & heat-treated, solvent, vacuumed and heat-treated and recovered/recycled E-glass fibre reinforced/epoxy composites were end-tabbed as described

in Section 3.4.3. Five of the twenty end-tabbed from each of these batches were attached with strain gauges as described in Section 3.4.4. The gauge length for all composite samples was 100 mm whilst the cross-head displacement used was 1 mm/minute.

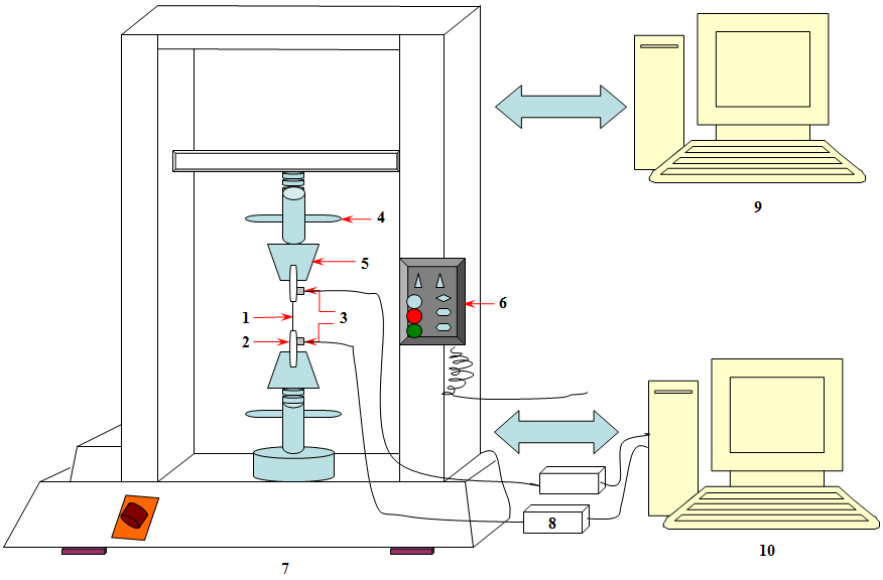

Figure 3.27 Schematic illustrations of the Instron mechanical test machine and the acoustic emission set up along with the data acquisition system: (1) Fibre bundle; (2) End-tabs; (3) PZT acoustic emission sensors; (4) Instron jaw locking device; (5) Jaw of Instron machine; (6) Instron machine control panel; (7) Instron machine; (8) Pre-amplifier; (9) Instron data acquisition system; and (10) Acoustic emission data acquisition system.

3.5.1.3 Acoustic Emission Monitoring

A two-channel Mistra 2004 data acquisition software system (Euro Physical Acoustics Corporation) was used for acquiring acoustic emission (AE) data. Two resonant piezo electric (PZT) transducers (Wide-band sensors) were surface-mounted on to the end-tabs at both ends of the fibre bundles using a soft paraffin wax (White Petroleum Jelly B.P, Thornton Ross) to ensure signal. These transducers were secured to the end-tabs with high-duty adhesive tape. Two parametric channels from the data acquisition systems were connected to the Instron machine to acquire the load and cross-head displacement data. The data acquisition parameters for capturing AE data are summarised in Table 3.2.

Simulated AE events were generated; using pencil lead breaks tests to ascertain the efficiency of the coupling between the aluminium/sample interfaces and to evaluate the wave speed. In these experiments, each recorded signal was analysed by the Mistra data acquisition system and eleven parameters were calculated and recorded from the waveforms: rise time, parametric 1 (loading), parametric 2 (extension), channels, duration, counts to peak, amplitude, average frequency, resonant frequency, energy and peak frequency.

Table 3.2 Summary of the data acquisition parameters that were used for acquiring AE data during tensile testing of the E-glass fibre bundles.

FT Band	6 dB
Pre-Amplifier	40 dB
Sampling rate	10 MSPS
Pre-Trigger	256.000
Sensors type	Wide-band sensors (WD)
Coupling agent	Vaseline
Peak definition time (PDT)	50 μs
Hit definition time (HDT)	100 μs
Hit lockout time (HLT)	100 μs

3.5.2 E-glass Fibre Characterisations

3.5.2.1 Sample Preparation from E-glass Fibre Bundle

The E-glass fibre bundles used for the tests were obtained from the samples prepared as described in Section 3.3. The specimens were made up of as-received, heat-treated and solvent-treated E-glass fibre bundles. Except for the scanning electron microscopy (Bock *et al.*) and optical microscopy analysis where fibre bundles were used directly to prepare experimental samples, E-glass fibre bundles were ground in a clean mortar and pestle (see Figure 3.28) to a fine powder for X-ray diffraction (XRD), mid-infrared spectroscopy, differential scanning calorimetry (DSC) and thermogravimetric analysis (TGA).

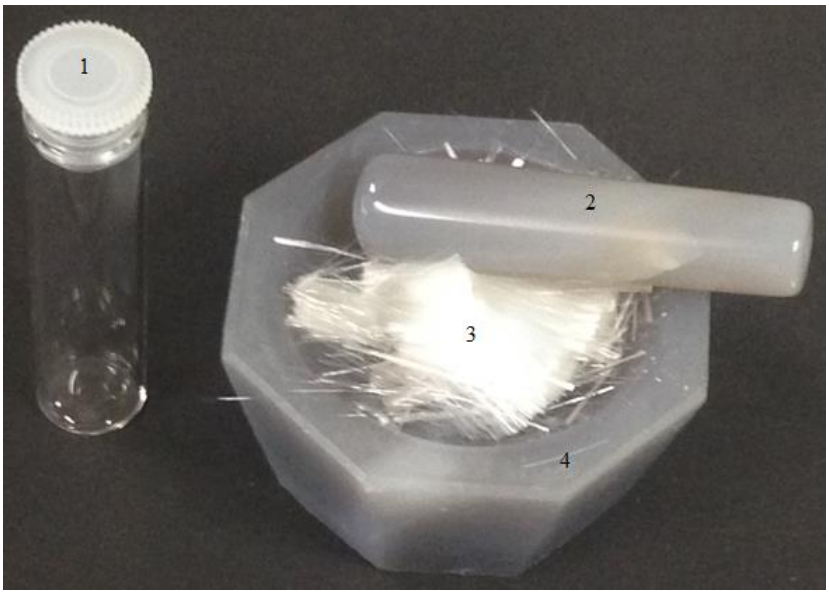

Figure 3.28 Photograph of powdered sample preparation tools (1) Sample container; (2) Pestle; (3) Chopped E-glass fibre bundles; and (4) Mortar.

3.5.2.2 SEM

The fibre bundles were carefully laid on a cutting plate, ensuring no contamination from handling or environment took place. The fibre bundles were cut to the appropriate length, using a sharp blade. SEM stubs were cleaned whilst carbon stickers were stuck on the stubs required, depending on number of samples being prepared. The fibre bundles were then laid on the carbon sticker and gently manipulated, using a wooden spatula in order to ensure a good bond between the fibre and the carbon sticker. Silver-dag was carefully dropped at the ends of each bundle to act as a conductor. After this the samples were coated two or three times with an electrically conductive thin film of platinum. These thin films were sputter coated on to the samples surface to prevent "charging", reduce thermal damage, and

enhance secondary electron emission. The samples were loaded into the electron chamber for surface examination and image taking individually.

3.5.2.3 XRD

This analysis was carried out using a X-ray diffractometer (Equinox 3000) supplied by Inel, France. This machine was equipped with a solid quadrant detector that measures angles 2 theta in the range 0-115° whilst the integrated time for this sample was ≈900 seconds. The X-ray tube emits Copper k alpha radiation and uses a germanium monochromator.

The samples were prepared as discussed in Section 3.5.2.1 and thereafter 100 ml was dispensed into the sample holder of XRD machine for analysis. The adaptor plate was placed at the bottom of sample holder to enhance its height. The sample was filled to level with the top edge of the filling area. The sample holder was placed at the central part of the sample rotator whilst the starter switch was pressed. The front cover of the X-ray set was closed and the XRD analysis started running. After the test was completed, the XRD spectrum was obtained and analysed using the Match software.

3.5.2.4 Mid-infrared Spectroscopy

About 2 ml of the specimen prepared in Section 3.5.2.1 was dispensed on the Golden gate attenuated total reflection (ATR) crystal plate mounted on Nicolet 8700 FTIR system supplied by Thermo Scientific (see Figure 3.29). The software parameters were set whilst the cone surface (powder press) was lowered to rest on the sample surface. A powder press

was used to provide even distribution and contact. ATR technique was used due to its advantage over diffuse reflection when analysing powder, in that the distortions due to scattering that occurs in diffuse reflection spectra does not occur in ATR spectra. The infrared scanning was carried out for about 120 seconds whilst the scanning wavelength was between 400 and 4000 wavenumbers (cm^{-1}).

Figure 3.29 Photograph of Nicolet 8700 FTIR system mounted with golden gate ATR crystal.

3.5.2.5 DSC and TGA

About 10 mg of the specimen prepared in Section 3.5.2.1 was dispensed in a platinum crucible. The machine used for this experiment was a DSC-TGA machine (NETZSCH STA

449 C) supplied from Germany (see Figure 3.30a). Twin crucibles were used in the heating chamber with one acting as reference whilst the other held the sample to be analysed.

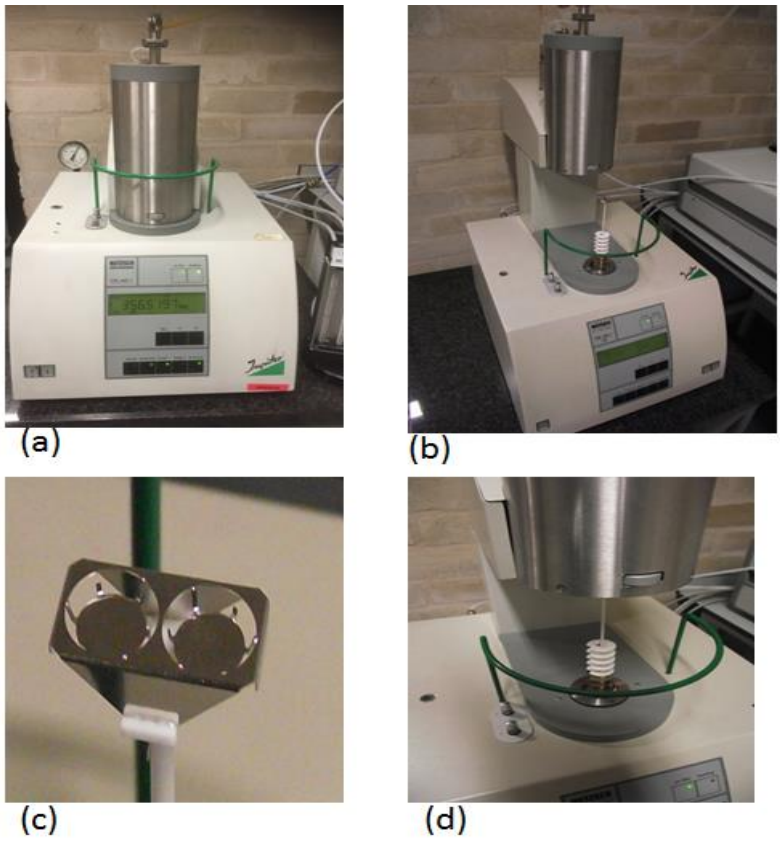

Figure 3.30 Photograph of DSC-TGA machine (NETZSCH STA 449 C).

The analysis was carried out in an air environment with a flow rate of 100 ml/min. The sample was heated from room temperature to 650 ºC at 10 ºC/min. After the temperature

reached 650 ºC, it was allowed to cool to ambient and the result was obtained for further analysis.

3.5.2.6 Optical Microscopy

The fibre bundle was impregnated using UV cured resin, which was cured by using a laser. This was done to hold the filaments together in order to prevent them from being disorientated; thus, making sure they are vertically aligned during potting. This was not necessary for the composite sample. Potting was carried out by holding the sample vertically using a clip. The sample was then placed inside the potting mould, making sure the clipped sample was centrally secured. Epofix resin and hardener were then prepared, using a stoichiometric ratio of 25:3. The resin was put in vacuum desiccator for 40 minutes to de-gas and was then gently poured into the mould. This was left for 24 hr to cure at room temperature. The sample was removed and post-cured at 70 ℃ for 1 hr. The sample was ground and polished, using 5 grades of polishing paper ranging from 240 to 4000 microns followed by 3 grades of polishing disc liquids ranging from 3 to 0.25 microns. The samples were inspected using an optical microscope (Axio-skop 2 MAT mot) with analysis software (Axio Vision), both supplied by Carl Zeiss Ltd.

3.5.2.7 Fibre Volume Fraction (V_f)

The crucibles and beakers used for this experiment were cleaned using distilled water and dried in an oven at a temperature of 40 ℃ for 30 minutes. After cleaning they were stored in a desiccator until required. A weighing balance (± 0.00001 g), and its accessories were used.

The temperature of the room was recorded prior to the experiment. Upon starting the experiment the weight of an empty crucible, m_c was measured and the composites were cut into smaller pieces to fit into the crucible. The weight of the crucible and composites were measured in air, $m_{i,}$ whilst the weights of the composite pellets were weighed in water, m_w prior to return into the crucible. The sample was then transferred into the furnace for a burn-off session. The burn-off temperature was 625 °C at an initial heating rate of 10 °C per minute and the dwell was 4 hrs. At the end of the cycle, the furnace was allowed to cool down to room temperature. The sample was removed and weighed, m_{cr}. V_f calculations were carried out, using the following equations:

Mass of crucible $(g) = m_c$ [35]

Initial mass of specimen $(g) = m_i$ [36]

Mass of specimen in water $= m_w$ [37]

Mass of crucible + recovered fibre $(g) = m_{cr}$ [38]

Mass after combustion – final mass $(g) = m_f = m_{cr} - m_c$ [39]

Volume of reinforcement $(cm^3) = vol_1 = \frac{m_f}{\rho_r}$ [40]

Density of reinforcement $(g/cm^3) = \rho_r$ [41]

Density of composite (specimen) $(g/cm^3) = \dfrac{(m_i \times k)}{(m_i - m_w)}$ [42]

Density of matrix $(g/cm^3) = \rho_m$ [43]

Weight percent of reinforcement $(\%) = w_f = \left[\dfrac{m_f}{m_i}\right]100$ [44]

Volume percent of reinforcement $(\%) = v_r = \left[\dfrac{m_f}{m_i}\right]100 \times \dfrac{\rho_c}{\rho_r}$ [45]

Weight percent of matrix $(\%) = w_m = \left[\dfrac{m_i - m_f}{m_i}\right]100$ [46]

Volume percent of matrix $(\%) = v_m = \left[\dfrac{m_i - m_f}{m_i}\right] \times \dfrac{\rho_c}{\rho_m} \times 100$ [47]

Void volume percent $(\%) = v_v = 100(v_r + v_m)$ [48]

Note: k is a constant which depends on the room temperature recorded during the experiment and the value was taken from the standard density chart.

4 RESULTS AND DISCUSSION

4.1 Introduction

This chapter summarises the results and analyses of the data obtained from the tensile testing of 2400 Tex E-glass fibre bundles. The initial discussion considers the tensile strengths of as-received E-glass fibre bundles at five gauge lengths. A comparison is then made with spread 2400 Tex E-glass at the corresponding gauge lengths. The rationale for inspecting the effect of spreading the fibres were: (i) it was noted that during the end-tabbing stage, the process of impregnating the bundle with the Scotch Weld 9323 resin (3M, UK) and the subsequent application of lateral pressure during curing (at room temperature) results in an average increase in the width from the as-received value of 6-8 mm to 16-17 mm; (ii) since this project was concerned with the effect of specified treatment on the tensile strength of E-glass fibre bundles, solvent extraction was used as a method to remove the acetone-soluble fraction of the binder (without any agitation at room temperature). It was noted that the binder distribution was variable in a commercial E-glass and spreading the fibres was shown by Wait to result in partial removal of the binder by mechanical means (Wait, 2016). Hence, the effect of spreading the filaments on the tensile strength was studied and compared with the as-received datasets at the appropriate gauge lengths. Since a

minimum of thirty samples were tested per batch, per class of treatment and statistical analyses were undertaken, a comparison was made with published literature.

The second section of this chapter considers the effect of specified treatments of 2400 Tex E-glass on the ultimate tensile strength, Young's modulus and failure strain of the corresponding composite.

4.2 Tensile Strength of As-received and Spread 2400 Tex E-glass Fibre Bundles

Figure 4.1 shows a summary of the average tensile strength of thirty individual fibre bundles per batch, tested at gauge lengths corresponding to 50, 80, 100, 150 and 200 mm for the as-received and spread fibre bundles.

At first sight, a number of general conclusions can be reached on inspecting Figure 4.1.

(i) The average tensile strength of the spread fibres is marginally higher. This was unexpected as intuitively, the mechanical-based method of removing the binder, as described in Section 3.3.2 would be expected to decrease the tensile properties due to unintentional damage during the spreading process. Possible reasons for these observed apparent higher tensile properties after spreading are as follows:

(a) spreading the filament in the bundle is known to straighten some of the intrinsically meandering filaments thus it is speculated that a greater proportion of the filaments are loaded axially;

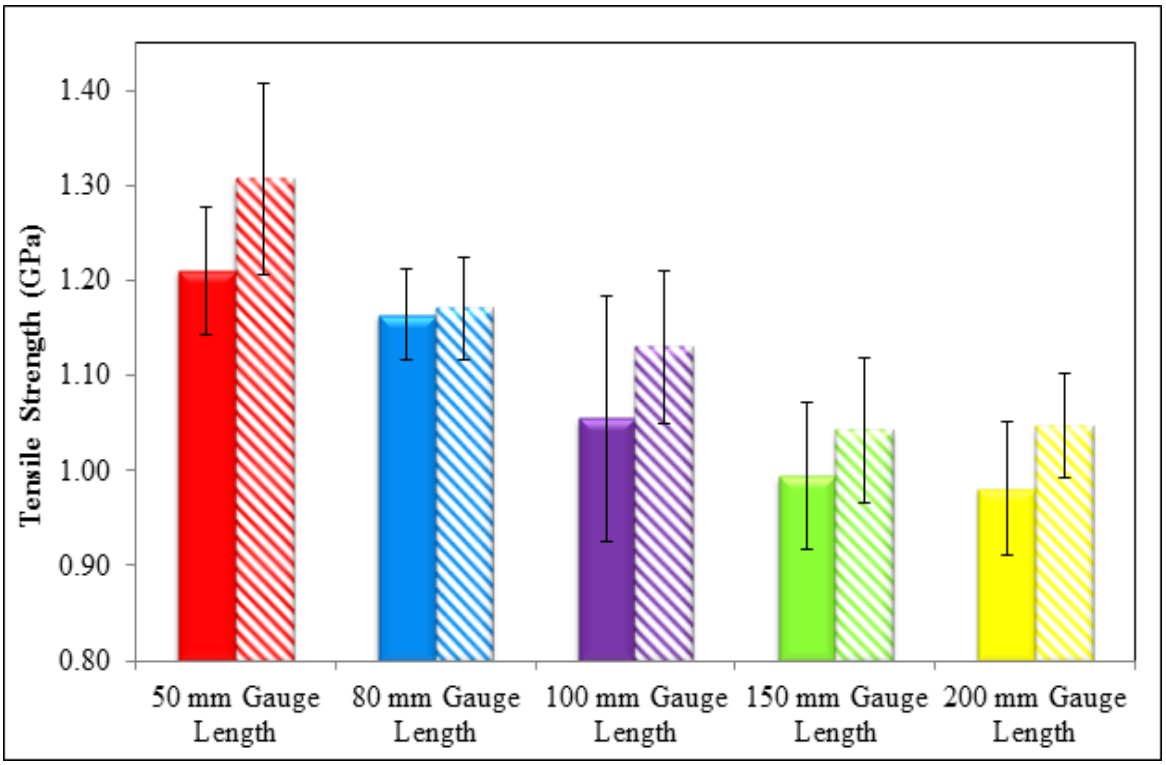

Figure 4.1 Histogram of average tensile strength of as-received (solid bars) and spread (shaded bars) E-glass fibre bundles tested at gauge lengths corresponding to 50, 80, 100, 150 and 200 mm.

(b) the process of spreading the filaments is known to remove some of the binder, especially in areas where the binder content was abnormally high (Wait, 2016). Therefore, it is possible that when using spread fibres, there is a greater probability of the filaments acting independently when loaded in tension; as opposed to loading a cluster due to the presence of excess binder. As will be seen in Section 4.1.1.3, the acoustic emission data during tensile testing resulted in a lower number of "hits"; this is interpreted as a reduction in filament-to-filament interaction and the possible reloading of fractured filaments by the

meandering and off-axis fibres and the presence of clusters of filaments in areas of high binder content. Furthermore, the relative slopes of the stress/strain traces (Section 4.1.1.1) for the spread fibre bundles were higher. This supports the view that the spread bundles may have contained a higher proportion of aligned filaments.

(c) It is reasonable to assume that the significance of meandering fibres will be lower as the gauge length is lowered. This may account, in part, for the superior apparent tensile strength of the spread 50 mm gauge length fibre samples.

(d) It is proposed that in the case of the spread fibres, the impregnation within the end-tab region may be more effective and that the subsequent loading of the filaments may have been more efficient.

(ii) The average tensile strength decreases as the gauge length increases for the as-received and the spread bundles. However, on inspecting the as-received dataset, it suggests that doubling the gauge length from 50 to 100 mm is seen to decrease the apparent tensile strength at 0.0032 GPa/mm; doubling the gauge length from 100 to 200 mm showed a tensile strength decrease at 0.0007 GPa/mm. The corresponding strength decrease as a function of the above-mentioned gauge lengths for the spread fibres is 0.0036 and 0.0008 GPa/mm respectively. In order to assess the statistical significance of these datasets, further analysis was undertaken to assess if the above-mentioned pairs of datasets were from the same population.

(iii) The scatter observed in the tensile strength for the 100 mm gauge length as-received 2400 Tex E-glass is significant when compared to the other datasets. Time constraints did not permit a new batch of thirty samples of the 100 mm gauge length samples to be re-tested but due consideration was given to possible reasons that may have contributed to the high degree of scatter. The most plausible reason for the abnormally high scatter in the 100 mm gauge length was the fact that it was the first set that was evaluated.

The procedures and protocols for handling, end-tabbing and storing the samples had to be developed. The experimental procedures for end-tabbing had to be developed by trial-and-error; retaining the original fibre architecture within the end-tab region was not possible as the resin system that was used had a relatively high viscosity (10-25 Pa.s at room temperature). Hence, in order to impregnate the centre of the as-received fibre bundle, it was necessary to massage the resin system into the bundle; this resulted in some unavoidable spreading. Failure at the leading-edge of the end-tab was unlikely as it was deburred, cleaned, dried, primed with a thin layer of the resin system and cured. The primed end-tabs were used in a secondary bonding operation when the fibre bundle was bonded to the end-tab. Ideally a capstan-type loading fixture should have been used but this was not available at the time of testing. Hence, elaborate measures were taken to ensure that the end-tabbing process did not damage the fibres.

Figure 4.2(a) shows the appearance of a typical as-received 2400 Tex E-glass fibre bundle. The coded items on the micrograph are as follows:

Region A-represents regions where significant variation in the trajectory of the filaments is observed. This undulating trajectory is a consequence of the winding pattern used during production where the filaments are wound on to a mandrel as described in the literature review. Since an "angle winding" sequence is used (as opposed to hoop winding), the partially wet bundles takes an undulating profile as the layers are built up. This pattern is "set" during the drying phase where the moisture is removed. Region-B shows partial localised charging on the micrograph and this was correlated in some instances to regions where the binder content was higher. Region – C illustrates areas where the fibre-to-fibre spacing was variable. The arrow shows some filaments meandering.

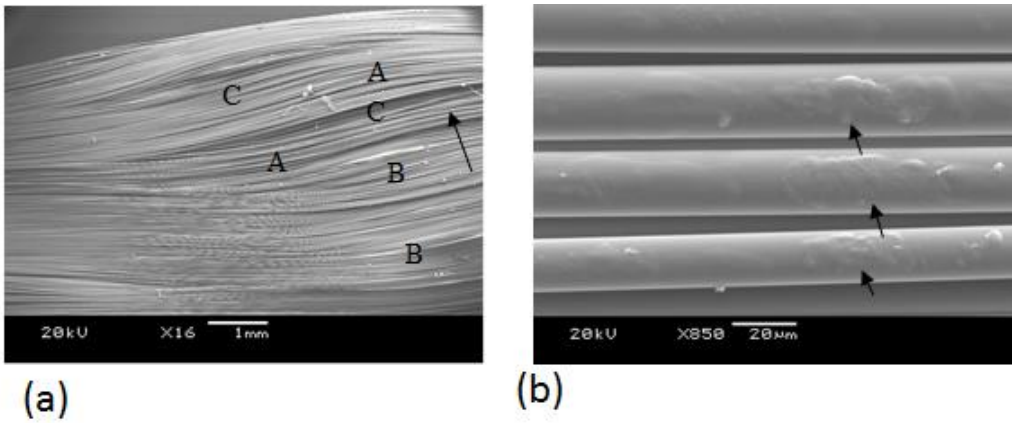

Figure 4.2 (a) Micrograph of a section of as-received 2400 Tex E-glass bundle showing the general filament trajectory. (b) Micrograph illustrating the variability in the binder distribution on the surface of the filaments (Murray, 2016).

Figure 4.2(b) shows two key features. The arrows indicate regions on the filaments where an uneven binder distribution is observed. The variation in the diameter of the individual filaments is also apparent.

Wait (Wait, 2016) undertook a detailed study on the distribution of binders in two classes of 2400 Tex E-glass fibres (the identity of the suppliers were withheld) and found significant variations – see Figure 4.3.

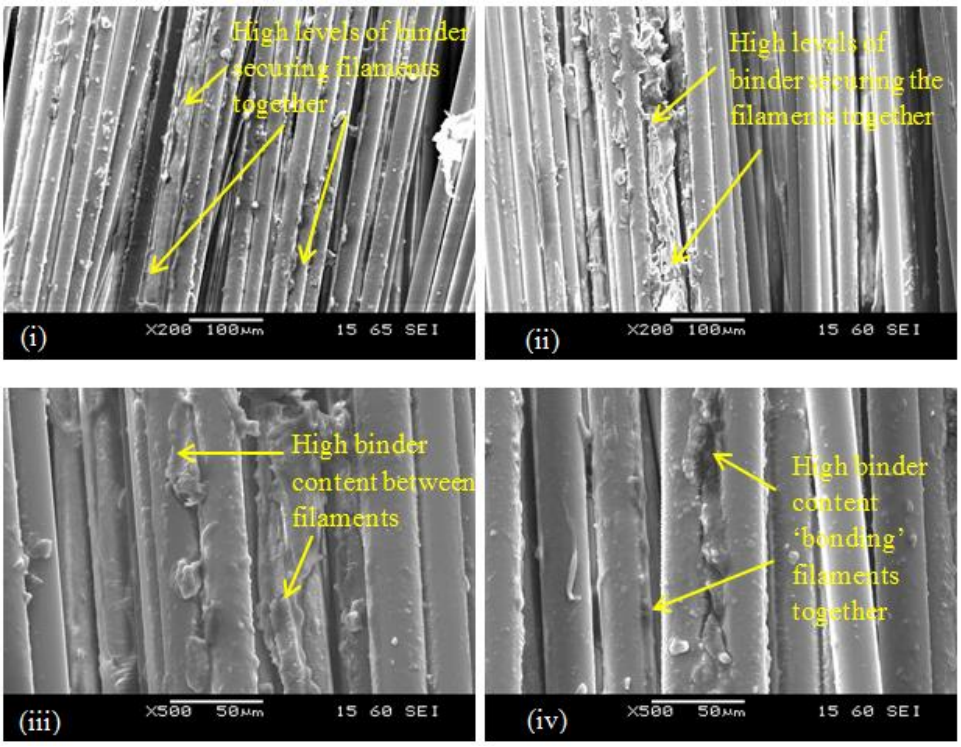

Figure 4.3 Micrographs reported by Wait (Wait, 2016) showing the variation in the binder distribution for a 2400 Tex E-glass fibre bundle from an undisclosed commercial supplier.

The conclusions that can be reached after inspecting these micrographs are:

(i) Due consideration needs to be paid to the relative binder distribution in the tensile test specimens. (ii) The factors that can give rise to variability in the tensile strength of E-glass fibre bundles include: (a) variability in the fibre diameter; (b) clusters of filaments held together by a relatively high volume fraction of the binder, possible enabling load-transfer when filaments break within the cluster; (c) the meandering filaments enabling load-transfer when they fracture; (d) variability in the axial loading of the filaments due to the undulating topology of the bundle; (e) the combination of the above-mentioned factors being present within a specified section of a gauge length; (f) the intrinsic flaw distribution in the filaments and the extrinsic unintentional damage caused during sample preparation and testing.

In addition to the above-mentioned issues, if operator-dependence on sample preparation and testing is considered, it is not surprising that inter-laboratory comparison will be difficult

4.2.1 Statistical Analyses

The statistical analyses were performed to investigate the influences of gauge length on the tensile strength of the E-glass fibre bundles. The F-test statistical analysis was conducted on the five sets of gauge lengths. The P-value was used to accept or reject the hypothesis of a relationship between the gauge length and the ultimate tensile strength. “P” is defined as

the probability of obtaining a result equal to or more than what was actually observed when null hypothesis (H_0) of a study is true, in other words:

a. To accept the hypothesis that the different gauge lengths have no influence on the tensile strength of E-glass fibre bundles, the value of P has to be equal to or higher than 0.05 with a confidence level of 95%.
b. To reject the hypothesis that the different gauge lengths will have an influence on the tensile strength of E-glass fibre bundle, the value of P has to be lower than 0.05

The P-value was calculated via an open-source statistical software package: 'QuickCalcs' (GraphPad Software, Inc. by Dr. Harvey Motulsky. http://graphpad.com/quickcalcs/PValue1.cfm). The value of F_0 (as shown in Table 4.1) for the full set of gauge lengths was calculated using Equation 4.1:

$$F_0 = \frac{SS_{Treatment}/(a=1)}{SS_E/(N-a)} \qquad [4.1]$$

$$SS_T = \sum_{i=1}^{a}\sum_{j=1}^{n} y_{ij}^2 - \frac{y_{ij}^2}{N} \qquad [4.2]$$

$$SS_{Treatment} = \frac{1}{n}\sum_{i=1}^{a} y_i^2 - \frac{y^2}{N} \qquad [4.3]$$

$$SS_E = SS_T - SS_{Treatment} \qquad [4.4]$$

where:

SS_T – the total corrected sum of squares.

$SS_{Treatment}$ – the sum of squares due to treatment.

SS_E – the sum of squares due to error.

With reference to Table 4.1, the values of F_0, the degrees of freedom for the numerator (DFn) were calculated using Equation 4.5:

DFn = Number of gauge lengths – 1 [4.5]

The degrees of freedom for the denominator (DFd) were calculated using Equation 4.6:

DFd = (Number of gauge lengths * Number of test specimens per gauge length) – (Number of gauge lengths) [4.6]

The values in Equations [4.1], [4.5] and [4.6] were used via the QuickCalcs program to calculate the P-Value. A summary of the F-test data for the as-received and spread fibre bundles is presented in Table 4.1. On inspecting Table 4.1, it is seen that the P-values for the as-received and spread fibre bundles are lower than 0.0001. This means that based on the hypothesis mentioned previously, the F-tests are rejected for the as-received and spread fibre bundles. Therefore, the conclusion is that the gauge length has an influence on the tensile strength for the as-receive and spread fibre bundles.

In order to expand the discussion on the influences of the gauge length on the tensile strength of fibre bundles, the T-test was used on selected pairs of gauge lengths. The paired gauge lengths considered were: (i) 50 mm with 100 mm; (ii) 100 mm with 200 mm; and (iii) 150 mm with 200 mm; see Table 4.1. Here, as before, the P-value was used to accept or to reject the hypothesis. The hypothesis will be accepted if the P-value is greater than 0.05. T_0 (as shown in Table 4.1) for the selected pairs was calculated using Equation [4.7].

$$T_0 = \frac{\overline{y_1} - \overline{y_2}}{S_P \sqrt{\frac{1}{n_1} + \frac{1}{n_2}}}. \qquad [4.7]$$

where:

$\overline{y_1}$ and $\overline{y_2}$ = sample mean values.

n_1 and n_2 = sample sizes.

S_p^2 = estimate of the common variance $\sigma_1^2 = \sigma_2^2 = \sigma^2$ computed from:

$$S_P^2 = \frac{(n_1 - 1)S_1^2 + (n_2 - 1)S_2^2}{n_1 + n_2 - 2} \qquad [4.8]$$

Degree of Freedom = Numbers of specimen tested - Number of gauge lengths [4.9]

The P-value was calculated by substituting the relevant values in Equations [4.7] and [4.9] via the open source software, Quickcalc.

With reference to Table 4.1 and the T-test of selected pairs, it is concluded that the gauge lengths up to 150 mm will influence the tensile strength of fibre bundles for the as-received and spread fibres.

Table 4.1 F-test and T-test results for tensile strength of specified gauge lengths for the as-received-1 (2 mm/min.) and spread E-glass fibre bundles.

No.	Comparison of Gauge Lengths	Statistical Test Type	F_0 or T_0	Degree of Freedom	P-Value	Conclusion
F-test and T-test for as-received E-glass fibre bundles.						
1	All gauge lengths for as-received fibres	F-Test	36.087	DFn =4 DFd = 145	0.0001	Statistically significant
2	50 mm versus 100 mm gauge length	T-test	5.865	58	0.0001	Statistically significant
3	100 mm versus 200 mm gauge length	T-test	2.778	58	0.0074	Statistically significant
4	150 mm versus 200 mm gauge length	T-test	0.721	58	0.4738	Not statistically significant
F-test and T-test for spread E-glass fibre bundles.						
5	All gauge lengths for spread fibres	F-Test	84.248	DFn =4 DFd = 145	.0001	Statistically significant
6	50 mm versus 100 mm gauge length	T-test	7.570	58	0.0001	Statistically significant
8	100 mm versus 200 mm gauge length	T-test	4.710	58	0.0001	Statistically significant
9	150 mm versus 200 mm gauge length	T-test	-0.220	58	0.8267	Not statistically significant
T-test of tensile strength for as-received and spread E-glass fibre bundles.						
10	50 mm gauge length (as-received versus spread fibres bundles)	T-test	-4.368	58	0.0001	Statistically significant
11	80 mm gauge length (as-received versus spread fibres bundles)	T-test	-0.471	58	0.6396	Not statistically significant
12	100 mm gauge length (as-received versus spread fibres bundles)	T-test	-2.710	58	0.0088	Statistically significant
13	150 mm gauge length (as-received versus spread fibres bundles)	T-test	-2.472	58	0.0164	Statistically significant
14	200 mm gauge length (as-received versus spread fibres bundles)	T-test	-4.079	58	0.0001	Statistically significant

In Table 4.1, the T-tests were also conducted to investigate the influence of spreading on the tensile strength of the fibre bundle for similar gauge lengths.

Figure 4.4 shows a comparison of the tensile strength of the as-received and spread fibre bundles with a gauge length of 100 mm along with a comparison with the published data. Possible reasons for the apparent higher tensile strength and the reduced scatter for spread E-glass fibres were discussed previously. The average tensile strength for 2400 Tex E-glass reported by Hill and Okoroafor (1995) for a 70 mm gauge length (0.97 GPa) is lower than that obtained in the current study. However, R'Mili *et al.* (2008) reported an average tensile strength (0.74 GPa) for 100 gauge length that is lower than published by Hill and Okoroafor (1995). These authors presented limited data on the standard deviation and the number of specimens tested.

In the current study, thirty individual test specimens were tested for each gauge length using the previously described method. The cross-head displacement rates used in the current study was 0.1 and 2 mm/minute. The initial experiments were conducted using a cross-head displacement of 2 mm/minute. However, for all subsequent tests, this was changed to 0.1 mm/minute primarily to aid the acquisition of discrete AE data.

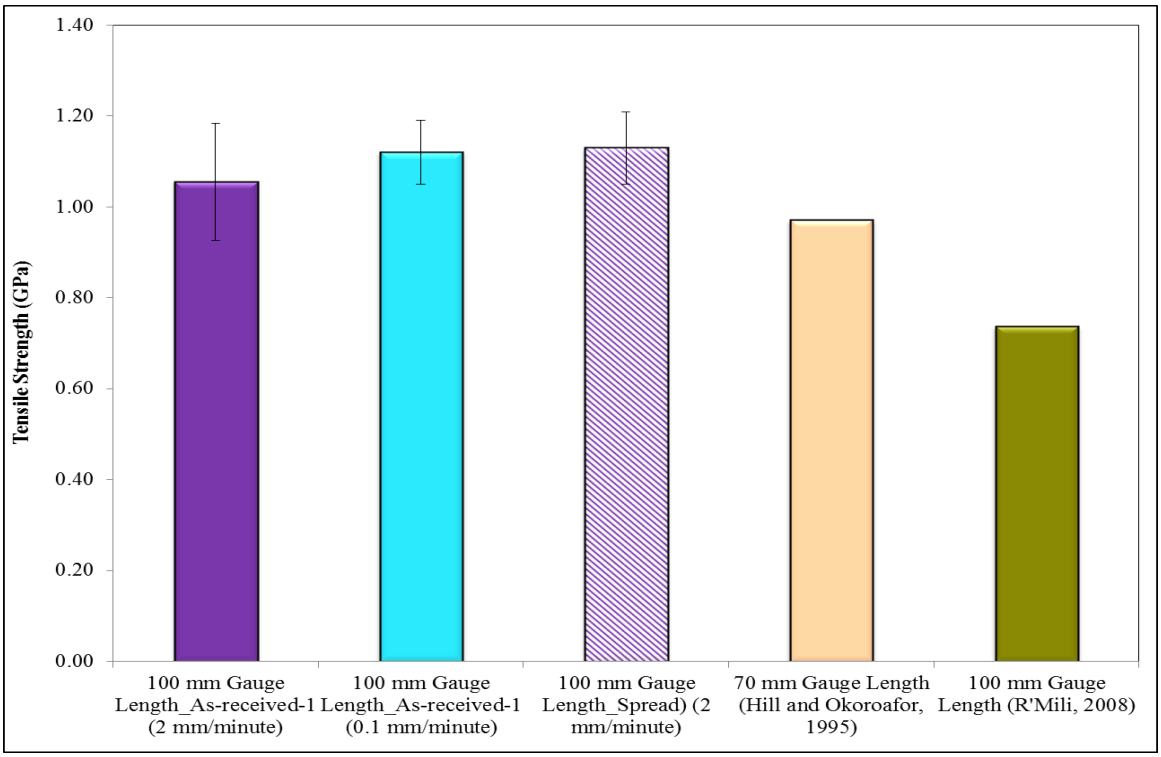

Figure 4.4 Comparison of tensile strength of 100 mm gauge length for the as-received and spread 2400 Tex fibre bundles along with published data for 2400 Tex E-glass.

In the current study, changing the rate of cross-head displacement from 2 to 0.1 mm/minute did not have any significant effect on the tensile failure strength of the 2400 Tex E-glass bundles tested in this programme. However, on comparing the scatter in the tensile strength datasets for the 0.1 and 2.0 mm/minute loading rate, the former is lower. It is proposed that this may be due to the increased loading rate, however, additional different loading rates need to be investigated prior to drawing any conclusions. Another possible reason for the higher scatter in the 2 mm/minute loading rate dataset may be due to the fact that it

represented the first series of experiments involving the fibre bundle test. The procedures for preparing the samples, end-tabbing and storing the samples until they were required for tensile testing had to be developed. Furthermore, the same applied to aligning and clamping the sample on the jaws of the mechanical test machine. It is conceivable that the scatter in the 2.0 mm/minute may have been due to the fact that it was the first set of samples tested where the various procedures were being optimised.

4.2.2 Weibull Analysis

The two-parameter Weibull distribution analysis was used to analyse the tensile strength data at five gauge lengths investigated Table 4.2 lists the Weibull shape (m) and the scale (σ_0) parameters for the as-received and spread 2400 Tex E-glass fibre bundles. With reference to the 100 mm gauge length samples that were tested at 2 mm/minute, the shape parameter was uncharacteristically low; possible reasons for this were discussed in the previous section. As stated previously, the cross-head displacement rate was changed to 0.1 mm/minute to accommodate AE data acquisition during tensile testing. As before, 30 individual specimens were used at the lower rate of loading. The corresponding Weibull parameters are summarised in Table 4.2 where it can be seen that shape parameter is 18.769. This is in line with the other dataset as a function of gauge length. This findings support the explanation made previously where it was stated that the 100 mm gauge length tested at 2 mm/minute represented the first series of experiments where the protocol was being developed.

Table 4.2 Weibull shape (m) and scale (σ_0) parameters for the as-received and spread 2400 Tex E-glass fibre bundles.

Gauge Length (mm)	As-received 2400 Tex E-glass fibre bundles		Spread 2400 Tex E-glass fibre bundles	
	Shape Parameter (m)	Scale Parameter (σ_0)	Shape Parameter (m)	Scale Parameter (σ_0)
50	21. 052	1.241	14. 629	1.352
80	28.954	1.186	24.888	1.196
100 (2 mm/minute)	9.409	1.110	16.621	1.165
100 (0.1 mm/minute)	18.769	1.148	-	-
150	14.426	1.030	15.78	1.078
200	16.339	1.012	21.874	1.072

Figure 4.5 shows the scatter plot for the Weibull modulus values for the as-received and spread fibre bundles along with that reported in the literature for E-glass fibre bundles. The dashed lines in Figure 4.3 represents the nominal Weibull shape parameter (m) value for synthetic fibres as proposed by Hull and Clyne (Hull and Clyne, 1996). The Weibull modulus (m) is often linked to the scatter in the data and it is generally assumed to be associated with the flaw distribution. The higher the Weibull modulus, the lower the scatter in the data (Thomason *et al.*, 2014b; Thomason, 2013; Lund, 2010; R'Mili *et al.*, 2008). Hull and Clyne (Hull and Clyne, 1996) stated that ceramics generally have Weibull modulus values in the range 2-15; in other words, significant variation in the tensile strength is to be expected. In the case of the fibre bundle test, the scatter in the data are likely to be a combination of the intrinsic flaw distribution in fibres and other issues such as: (i) the alignment of the fibres within the bundles; (ii) fibre misalignment caused by end-tabbing, (iii) fibre-to-fibre contact during tensile loading; (iv) uneven loading due to misalignment in

the loading of the specimen in the jaws of the mechanical test machine; (iv) unsymmetrical end-tab pairs; in other words, issues relating to experimentally-induced variability; and (v) the binder distribution within specified lengths obtained from the creel.

With reference to Figure 4.5, all but one of the single-filament and the fibre bundle tensile test are seen to fall within the banding between 2-15 for the shape parameter. There is a cluster between 15 – 20 for the shape parameter for the as-received and spread 2400 Tex E-glass fibres, and a cluster between 20 - 28. These values are significantly higher than those reported in the literature for the single bundle tensile testing for the as-received E-glass. At the time of writing, the author could not offer an explanation for the higher shape parameters obtained other than to suggest that this is influenced by the careful sample preparation methods used. Further research is necessary, using a large sample population, to assess the Weibull shape parameter for commercial E-glass.

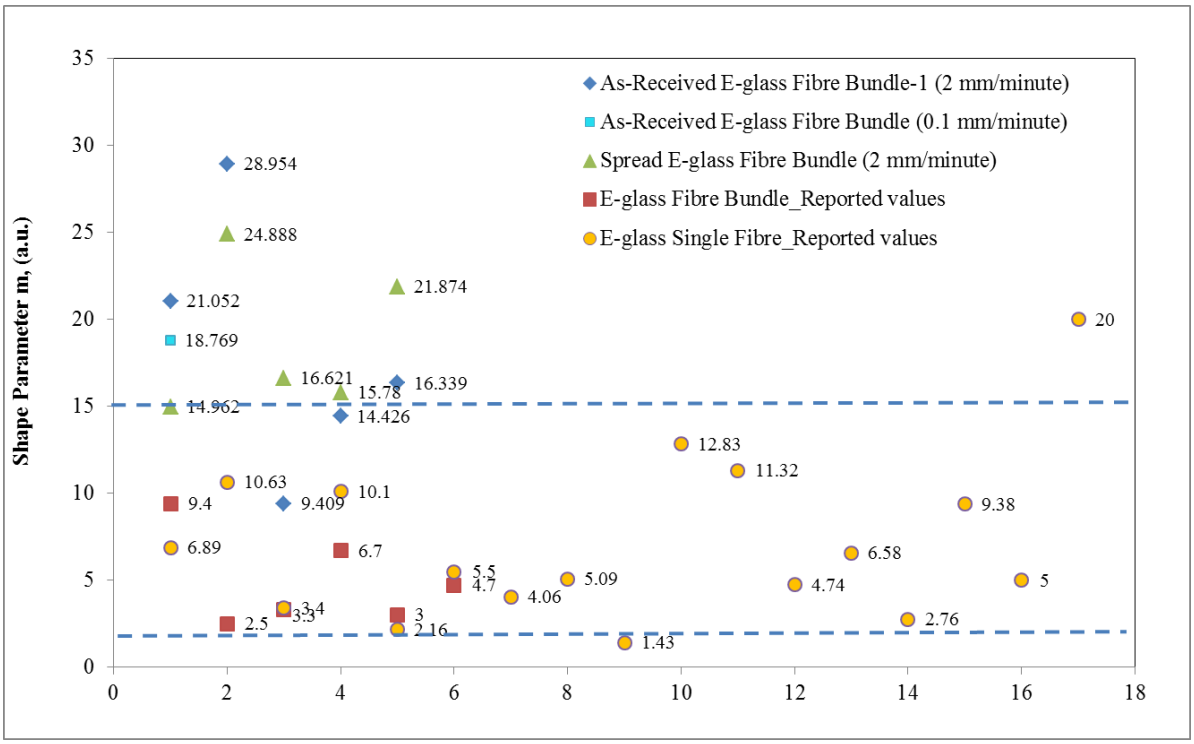

Figure 4.5 Weibull shape parameters for 100 mm gauge length 2400 Tex E-glass: (i) current as-received fibre bundle-1 (2 mm/minute) study data - solid diamond; (ii) Spread fibre bundle – current study data – solid triangle (iii) Reported fibre bundle data – solid square.

Figure 4.6 shows the Weibull scale parameters as a function of gauge length for the 2400 Tex E-glass fibre bundles. In all the cases, the dataset for the spread fibre bundles was higher than that observed for the as-received bundles; this is consistent with the data in Figure 4.1. It is noted that the observed increase in the scale parameter for the 80 mm gauge length spread bundles is only marginal.

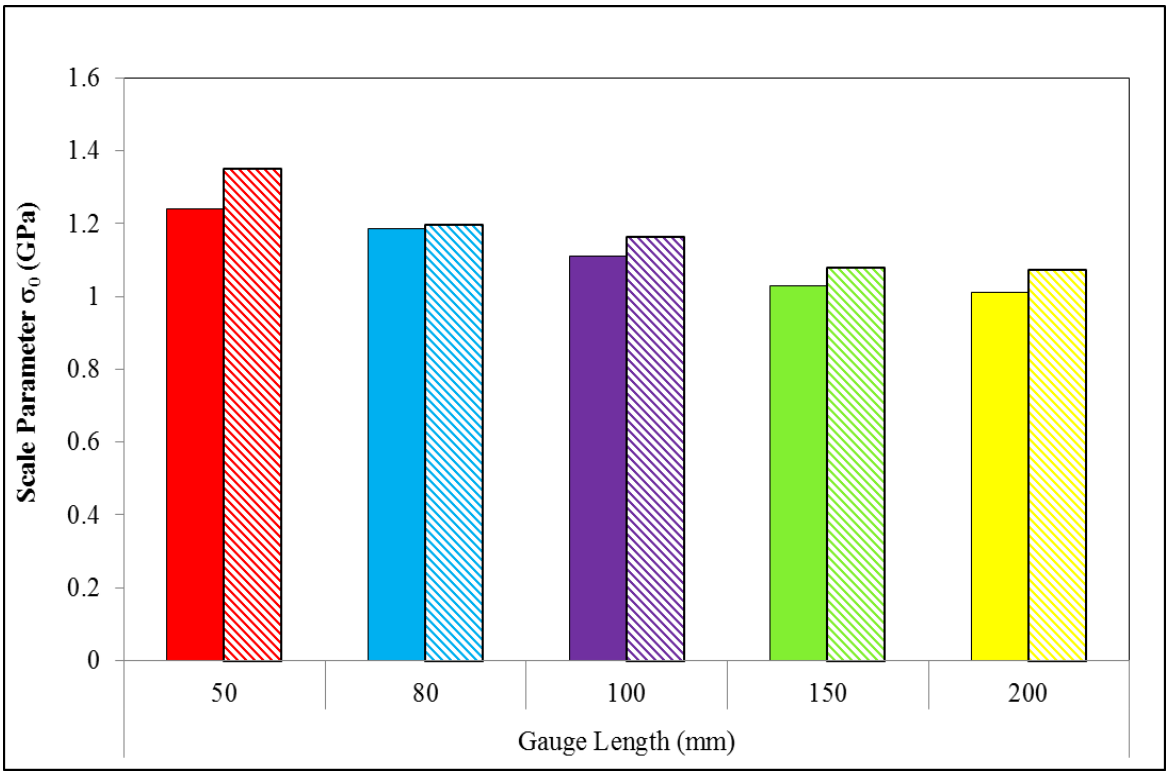

Figure 4.6 Representation of the Weibull scale parameters for the as-received and spread E-glass fibre bundles as a function of the gauge length.

The Weibull scale parameter (σ_0) is the tensile strength of the fibre bundle with a probability of survival ($P(\sigma)$) at 63.2% in the Weibull survival plot (see Figures 4.7 (a and b)). The scale parameter is seen to decrease marginally as the gauge length increases. Possible reasons for this include:

(a) a higher probability of encountering flaws as the gauge length is increased (as discussed in the literature review section); (b) the factors mentioned previously such as meandering fibres leading to entanglements and uneven tensile loading; (c) binder content and

distribution leading to localised load-transfer where each filament is no longer acting independently; (d) better load-transfer efficiency within the end-tab for the spread fibre bundles; (e) the variable filament diameter.

Observations carried out by the author and other colleagues of the Sensors and Composites Research Group members (University of Birmingham) suggest that the uniformity of the binder distribution and the width of the bundle were dependent on its position within the creel. Furthermore, observation made by the current author suggests that the integrity of the bundle can be influenced by the manner in which it was stored. In other words, the top and bottom of the creel in some instances displayed some evidence of damage caused by handling. Hence, considering the various factors discussed, the observed variability inter and intra-laboratory data is to be expected.

The unexpected finding in this study was the apparent higher tensile strength for the spread fibres at the five gauge lengths investigated. The reasons for this were discussed previously.

Figures 4.7 and 4.8 show the Weibull survival probability plots for the as-received and spread E-glass fibre bundles respectively. The survival probability is equal to one subtracted from the failure probability $P(\sigma)$. The filaments in the fibre bundle will not fracture when the survival probability is equal to 1. In Figure 4.7, the relative slopes for the as-received E-glass fibre bundles at 50, 150 and 200 gauge lengths are similar. The 80 mm gauge length dataset exhibits a marginally steeper slope but the 100 gauge length dataset is abnormal.

The most probable reason for this was discussed previously – it was the first set that was tested and behaviour of this dataset may be reflective of sample preparation, storage conditions and unintentional artefacts introduce during loading and tensile testing.

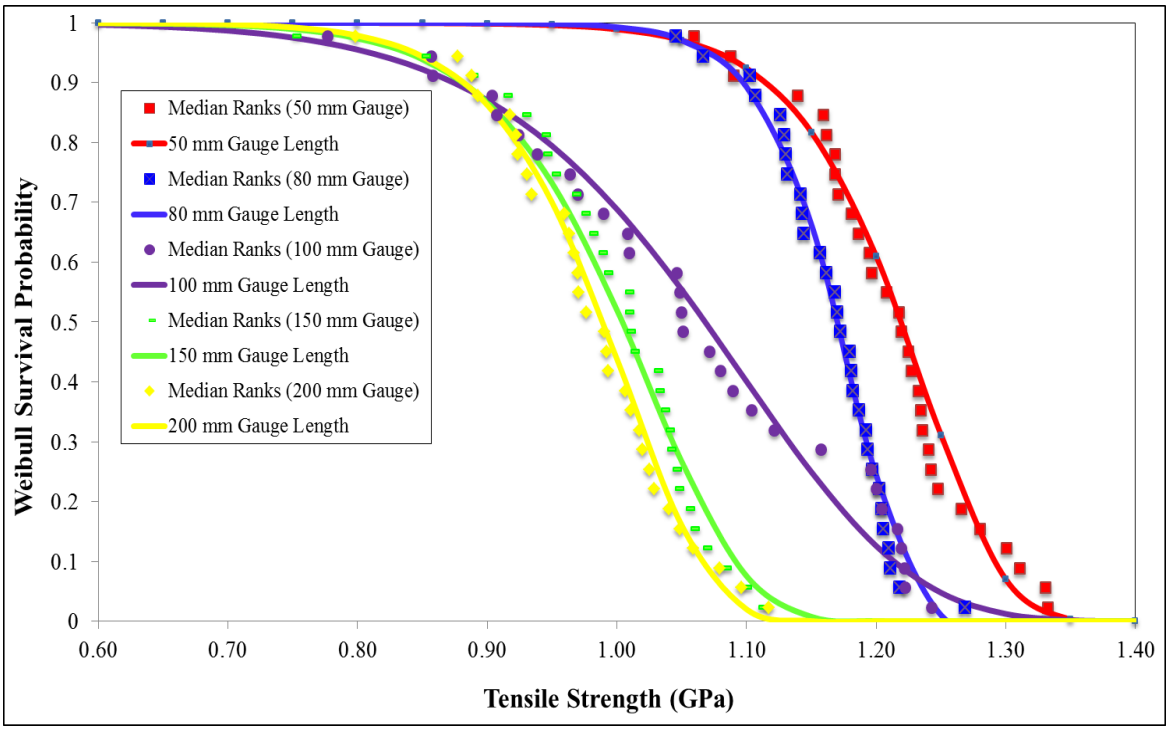

Figure 4.7 Weibull survival probability plot for the tensile strength of as-received 2400 Tex E-glass fibre bundles.

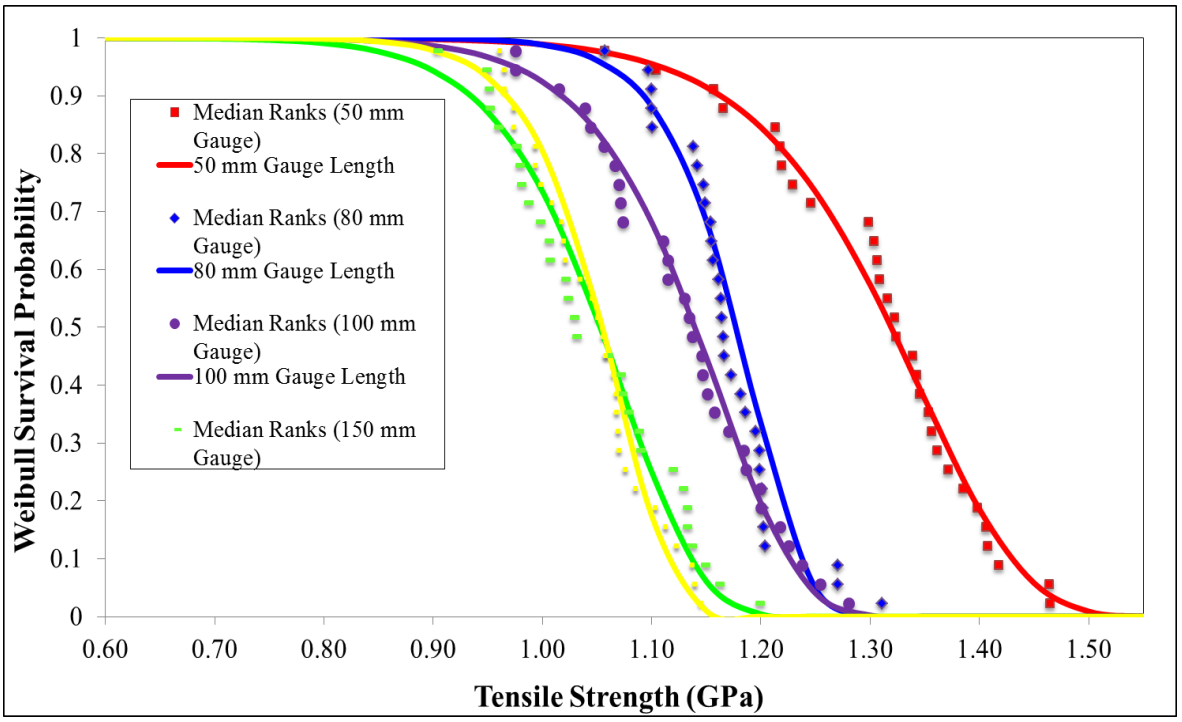

Figure 4.8 Weibull survival probability plot for the tensile strength of spread as-received 2400 Tex E-glass fibre bundles.

4.2.3 Tensile Stress/Strain Behaviour of E-glass Fibre Bundle

Typical stress/strain traces for the as-received bundle are shown in Figures 4.9 and 4.10 respectively.

Figure 4.9 shows typical stress/strain curves for the as-received fibre bundlees at the five gauge lengths. With the exception of 50 mm gauge length, the slope for the 80, 100, 150 and 200 mm gauge length are similar. The significantly lower slope observed for the 50 mm gauge length cannot be explained. However, this trend with short gauge length (50 mm and

below) giving lower slope has been observed for T700 (Murray, 2016). It is speculated that, this may be due to the compliance of the machine not being taken into consideration. Figure 4.10 shows typical stress/strain traces for the 2400 Tex E-glass bundles where the highest tensile strength data from each dataset is represented (as opposed to the lowest shown previuosly in Figure 4.9.

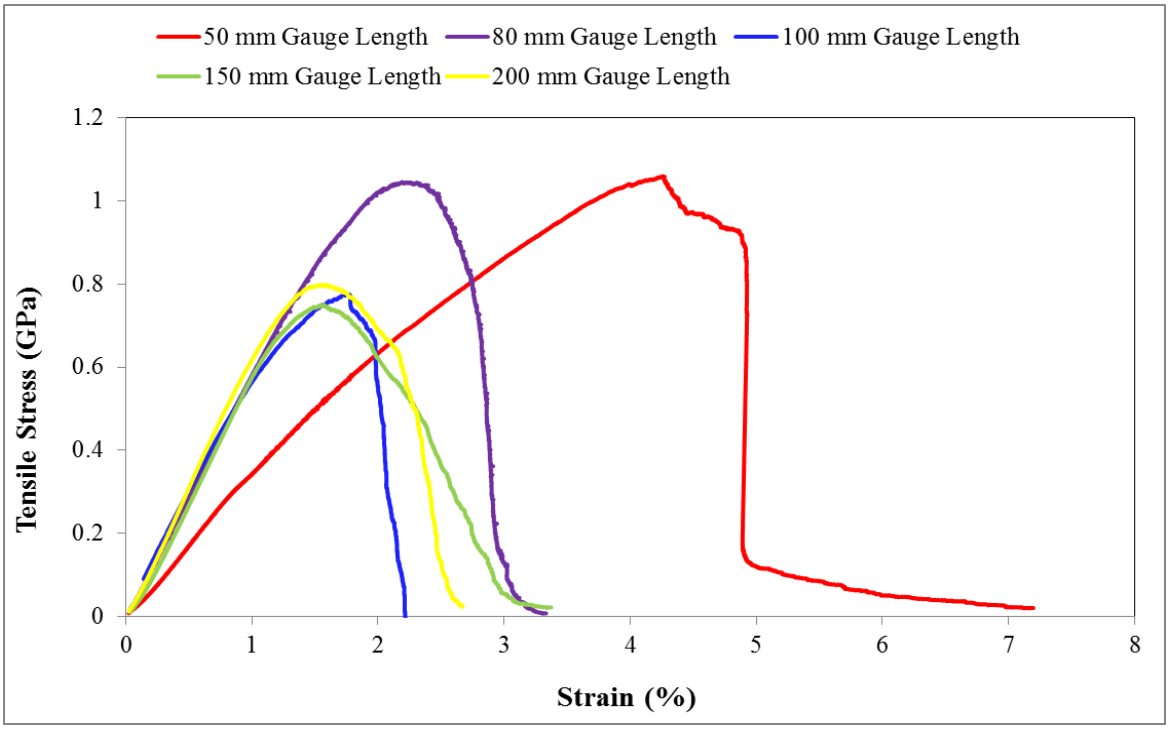

Figure 4.9 Stress/strain plots for as-received 2400 Tex E-glass fibre bundles as a function of gauge length. This dataset represent the lowest tensile strengths per gauge length.

Inspecting the data shown in Figure 4.10, it can be seen that the 50 mm gauge length is once again different to that observed for the 80, 100, 150 and 200 mm gauge lengths. A possible reason for this discrepancy was discussed previously. The slope for the 200 mm gauge length is marginally higher when compared to the 80, 100 and 150 mm gauge lengths.

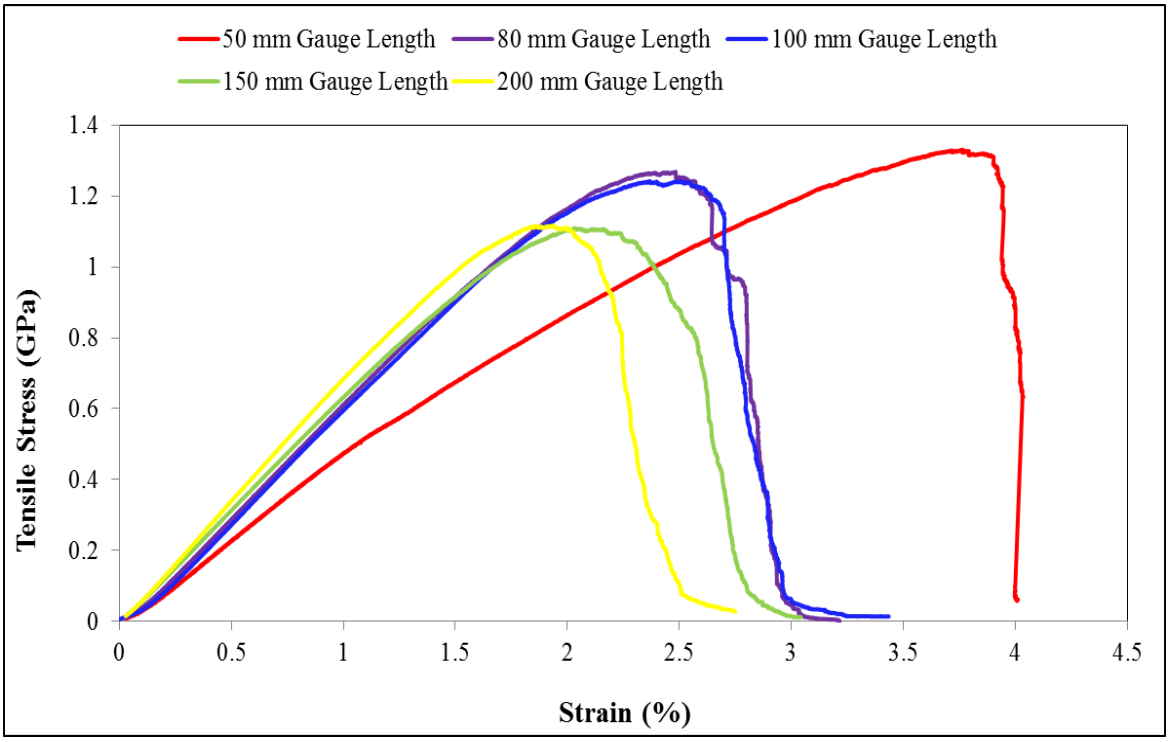

Figure 4.10 Stress/strain traces for the as-received 2400 Tex E-glass fibres bundles as a function of gauge length. Here the highest tensile data are presented.

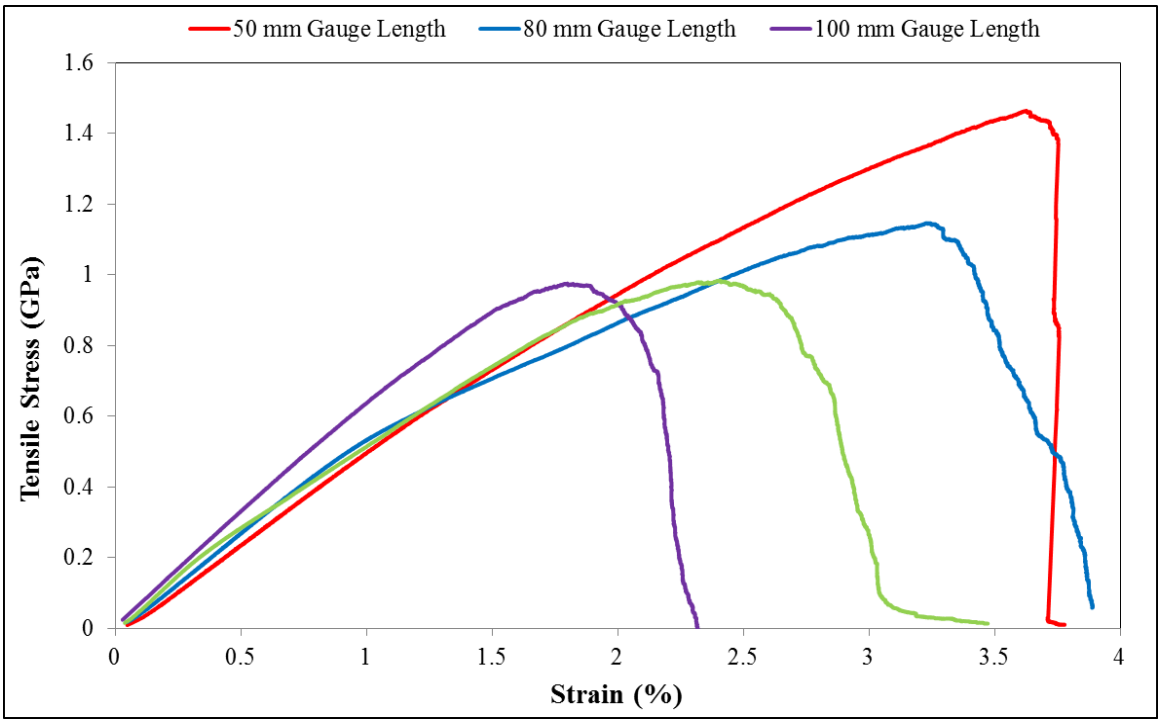

Figure 4.11 Stress/strain traces for the spread 2400 Tex E-glass fibres as a function of the gauge length. Here the highest tensile strengths obtained for each of the gauge lengths is presented.

Unlike the previous datasets for the as-received E-glass fibre bundles, the spread bundles show a somewhat different behaviour (see Figures 4.11 and 4.12). With reference to Figure 4.11, the slopes for the 100 and 200 gauge length are higher than that observed for the other gauge lengths. However, in this instance, the slope for the 50 mm gauge length is similar to that observed for the 80 and 150 mm gauge lengths. Figure 4.12 shows stress/strain traces for the spread 2400 Tex E-glass where the lowest tensile strengths are represented at each of

the gauge lengths tested. The plotted result of the 50 mm gauge length tensile specimens shows that the slope for this gauge length is once again lower.

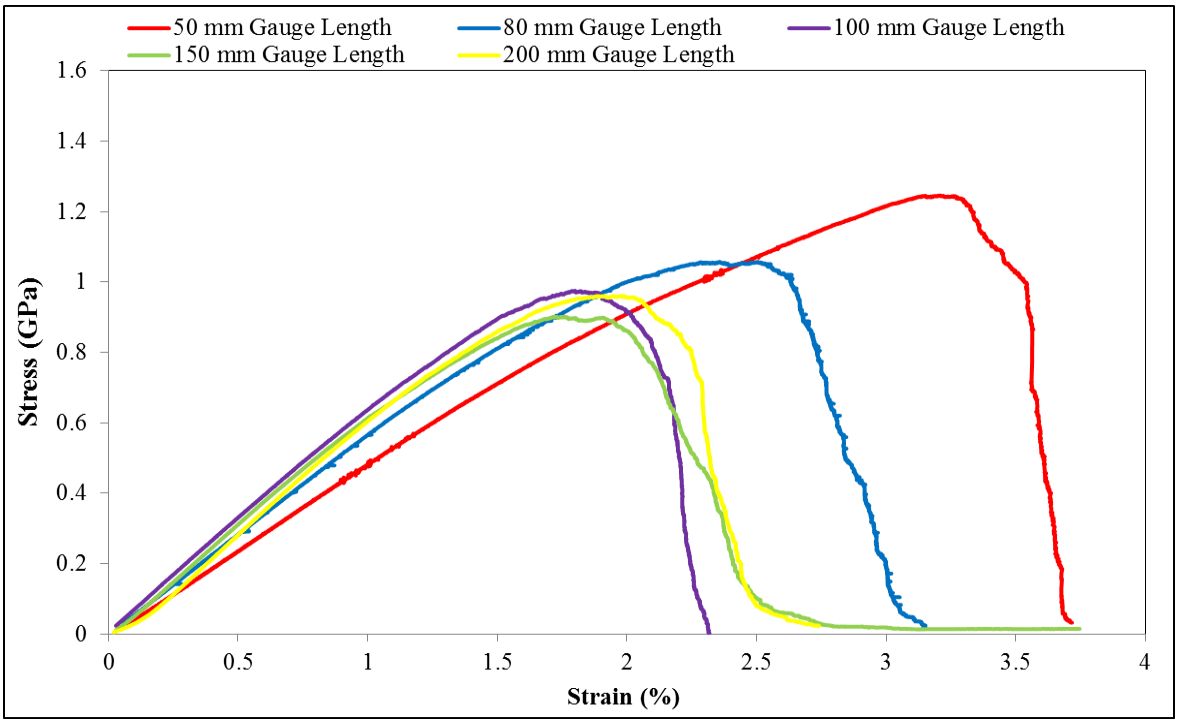

Figure 4.12 Stress/strain traces for the spread 2400 Tex E-glass bundles as a function of gauge length where the lowest tensile strengths per data set have been plotted.

A summary of relative slopes for the as-received and spread samples at all the gauge lengths investigated are summarised in Figure 4.13.

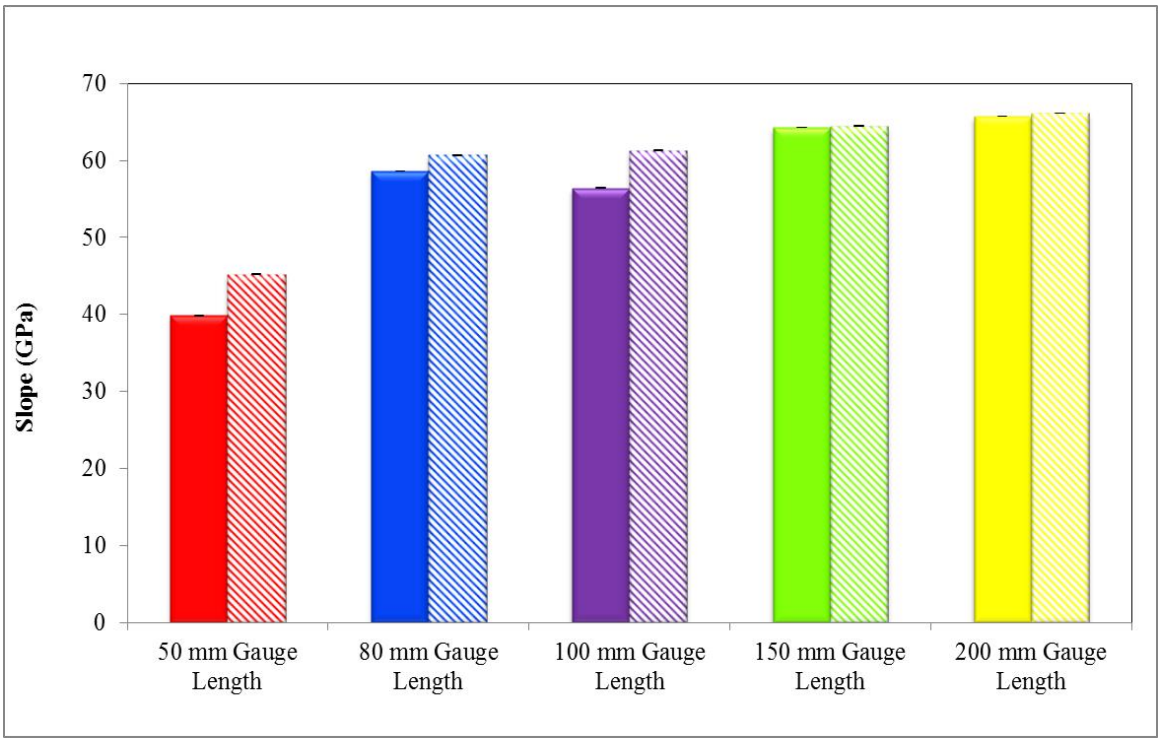

Figure 4.13 Averages of the slopes obtained from all the stress/strain traces at the various gauge lengths.

In Figure 4.13, the relative slopes of the stress/strain traces for the spread fibre bundles are marginally higher than their as-received counterparts for gauge lengths corresponding to 50, 80 and 100 mm. The slopes for the 150 and 200 mm gauge lengths were marginally higher that the other gauge lengths, however, the slopes were similar for the as-received and spread cases.

The trends in the tensile strength for the as-received and spread datasets were discussed previously. A commentary on the stress/strain traces is not as straightforward because: (i) the 50 mm gauge length for the as-received E-glass bundle showed an anomalous behaviour

with regard to the slope. However, this discrepancy was not observed with the spread E-glass bundles. (ii) The slopes for the 50, 80 and 100 mm gauge lengths were higher for the spread bundles when compared to the as-received dataset. However, higher slopes were observed for the 150 and 200 mm gauge lengths but in this instance, the as-received and spread datasets displayed similar slopes. Thus, it is difficult to derive any definite conclusion. The possible options to consider are: (i) significant variability in the 2400 Tex E-glass bundles as a function of position within the creel. Regrettably, the position of the samples from within the creel was not recorded as it was not known at the time that this could have an influence on the binder; (ii) variability in the degree of manually-assisted spreading. In other words, the distribution of the filaments, across the width of the specimen was not always uniform; (iii) unintentional damage caused during spreading but this was not evident from the tensile strength data. However, unintentional damage caused during sample preparation (end-tabbing), storage and tensile testing cannot be discounted.

4.2.4 Acoustic Emission Analysis

A piezo-electric transducer (Wide Band) was attached to each of the end-tabs, as described previously in Section 3.5.1.3 during tensile testing of the single fibre 2400 Tex E-glass bundles. Figure 4.14 represents the average cumulative acoustic emission hits recorded during the tensile tests. At each gauge length, the number of AE hits for the unfiltered as-received fibre bundles were greater when compared to the spread E-glass bundles. The magnitude of the scatter in the cumulative AE hits was variable with the highest being noted for the spread bundle 150 mm gauge length followed by the 200 mm gauge length (as-

received and spread). With the exception of the 100 mm gauge length, the general trend observed in Figure 4.14 is that the cumulative AE hits increases as a function of the gauge length for the as-received and spread fibre bundles. The 100 mm gauge length samples for the as-received E-glass bundles were highlighted as an anomaly previously when considering the Weibull survival plots (see Figure 4.7). It is speculated that the significantly lower cumulative hits recorded at 100 mm gauge lengths may indicate that a large proportion of the filaments had sustained some damage during sample preparation, storage and subsequent handling prior to mechanical testing.

With the exception of the 100 mm gauge length samples, the general trend in the cumulative hits recorded is a progressive increase as the gauge length is increased. This trend is consistent with the discussion presented previously with regard to the relationship between the tensile strength and the gauge length; it decreased as the gauge length was increased. However, with reference to Figure 4.14, the number of filaments in the 2400 Tex E-glass bundle is approximately 4000. The cumulative hits recorded for each of the gauge lengths for the as-received and spread E-glass bundles is observed to be significantly higher than the number of filaments.

The following section presents a general discussion on the data presented in Figure 4.14 where the as-received and spread cumulative AE hits are compared.

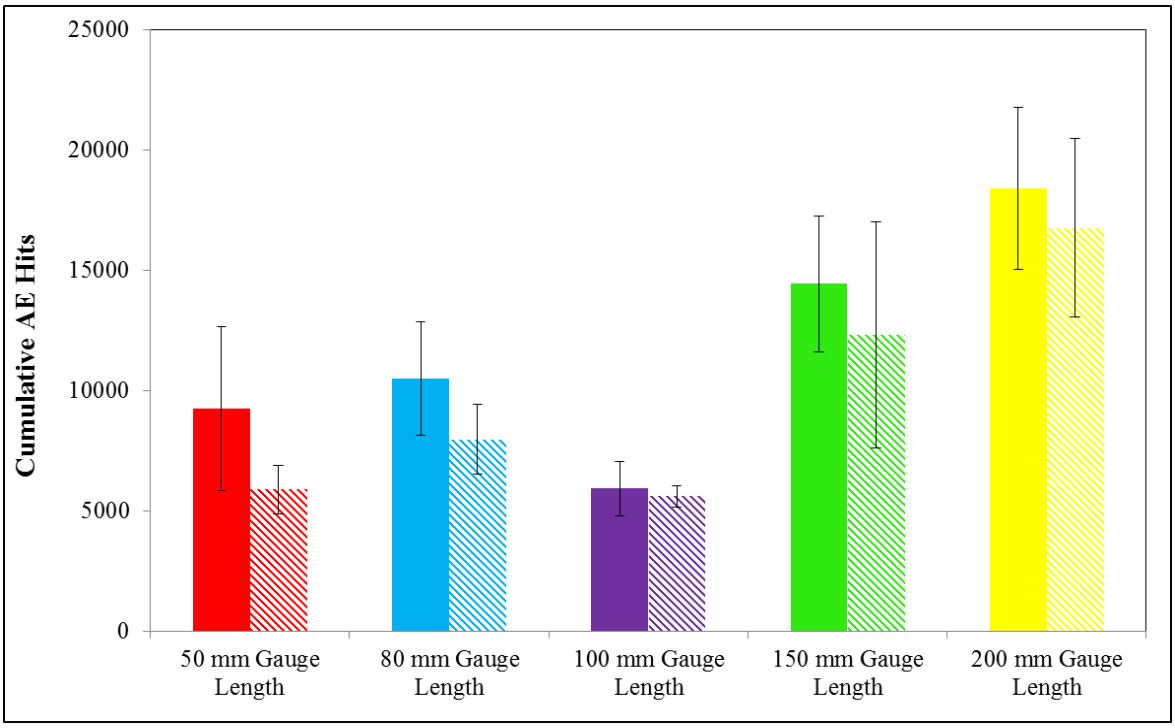

Figure 4.14 Summary of the unfiltered cumulative hits recorded during the tensile tests of 2400 Tex E-glass bundles at specified gauge length.

As the gauge length is increased, the probability of encountering a higher number of meandering fibres, flaws etc, as described previously, will be higher. By implication, this will mean that the acoustic activity in samples with a longer gauge length and a higher degree of misaligned fibres would be expected to be higher. In addition to characteristic acoustic activity resulting from the fracture of filaments during tensile loading, other signatures due to inter-filament friction, constriction-induced friction caused by the meandering filaments would be expected to be higher. In the case of the spread fibre bundle the degree of alignment in the spread samples is known to be higher. Therefore, the

spread bundles would be expected to exhibit a lower cumulative AE hits when compared to the as-received samples. This is observed in Figure 4.14.

A number of suggestions can be offered to account for this observation including the following: (i) In areas of high binder distribution, the fracture of filaments within these areas may have enabled reloading of the fractured fibres thus enabling them to be undergo further fracture; (ii) The recoil upon the fracture of a filament may have impinged or impacted on the surviving fibres generating acoustic activity; (iii) Multiple fibre fractures within a single filament caused by the shock-wave and recoil during the fracture of a filament; (iv) Multiple fibre fractures within the end-tab regions; (v) Reloading of fractured fibres because of the presence of meandering and/or twisted filaments within the bundle. In other words, the sections with meandering filaments act as a "rope" where it tightens as the applied load is increased. This compaction of the filaments will lead to inter-filament interactions and possible enable significant re-loading of fractured filaments. (vi) Matrix cracking within the end-tab regions; (vii) The binder fracturing; and (viii) Inter-filament contact and abrasion as the applied load is increased (ix) echo of fractures recorded by one sensor received and recorded by the second sensor.

If the above-mentioned scenarios are true, the slopes and the peak tensile failure loads would be expected to be higher for the case where the filaments are more aligned. This was observed for the 50 mm, 80 mm and 100 mm gauge length. However, the relative slopes for the 150 mm and 200 mm gauge lengths for the as-received and spread cases were similar.

Above a specified gauge length, the differences in the slopes would be expected between the spread (aligned) and as-received (not aligned) fibre bundles. This is not the case for the 150 mm and 200 mm gauge length specimens where the slopes are similar. It is therefore possible that this is likely due to the consistency in the method of spreading, sample preparation and testing. On the other hand, it is possible that above a specified gauge length, the probability of encountering a higher population of flaws will be reduced to a point where a constant value can be assumed. If this argument is correct, it can also be applied to the number of meandering fibres where above a specified gauge length, a near-constant value for the degree of meandering can be assumed. This hypothesis is apparent when inspecting the 150 mm and 200 mm gauge length in Figure 4.14.

4.3 The Effect of Specified Methods of Binder Removal on the Tensile Properties of 2400 Tex E-glass

The previous section was concerned with the tensile strength of as-received and spread E-glass fibre bundles. As mentioned previously, fibre spreading was used as a means for partially removing the binder via a mechanical fibre spreading technique. It was established that the act of spreading the fibres was not detrimental to the tensile strength of the E-glass bundles. The following section is concerned with the tensile strength of lubricated and also where the binder was partially removed using acetone. The data from these were compared with as-received and lubricated fibre bundles.

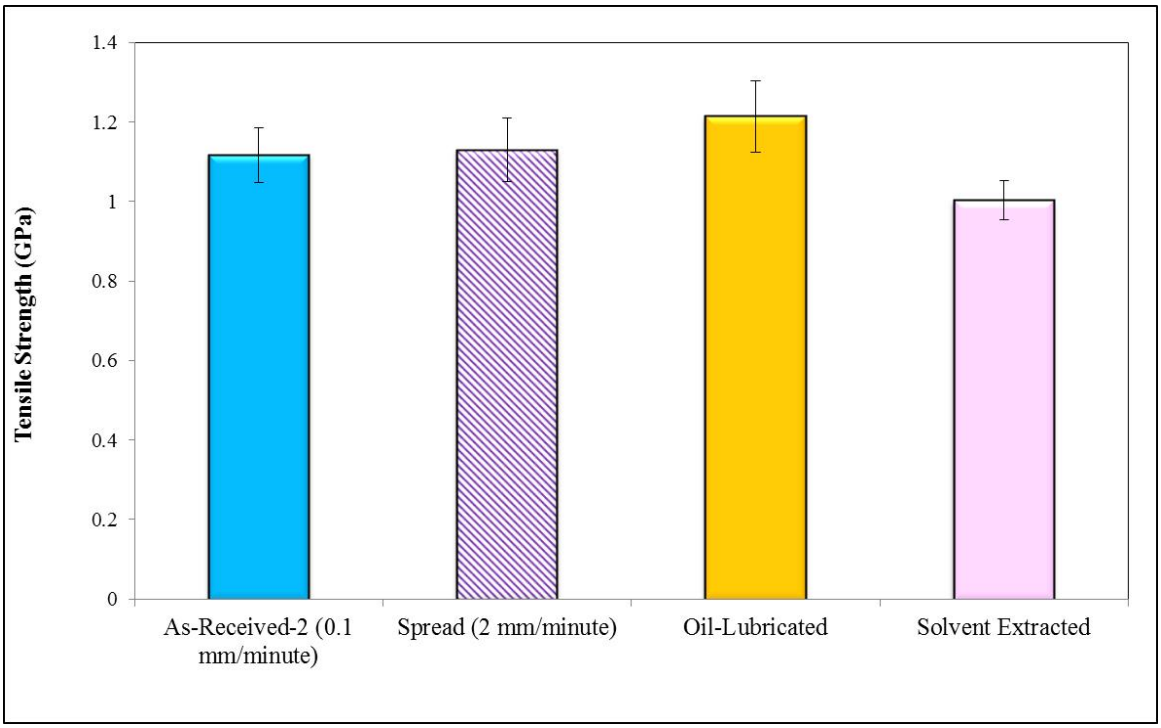

Figure 4.15 Summary of the tensile strengths for 2400 Tex E-glass where the binder was removed using solvent extraction. The data for the oil lubricated bundles has also been included. As before, statistical analyses were performed using the F-tests involving the full dataset. The data presented in Table 4.3 states that the tensile strength for the as-received, lubricated and acetone-treated bundles is statistically significant.

Figure 4.15 shows the average tensile strength of thirty samples for as-received, spread, lubricated and solvent-extracted 2400 Tex E-glass bundles. From here on, all the tensile tests were conducted using a cross-head displacement rate of 0.1 mm/minute. However, the data for spread bundles tested at 2 mm/min was included to be compared with treated bundles. Also, the data for the 2 mm/minute has been included to demonstrate that changing

the cross-head displacement rate of 2 mm/minute did not show any statistically significant difference in the tensile strength (see Table 4.3). On inspecting Figure 4.15, it is seen that the oil-lubricated tensile bundle displayed a marginally higher tensile strength. However, the solvent-treated E-glass bundle displayed a lower tensile strength.

Table 4.3 F-test and T-test results for tensile strength of specified treatment for the as-received-1 (2 mm/min.) and spread E-glass fibre bundles.

No.	Comparison of E-glass Sample Types	Statistical Test Type	F_0 or T_0	Degree of Freedom	P-Value	Conclusion
1	All E-glass fibre bundle samples	F-Test	10.475	DFn =2 DFd = 87	0.0001	Statistically significant
2	As-received-2 (0.1 mm/min.) versus oil lubricated E-glass fibre bundles	T-test	-4.052	58	0.0002	Statistically significant
3	As-received-2 (0.1 mm/min.) versus spread E-glass fibre bundles	T-test	-4.498	58	0.6200	Statistically significant
4	As-received-2 (0.1 mm/min.) versus solvent-extracted E-glass fibre bundles	T-test	-0.734	58	0.4661	Statistically significant
5	Oil lubricated versus solvent-extracted E-glass fibre bundles	T-test	2.627	58	0.0110	Statistically significant

4.3.1 Weibull Statistical Analysis

The shape parameter, m suggests that the tensile strength of solvent-extracted specimens has a lower scatter when compared to the oil-lubricated and as-received samples. This is

contrary to the reasons proposed previously when discussing the tensile strength data and it is difficult to offer any convincing arguments to explain this observation. A more likely explanation is that on evaporation, acetone leaves a residue on a particular region of the fibres as a tidemark. The mode of withdrawing the bundles from the rig may have resulted in a fine coating being reapplied to the separated filament as a tidemark. The filaments after acetone-treatment were separated, making subsequent handling difficult.

Table 4.4 Summary of the Weibull shape (m) and scale (σ_0) parameters for as-received, oil-lubricated and solvent-extracted E-glass fibre bundles.

E-glass Bundle Type	Shape Parameter (m)	Scale Parameter (σ_0)
Oil-lubricated	15.605	1.255
As-received-2 (0.1 mm/min.)	18.769	1.148
Solvent-treated	23.595	1.025

The scale parameter (σ_0) shows that oil-lubricated samples have higher survival rates at a higher tensile strength than the as-received and solvent-extracted fibre bundles; as expected, this is reflected in the tensile strength data. It is clear from Figure 4.16 that the survival probability was in the order oil-lubricated> as-received> solvent-treated E-glass bundles. However, the reason for the shape parameter being higher for the solvent-treated E-glass bundle remains as yet unexplained.

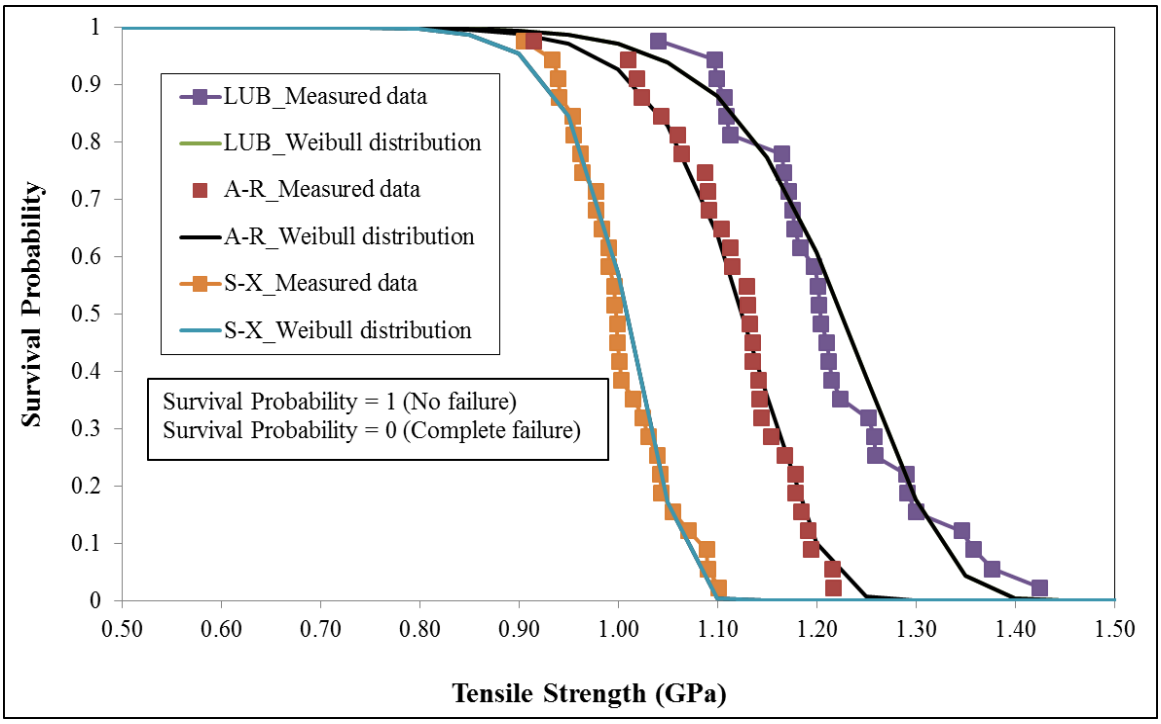

Figure 4.16 Survival probability for the tensile strength of as-received-2 (0.1 mm/min.), lubricated and solvent extraction E-glass fibre bundles.

R'Mili *et al.* (2008), proposed that the higher tensile strength exhibited by the lubricated fibre bundle could be caused by the following factors: (i) They claimed that the wettability of the lubricated samples enhances better fibre filament orientation when compared to the dry bundles. This is debatable because their samples, like those in the current work, were end-tabbed. Therefore, the relative spatial orientation of the fibre bundle is effectively fixed. However, it was established previously that the distribution of the binder was not even, and that meandering fibres are present in the bundle. Therefore during tensile loading, the meandering fibres will effectively act like a "rope" whereas the tensile load

increased, the constriction or compaction of the filaments within the rope will increase. In areas where there is a lower binder content, the probability of fibre-to-fibre contact will be higher. The opposite will be true in regions where excess binder is present (as shown preciously). Therefore, the proposal by R'Mili *et al.*, that "enhances better fibre filaments orientation" is not a likely scenario. These authors also suggested that the fibres in the lubricated samples acted independently, thereby avoiding inter-filament friction. This statement too is debatable as by definition, introducing a lubricant into the bundle will lubricate the filaments provided that the passage of the lubricant (non-polar in this case) will penetrate and impregnate silane-compatible binder. It is accepted that the probability of direct inter-filament contact and hence friction will be minimised by the presence of a layer of lubricant between the filaments. The original conclusions made on the effect of lubricants on the tensile strength of E-glass bundles stated by Hills and Okoroafor (1995), were echoed later by R'Mili *et al.* (2008).

The following discussion is concerned with the partial removal of the binder by treatment with acetone for 72-hours. With reference to Figure 4.15, it is seen that the acetone-treated E-glass bundles exhibited the lowest tensile strength when compared to the as-received and lubricated bundles. Removing the protective binder from the surface of the E-glass filaments will: (i) expose them to atmospheric moisture – it was established in the literature review that this is detrimental to the mechanical properties of glass fibres, in general (Petersen *et al.*, 2013); (ii) removing the acetone-soluble fraction of the binder is likely to enhance the probability of direct fibre-to-fibre contact in other words, increasing friction;

this is known to reduce the tensile strength of pristine E-glass. Therefore, it is reasonable for this to occur when the binder is removed. The removal of physisorbed components of the binder will also result in exposure of the filaments to the above-mentioned issues. It is known that the organo-silanes generally tend to form a covalent bond on the surface of glass fibres. Thus, it is unlikely that this component can be removed by a solvent such as acetone as claimed by Liu *et al.* (Liu *et al.*, 2007; Liu *et al.*, 2008). Film former, anti-static agents, lubricant etc are also known to be present in the binder, and hence, removing these protective layers is also likely to be detrimental to the mechanical properties of E-glass (Zhandarov and Mader, 2015; Cech *et al.*, 2002; Thomason, 2001; Zinck *et al.*, 2001).

The visual appearances of the as-received, lubricated and solvent-treated E-glass were as follows: The as-received 2400 Tex was "stiff" because of the presence of the binder. Moreover, it retained its curved shape when samples were being obtained from the creel. The solvent-treated samples on the other hand splayed out like a brush, as the solvent evaporated, when they were taken out of the acetone conditioning tube. The lubrication of the E-glass bundles was carried out on a pre-shaped aluminium foil. After immersion in the lubricant for 5-minutes, the samples were removed and placed on an empty tray for 10-minutes prior to testing; this resulted in the sample straightening presumably because of the penetration of the lubricant in between the filaments.

The next section is concerned with the acoustic emissions that were generated during tensile testing of the as-received, acetone-treated and lubricated E-glass bundles. The justification for selecting a method for filtering the AE data are also addressed.

4.3.2 Acoustic Emission Monitoring During Tensile Testing of E-glass Bundles

Figures 4.17 (a, b and c) show the unfiltered AE hits plots of amplitude versus displacement (parametric 2 mm) for the as-received, oil-lubricated and acetone-extracted E-glass fibre bundles respectively.

With reference to Figures 4.17, a common feature in the as-received and solvent-treated bundles is the presence of three distinct AE clusters: (i) above 85 dB; (ii) between 55 and 75 dB; and (iii) below 55 dB. The solvent-treated E-glass bundles clearly showed the presence of the third cluster below 55dB; this was less prominent in the as-received dataset and it was hardly present in the lubricated bundle. In the lubricated case, the AE hits were mainly concentrated in the cluster above 80 dB. This has been designated by previous authors as representing fibre fracture (R'Mili *et al.*, 2008). The hits in the as-received samples are seen to congregate towards the far right-hand side or towards the end of the tensile tests. However, the onset of a significant number of AE hits being detected is lowest for the lubricated bundle followed by the as-received and solvent-treated samples.

(a)

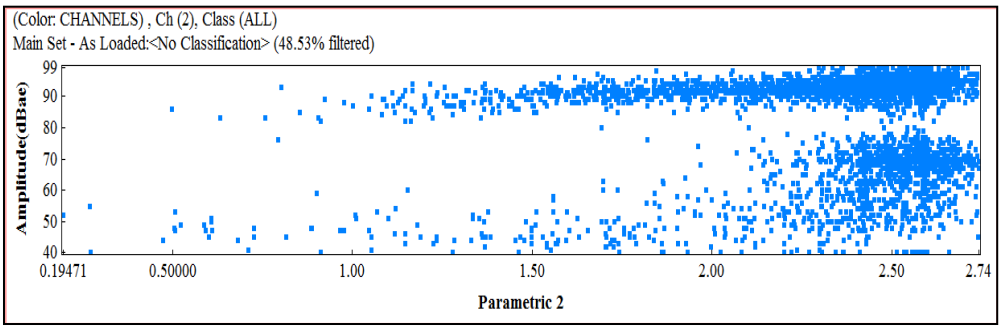

(b)

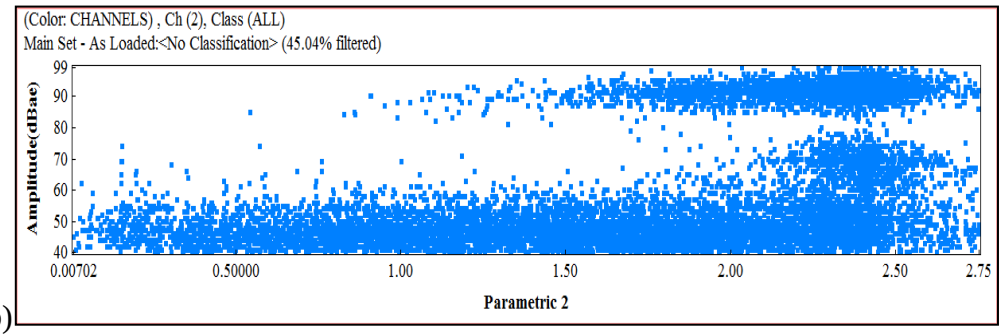

(c)

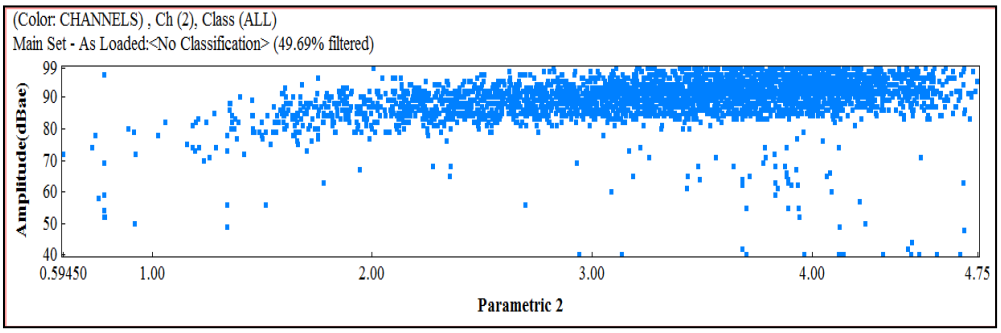

Figure 4.17 Raw AE hits datasets for channel 2 showing amplitude (dB) versus parametric (displacement, mm) plot for: (a) as-received; (b) solvent-treated; and (c) oil-lubricated E-glass bundles.

On the basis of the data presented in Figures 4.17, the necessity for filtering the data was considered for the following primary reason - the number of filaments in the bundle was significantly lower that the total AE hits obtained. A possible reason for the occurrence of multiple AE hits was discussed previously. However, the general trend in the literature was based on the assumption that not all the AE hits were caused by the fracture of individual filaments. For example, the spurious AE hits have been attributed to fibre-to-fibre interactions (R'Mili *et al.*, 2008), environmental conditions (Petersen *et al.*, 2013), data acquisition parameters (Monnier *et al.*, 2012), echo from another sensor (Asokan *et al.*, 2012) and machine noise (Gao *et al.*, 2011).

In the current study, the decision was taken to filter the AE data. The filtering was based on the observation that in the oil-lubricated bundles, they failed at higher absolute energy ($\geq$ 6,000 attoJoules) with a duration equal to or greater than 250 micro-seconds. It was assumed that the lubrication resulted in minimising the detrimental filament-to-filament contact, thus leading to the filaments being able to achieve their ultimate tensile strength. In other words, like previous researchers, the author of this work assumed that inter-filament contact would lead to degradation in the tensile strength of the E-glass filaments. Justification for these assumptions is given below by referring to published papers:

(i) Inter-filament contact leading to a degradation in the tensile strength (R'Mili *et al.*, 2008).

(ii) Humidity and temperature (Petersen *et al.*, 2013).

(iii) Machine noise (Hill *et al.*, 2012; Gao *et al.*, 2011)

(iv) AE data acquisition parameters (Jin *et al.*, 2014; Kouvarakos and Hill, 1996)

(v) Echo recorded from the fractured received from paired sensor (Asokan *et al.*, 2012; Guild *et al.*, 1980)

Therefore, the parameters that were used for filtering the AE data were:

(a) Considering only hits above ≥ 6,000 atto-Joules absolute energy; and

(b) Considering only AE hit durations that were equal to or greater than 250 micro-seconds.

With reference to the unfiltered presented previously in Figures 4.17 their filtered counterparts is presented in Figures 4.18.

(a)

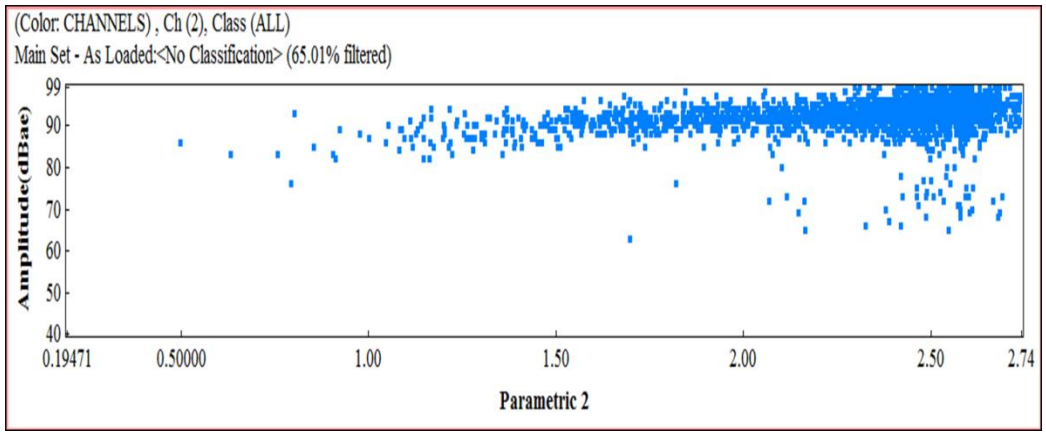

(b)

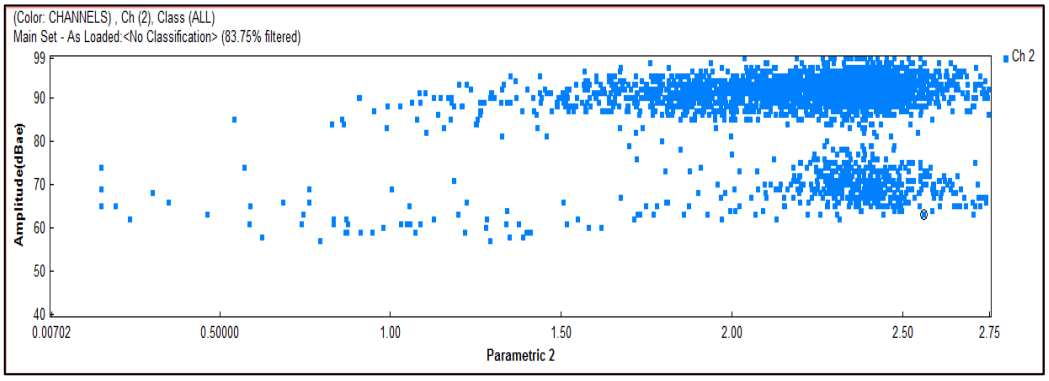

(c)

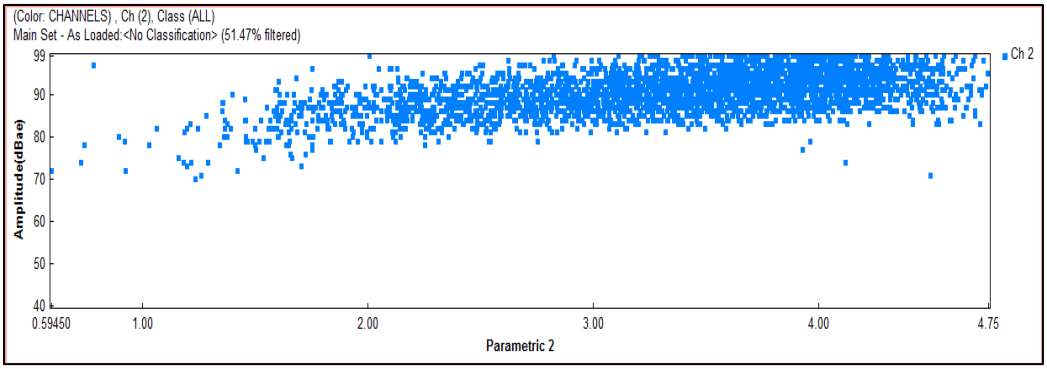

Figure 4.18 Plots showing the effect of the filtering that was carried out on the raw AE datasets for channel 2 for: (a) as-received; (b) solvent-treated; and (c) oil-lubricated E-glass bundles.

On comparing Figures 4.17 for the raw datasets for channel 2 with Figure 4.18 representing the filtered dataset, it is seen that filtering leads to the removal of all the AE clusters below 60 dB. It is therefore assumed that all AE hits, other than that representing the fracture of filaments have been filtered. The other consequence of this mode of filtering is that the total number of hits is below the filament count.

Figure 4.19 shows representative stress/displacement traces with superimposed cumulative AE hits for: (i) as-received; (ii) lubricated; and (iii) acetone-treated E-glass bundles.

In Figures 4.17 the parametric channel is activated only when an acoustic event is detected. Hence, as stated previously, in the as-received and lubricated cases, AE events were not detected until approximately after 0.25 and 0.5 mm of displacement for the as-received and lubricated samples respectively. However, in the case of the solvent-extracted sample, the AE events were detected from the onset of the tensile test.

The next section of this thesis is concerned with the effect of heat-treatment on the tensile strength of E-glass fibre bundles. The AE filtering method developed here was applied to the heat-treated specimens.

(a)

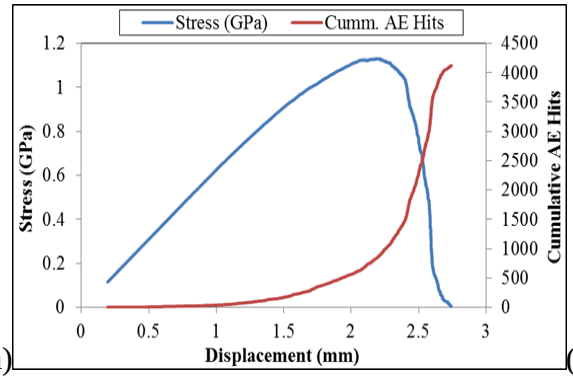

(b)

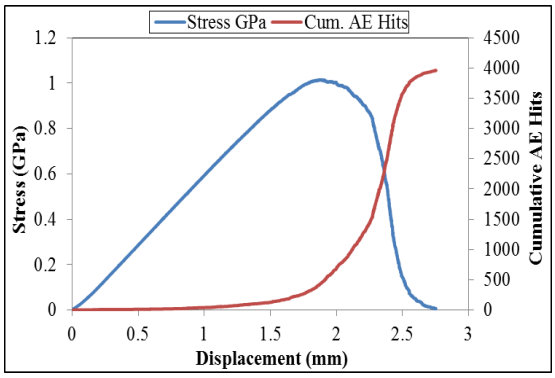

(c)

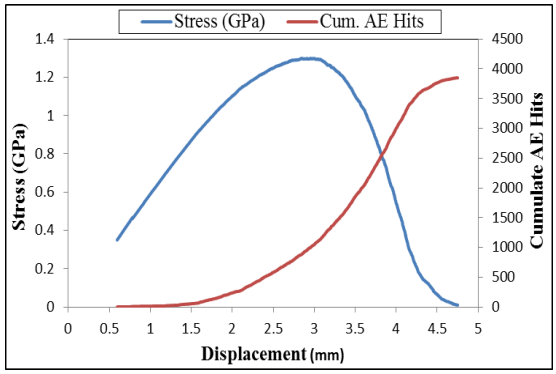

Figure 4.19 Representative stress/displacement traces for the: (a) as-received; (b); solvent-treated and (c) lubricated E-glass bundles. The cumulative AE hits have been superimposed on the traces.

4.4 Effect of Heat Treatment Temperature on the Tensile Strength of the As-received E-glass Fibre Bundles

A number of previous researchers have shown that, subjecting E-glass fibres to temperatures above 250 °C leads to a degradation in the tensile strength (Jenkins *et al.*, 2015a; Thomason *et al.*, 2014a; Thomason *et al.*, 2014b; Feih *et al.*, 2011; Ya *et al.*, 2008;

Kennerley, 1998; Kennerley *et al.*, 1997; Loewenstein, 1962; Thomas, 1960). The current study was undertaken to find plausible reasons for this strength degradation in E-glass as a function of temperature. This is of importance because E-glass represents over 70% of the reinforcements used to manufacture composites globally. Hence, if the reasons for the degradation in the tensile strength as a function of temperature could be identified, it was envisaged that it would be possible to develop a technique to overcome it.

Figure 4.20 shows the summary of the average tensile strength of thirty samples each of E-glass fibre bundles that were heat treated at 450 °C, 550 °C and 650 °C.

Subjecting E-glass fibres to 450 °C for two hours led to a 70% decrease in the tensile strength when compared to the as-received state. Thermal treatment at 550 °C and 650 °C for two hours led to tensile strength degradation between 90 – 95%.

The reasons reported in the literature range from:

(i) removal of water from the surface of the glass fibres (Loewenstein, 1962);

(ii) cracks forming when the hydrated layer on the glass fibre surface is removed above 250 °C (Feih *et al.*, 2011b; Kennerley, 1998);

(iii) crystallisation during slow-cooling; and

(iv) residual stresses.

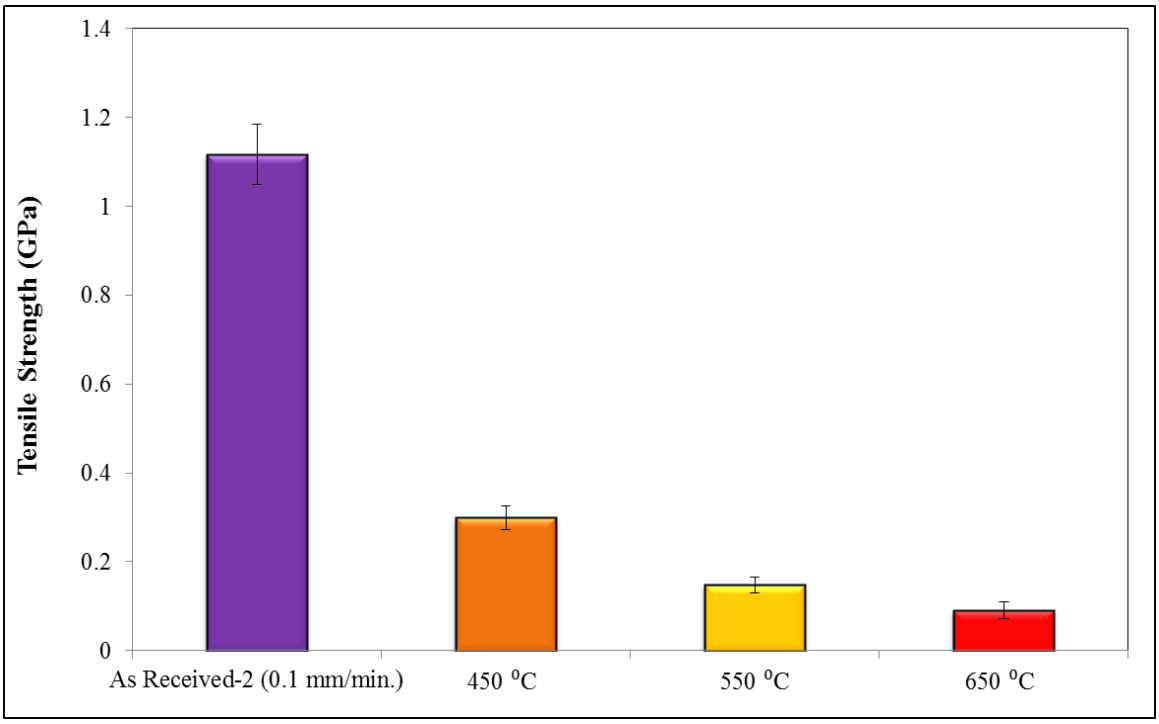

Figure 4.20 Average tensile strengths for E-glass fibre bundles that were heat treated at three specified temperatures for two hours.

Significant effort was expended to inspect the surface of the as-received and heat-treated E-glass using SEM. The motivation for this analysis was to determine if the heat-treatment led to any obvious surface features such as blisters, cracks or any other features that could be attributed to the observed loss in the tensile strength as a function of heat treatment. Some of the micrographs shown here were generated by Dr Winson Kuo of Johnson Matthey. This was because at that time the Metallurgy and Materials building at the University of Birmingham was being refurbished.

Figure 4.21 shows typical high-magnification images of as-received E-glass fibres. In general, the as-received E-glass fibres tended to exhibit a relatively smooth surface. It was not possible to state with any certainty if the debris on the surface of the fibres was introduced during storage or if they were part of the original surface. In some instances, significant binder was found to be present on the surface of the E-glass filaments. Typical representative micrographs showing binder-rich regions are shown in Figures 4.22. In addition to the binder-rich areas on the surface of the E-glass fibres, the other notable feature is the "spots" on the surface. The actual origin of this feature was not identified in the current study but it may represent volatilisation of some component of the binder during drying. It is emphasised that this was not observed on any of the other as-received samples inspected by the author or other members of the research team. Figures 4.23 show typical micrographs corresponding to E-glass fibres that were subjected to 650 °C for two hours in air. In general these samples exhibited a featureless smooth surface.

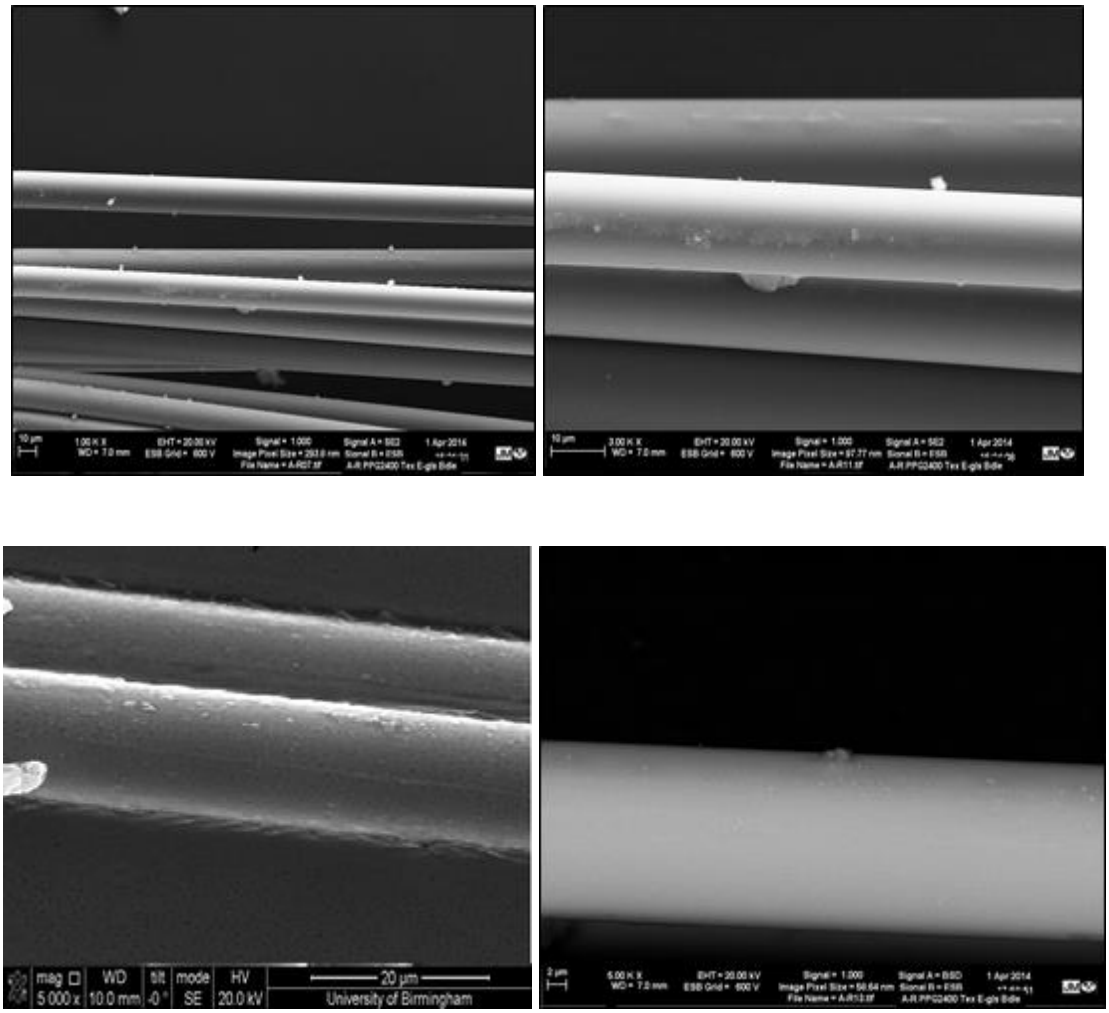

Figure 4.21 SEM micrographs showing typical surfaces of as-received E-glass fibres.

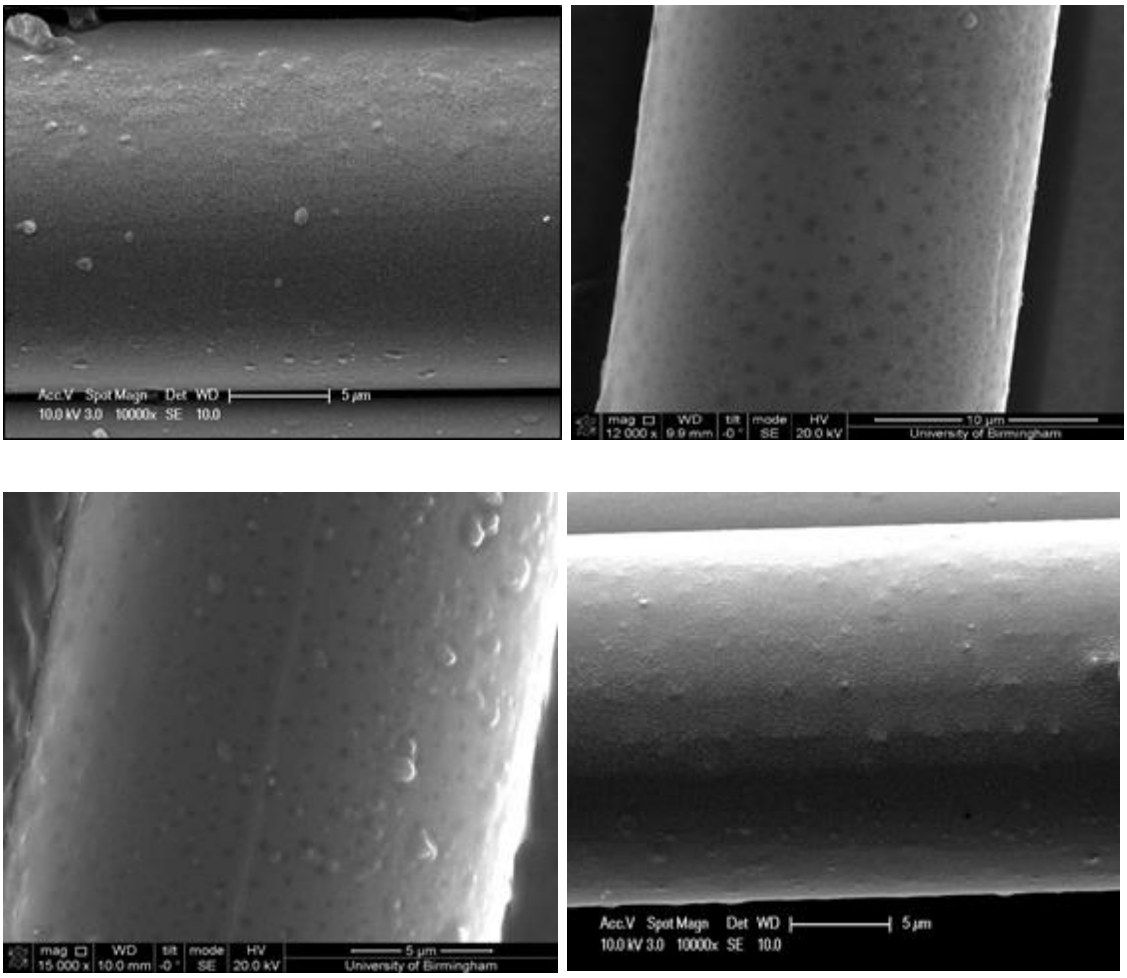

Figure 4.22 SEM micrographs showing binder-rich regions and "spots" that were not observed previously.

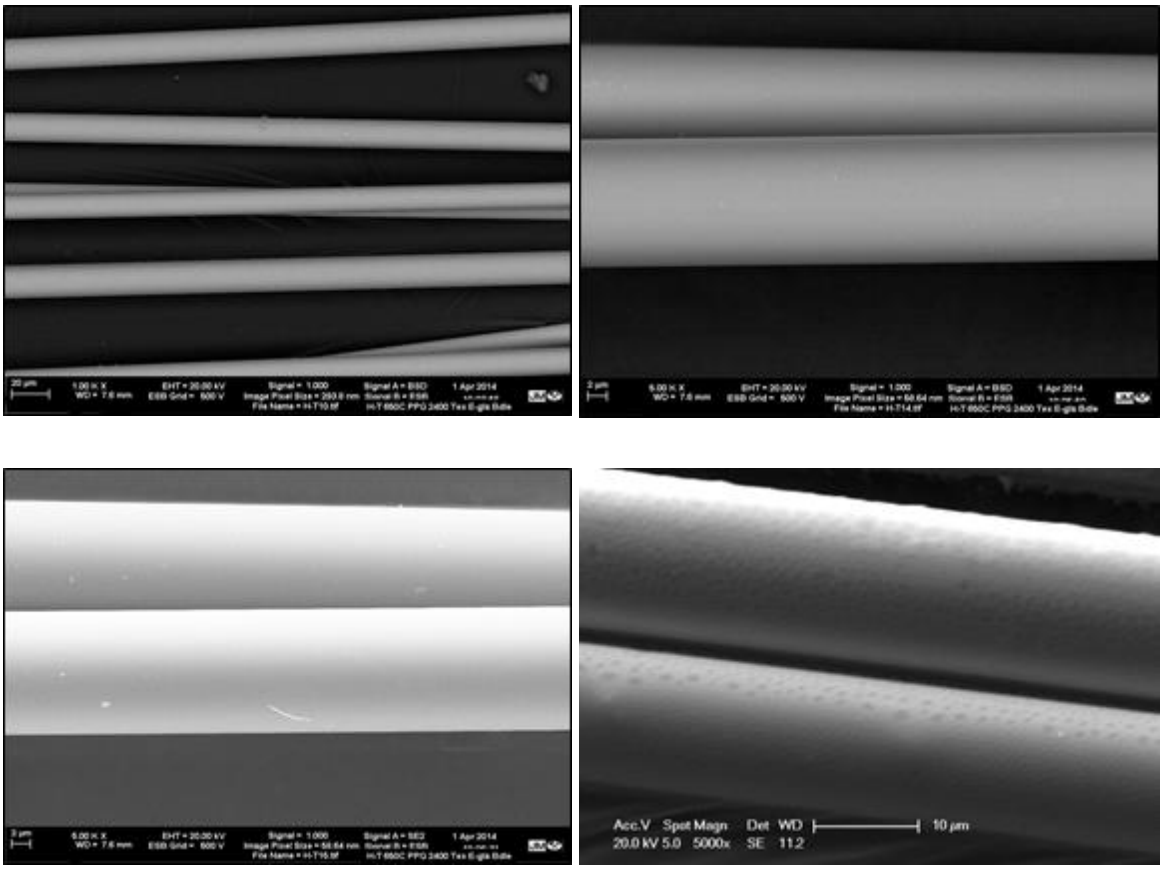

Figure 4.23 Typical SEM micrographs illustrating the surface features observed for E-glass fibres that were heat treated for two hours at 650 °C.

4.4.1 Weibull Analysis of Heat-treated E-glass Bundles

Table 4.5 presents a summary of the Weibull shape (m) and scale (σ_0) parameters for the heat treated E-glass fibre bundles and Figure 4.24 shows the Weibull survival probability plots for the heat-treated E-glass fibre bundles. It is clear from Table 4.5 that the Weibull modulus (m) for the heat treated samples is one of the lowest that was observed in the

current study. It was observed that heat treating E-glass resulted in rendering the filaments extremely brittle. This was most pronounced when the fibres were treated at 650 °C.

Table 4.5 Calculated values of Weibull parameters (m and σ_0) for the heat-treated fibre bundles.

H-T Temperature (°C)	m	σ_0
450	12.739	0.311
550	9.3374	0.155
650	4.8191	0.095

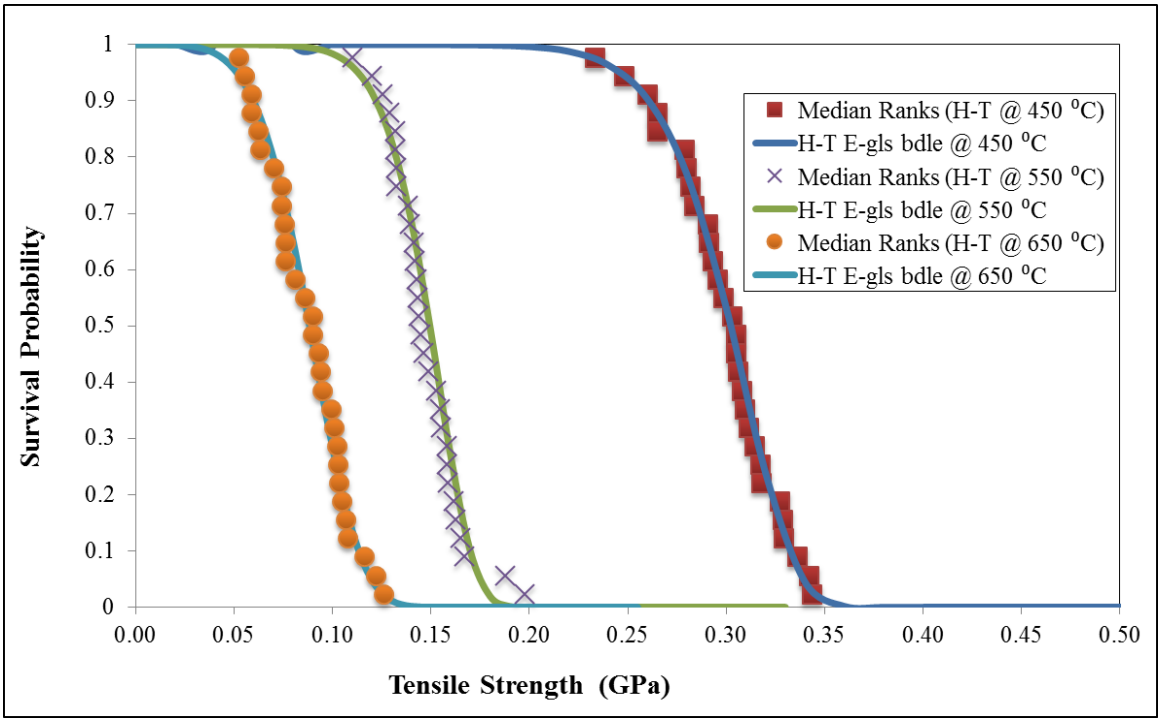

Figure 4.24 Survival probability of thermally conditioned E-glass fibre bundles at temperatures 450 °C, 550 °C and 650 °C.

The Weibull survival plots shown in Figure 4.24 show that the tensile strength of E-glass is degraded significantly as a consequence of heat treatment at 450 °C, 550 °C and 650 °C.

Figure 4.25 shows the average failure strain of thirty individual samples of E-glass fibre bundles that were treated at 450 °C, 550 °C and 650 °C. It is seen that the failure strain decreases as the heat treatment temperature increases. This is consistent with the observation where the brittleness of the filaments increased (during handling) as a function of the heat treatment temperature.

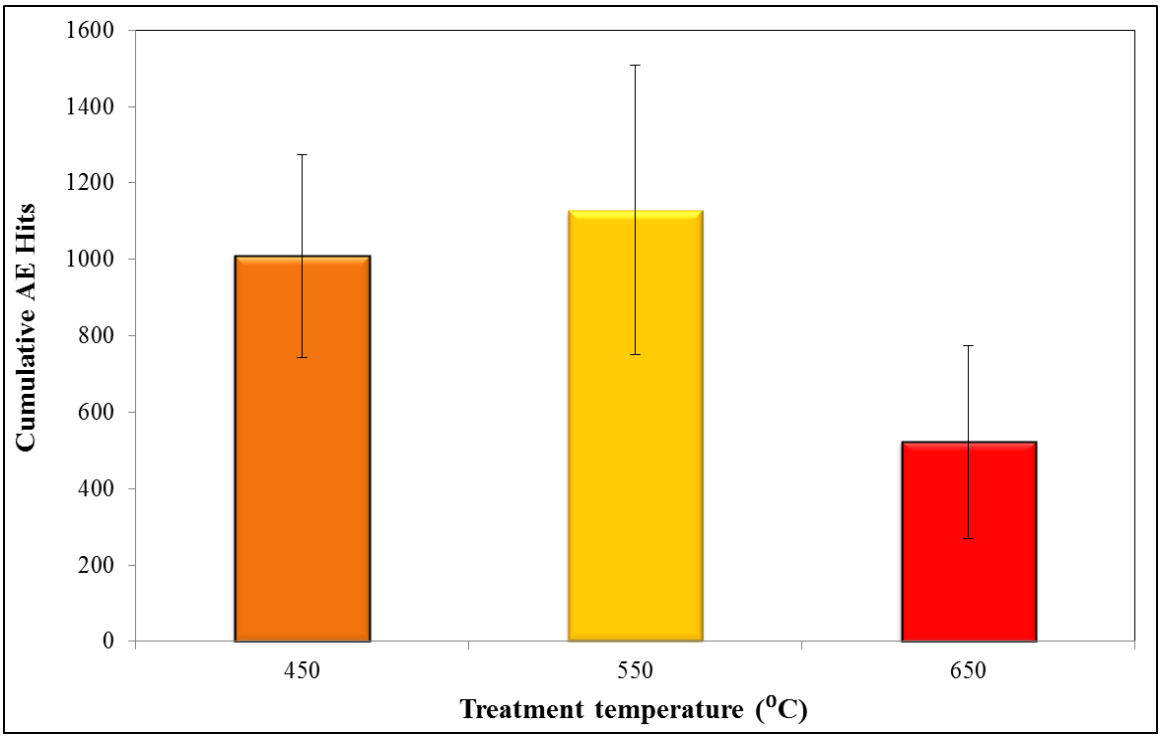

Figure 4.25 Average failure strain of 30 individual E-glass fibre bundles, per heat treatment temperature. The samples were treated for two hours at 450 °C, 550 °C and 650 °C.

Figure 4.26 shows representative tensile stress/strain traces for as-received and three heat-treated E-glass fibre bundles that were subjected to heat treatment for two hours at 450 °C, 550 °C and 650 °C. The drastic reduction in tensile strength and the failure strain for the heat treated samples is readily apparent when compared to the as-received E-glass bundle. It is interesting to note that the slopes for the four traces are similar.

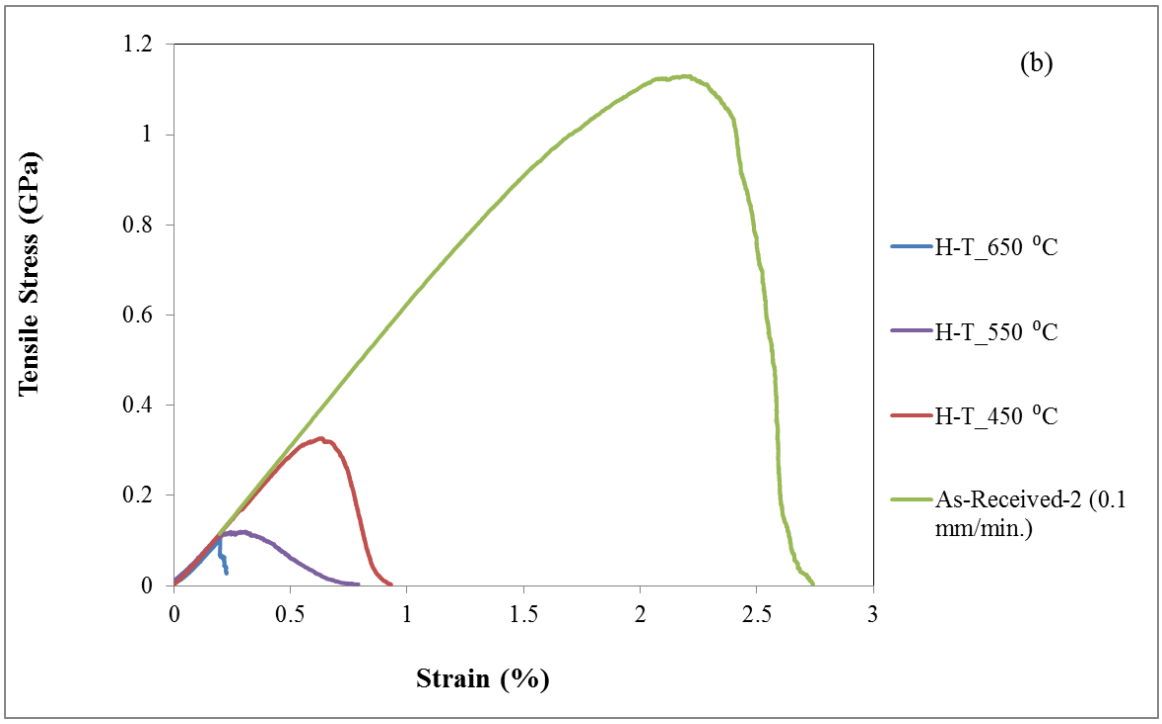

Figure 4.26 Influence of thermal conditioning at different temperatures on slope, failure strain and tensile strength for the as-received E-glass bundles and three samples that were conditioned at 450 °C, 550 °C and 650 °C for two hours.

The final set of experiments conducted in this series was to determine if the presence or absence of the binder during heat treatment could have contributed to the degradation in the tensile properties of E-glass. The rationale for the treatment methods considered were as follows:

As-received E-glass: This served as the reference or benchmark.

Solvent extraction followed by heat treatment in a vacuum at 650 °C for two hours – this was undertaken to investigate if the presence of oxygen could have contributed to the observed

degradation in the tensile properties. In other words, if the components of the binder could have oxidised to create a brittle surface and/or if the oxidised layer reacted with the surface of the E-glass.

As-received sample that was heated in a vacuum at 650 °C for two hours – as discussed above.

Solvent extraction followed by heat treatment in air at 650 °C for two hours – this was performed to determine if the removal of the binder, prior to heat treatment would lead to a greater reduction in the tensile properties.

As-received sample that was heated in air at 650 °C for two hours as discussed above.

Figure 4.27 presents a summary of the results obtained from the above-mentioned study. The main conclusion that can be reached from this set of experiments is that the absence of air or oxygen is seen to result in a somewhat smaller reduction in the tensile strength when compared to the situation where the heat treatment was conducted in air.

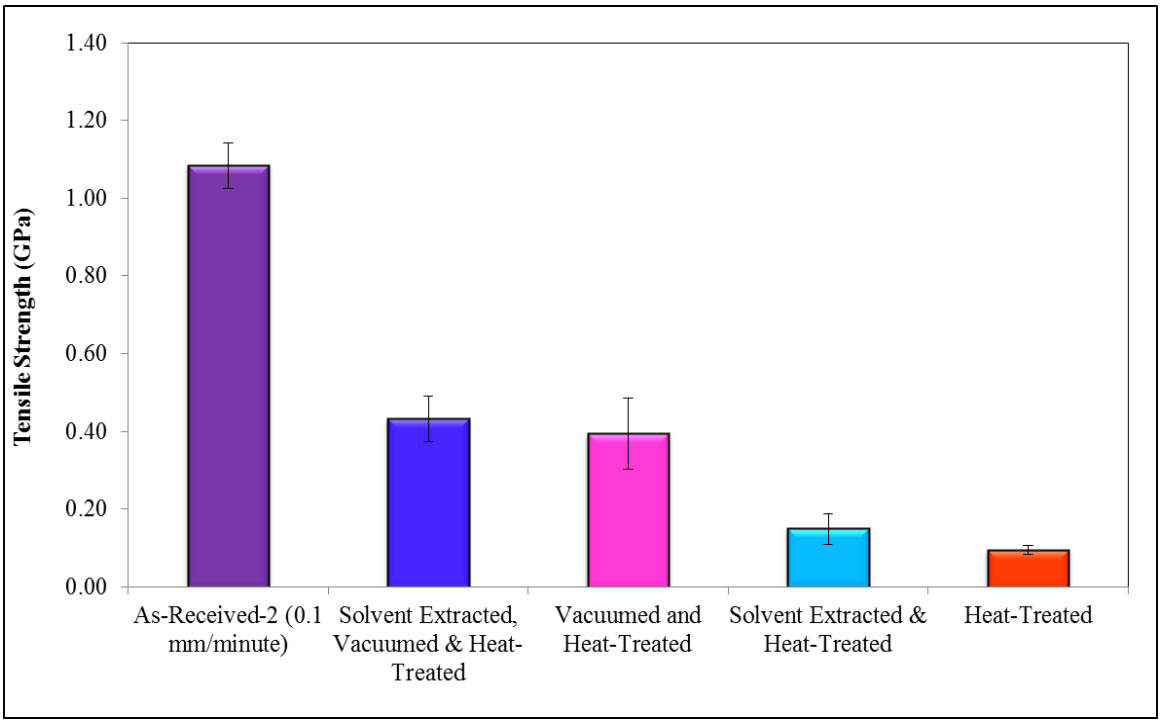

Figure 4.27 Effect of specified methods for removing the binder and heat treatment at 650 °C for two hours.

4.5 Mechanical Properties of Composites With and Without Specified Treatment

This section reports on the mechanical properties of fibre reinforced composites (FRC) manufactured using (i) as-received; (ii) heat-treated; (iii) solvent-extracted; (iv) solvent-extracted and heat-treated; (v) vacuumed and heat-treated; (vi) solvent-extracted, vacuumed and heat-treated; and (vii) recycled E-glass fibre composites. The matrix system used was LY3404 resin and XB3403 hardener (supplied by Huntsman Corporation, UK).

Thirty samples each of the (i) as-received; (ii) heat-treated; (iii) solvent-extracted; and (iv) solvent-extracted and heat-treated E-glass fibre reinforced composites were tested. Surface-mounted electrical resistance strain gauges were used on eight samples from each set.

Twenty samples of the (i) vacuumed and heat-treated, (ii) solvent-extracted, vacuumed and heat-treated, and (iii) recycled E-glass reinforced composites were tested. In this instance, five samples each of the above-mentioned samples were strain gauged prior to testing.

In order to enable comparison between the datasets, the tensile strengths and moduli were normalised to 60% fibre volume fraction; the fibre volume fractions were derived experimentally using the burn off technique as specified in Section 3.5.3.7. The rule-of-mixtures was used to compute the modulus of the various composites that were evaluated in this project. The predicted normalised E-glass fibre strength and modulus were compared to the normalised measured (i) as-received; (ii) heat-treated; (iii) solvent-extracted; (iv) solvent-extracted and heat-treated; (v) vacuumed and heat-treated; (vi) solvent-extracted, vacuumed and heat-treated; and (vii) recycled strength and modulus of reinforcement used in the E-glass composite.

With reference to Figure 4.28, two sets of data are displayed for each sample type: (i) strain data measured via the surface-mounted electrical resistance strain gauges; and (ii) data obtained via the displacement transducer of the Instron 5566 mechanical test machine. Since over 30 individual fibre reinforced composites test specimens were tensile tested, it was not practical to surface-bond electrical resistance strain gauges on every specimen.

Hence, a minimum of 5 specimens per batch of surface-treatments were strain gauged; the displacement data for the remainder were obtained by the cross-head displacement data. There was no evidence to suggest that slippage of test specimen within the end-tab or the jaws of the mechanical test machine were an issue. Furthermore, the minimum and maximum % discrepancy between the strains computed using the surface-mounted electrical resistance strain gauges and the cross-head displacement are 0.5% and 4.5% respectively. Hence, on inspecting the data-pairs presented in Figure 4.28, the inference of the strain data from the cross-head displacement is acceptable. A similar conclusion was reached when considering the Young's moduli of test pieces after they were calculated using the displacement data from the mechanical test machine and the strain data obtained from the surface-mounted electrical resistance strain gauges.

Due care and attention was taken to inspect the strain gauge data prior to reporting the ultimate failure strains for the composite because in some instances, the nature of the longitudinal splitting in the unidirectional materials meant that the strain gauge was damaged in the process. In such instances, the cross-head displacement data were used

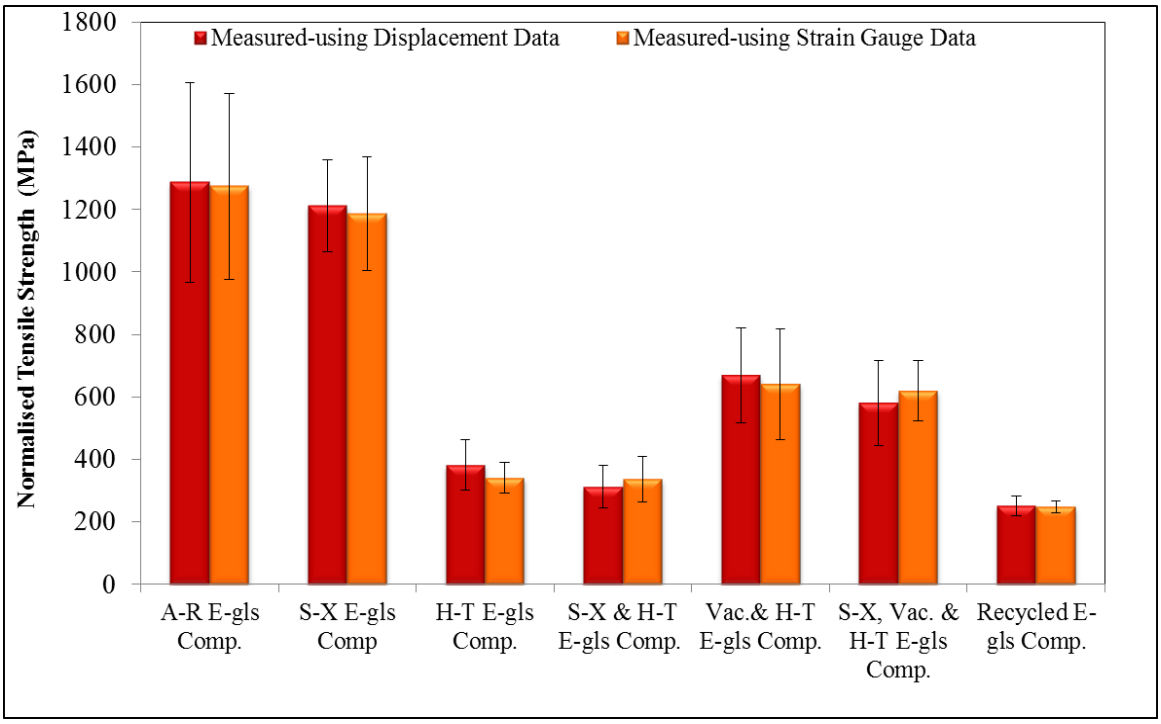

Figure 4.28 Normalised tensile strength of composites manufactured from as-received and treated E-glass fibre bundles. The paired maroon and pink bars represent the displacement data obtained from the mechanical test machine and the surface-mounted electrical resistance strain gauges respectively. The tensile data were normalised to 60% V_f.

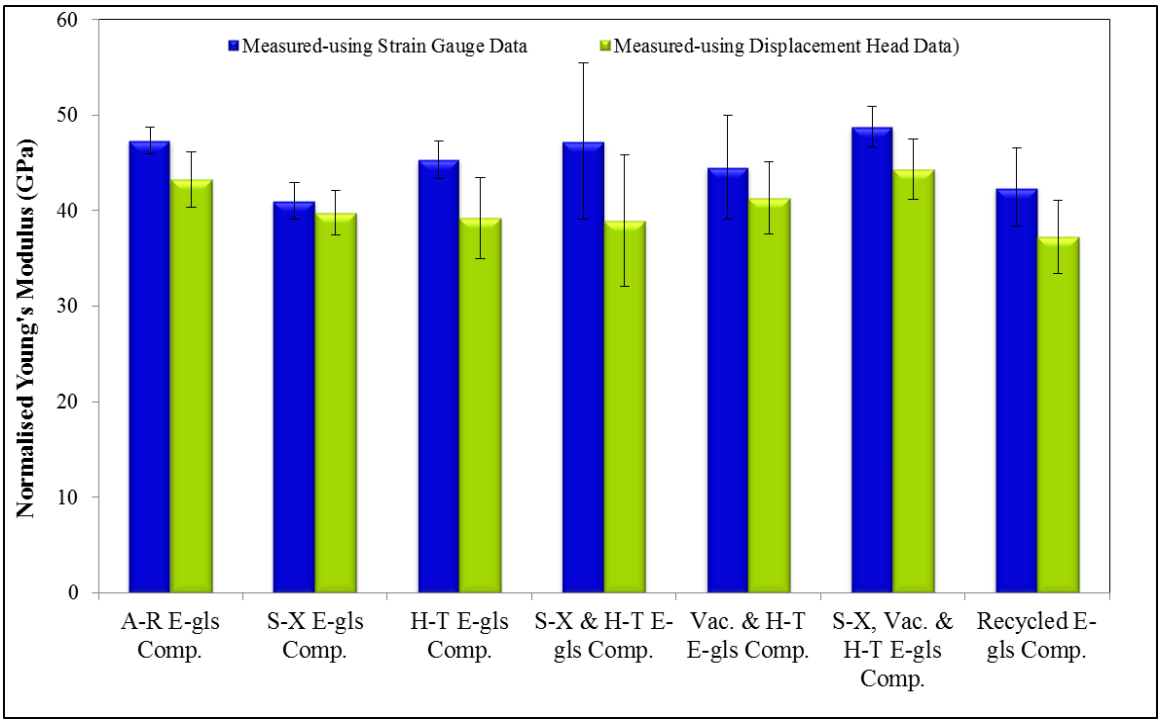

Figure 4.29 Normalised modulus of composites manufactured from as-received and treated E-glass fibre bundles. The paired blue and green bars represent the Young's moduli calculated using the displacement data from the mechanical test machine and the electrical resistance strain gauge respectively. The tensile data were normalised to 60% V_f.

4.6 Properties of E-glass Fibre Composites with and without Specified Treatments

Typical stress-strain traces for the composites evaluated in this series of experiments are shown in Figure 4.30.

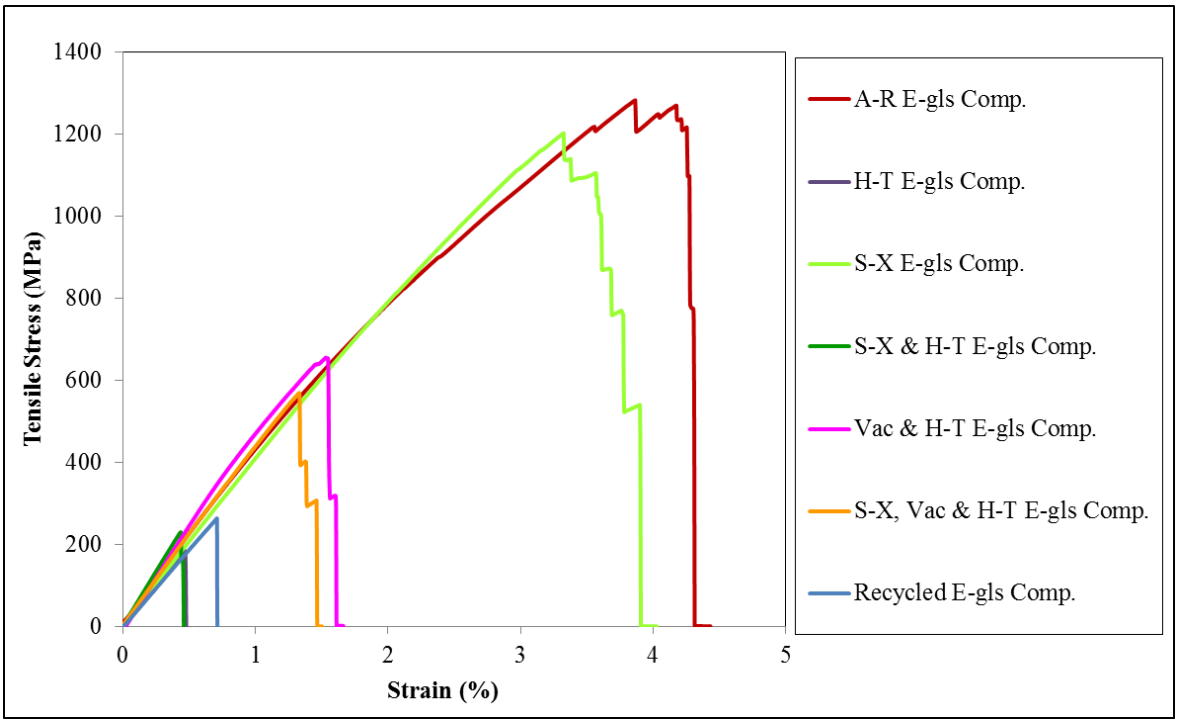

Figure 4.30 Typical stress/strain plots for the composites evaluated in this series of experiments. A-R=as-received. S-X=Solvent-treated. H-T=Heat treated at 650 °C for two hours. Vac.= Heat treated in a vacuum. Recycled = An as-received composite where the fibre bundle was recovered via degradation of the matrix at 650 °C for two hours followed by re-impregnation to manufacture the secondary composite.

The predominant failure mode observed was longitudinal splitting initiated at transverse fractures of the fibres. The degree of scatter seen in the data presented in Figure 4.28 is significant and the following reasons are proposed for this observation. (i) the decision was made not to use prepregs or filament winding to manufacture the composites because: (a) retaining the fibre orientation in the prepregs when the matrix was removed would have

been very difficult; and (b) the heat-treated fibres were too fragile to be subjected to conventional manufacturing processes to produce composites. Hence, the methodology for manufacturing single-tow or bundle composites was developed. This enables the various treatments to be investigated, and the composites to be manufactured, after each specified treatment.

However, it was recognised that the use of single-bundle composite would make it more sensitive to fabrication-induced flaws when compared to multi-layered composites. The type of flaws that were observed in the fibre bundles were (i) fibre undulations and splits in the bundle; (ii) variable binder content; (iii) variable fibre diameter; (iv) unintentional off-axis movement caused by the resin during end-tabbing; and (v) fibre damage caused by manual handling during and after specified treatments.

Table 4.6 presents a summary of previously reported tensile properties for E-glass composites. Accepting that the resin systems are different, the normalised data suggests that the data obtained in this study is comparable to that reported previously.

Table 4.6 Summary of previously reported tensile properties of E-glass/epoxy composites (Mahato *et al.*, 2016[1]; Durai Prabbhakaran *et al.*, 2013[2]; Samborsky *et al.*, 2012[3]; Fernando and Al-Khodairi, 2003[4]; Clements and Moore, 1978[5]). The data from the current study has been included in the last column.

Property						
	1	2	3	4	5	Current
Tensile Strength (GPa)	0.52	1.02	1.18	1.16	1.37	1.25
Young's Modulus (GPa)	20.5	48	43.2	43.69	56.16	52
Normalised (60% V_f) Young's Modulus (GPa)	-	49	-	41.4	-	50
Failure Strain (%)	2.4	2.4	2.92	2.93	2.4	3.73
Fibre volume fraction (%)	59	59	-	62.20	70	62
Void content (%)	-	-	-	0.6	-	0.6

Table 4.7 Fibre volume fraction of the composites manufactured in this current study using as-received and treated E-glass/epoxy composites.

E-Glass Composites Sample	Fibre Volume Fraction (V_f)
As-received E-glass/epoxy	62
Heat-treated E-glass/epoxy	60
Solvent-treated E-glass/epoxy	63
Solvent-treated & the heat treatment	57
Vacuumed, followed by heat treatment E-glass/epoxy	67
Solvent-treated, then vacuumed followed by heat treatment E-glass/epoxy	66
Recycled E-glass/epoxy	56

Figures 4.31 and 4.32 present a summary of the un-normalised and normalised tensile strengths respectively for the composites manufactured and evaluated in this series of experiments. The normalisation was carried out to 60% V_f to enable comparison between the datasets. The relative order of the data does not change significantly because as shown in Table 4.7, the fibre volume fractions for the composites ranged between 56-67%. This variability was primarily due to the fact that the composites were manufactured from single-bundles and the impregnation was carried out manually.

With reference to the data presented in Figures 4.31 and 4.32, the effects of the specified treatment on E-glass fibre are discussed per type of treatment.

(i) As-received E-glass composite: The reasons for the large scatter were discussed previously. The tensile strength reported here is comparable to that reported in the literature when considering normalised fibre volume fractions (see Table 4.7). Therefore, it can be assumed that the quality of the unidirectional composite in this study is acceptable.

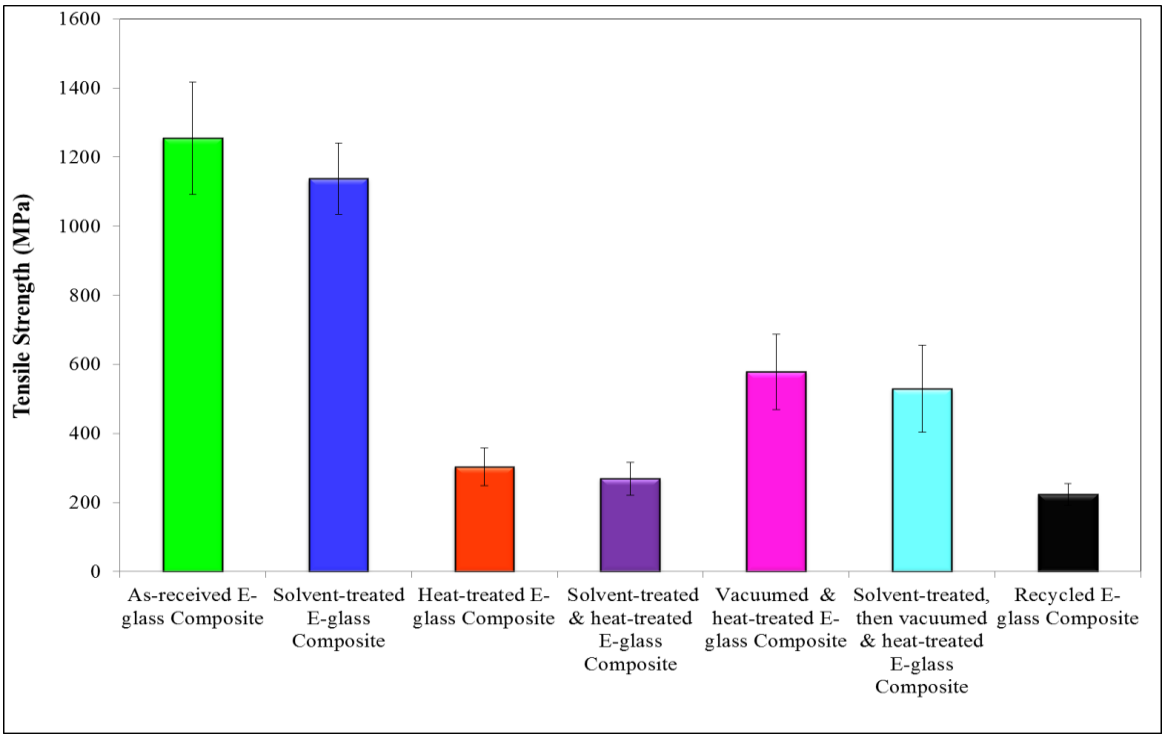

Figure 4.31 Summary of the tensile strengths for the composites manufactured in this current study using as-received E-glass fibres and reinforcement that were subjected to specified treatments. The data presented here were not normalised.

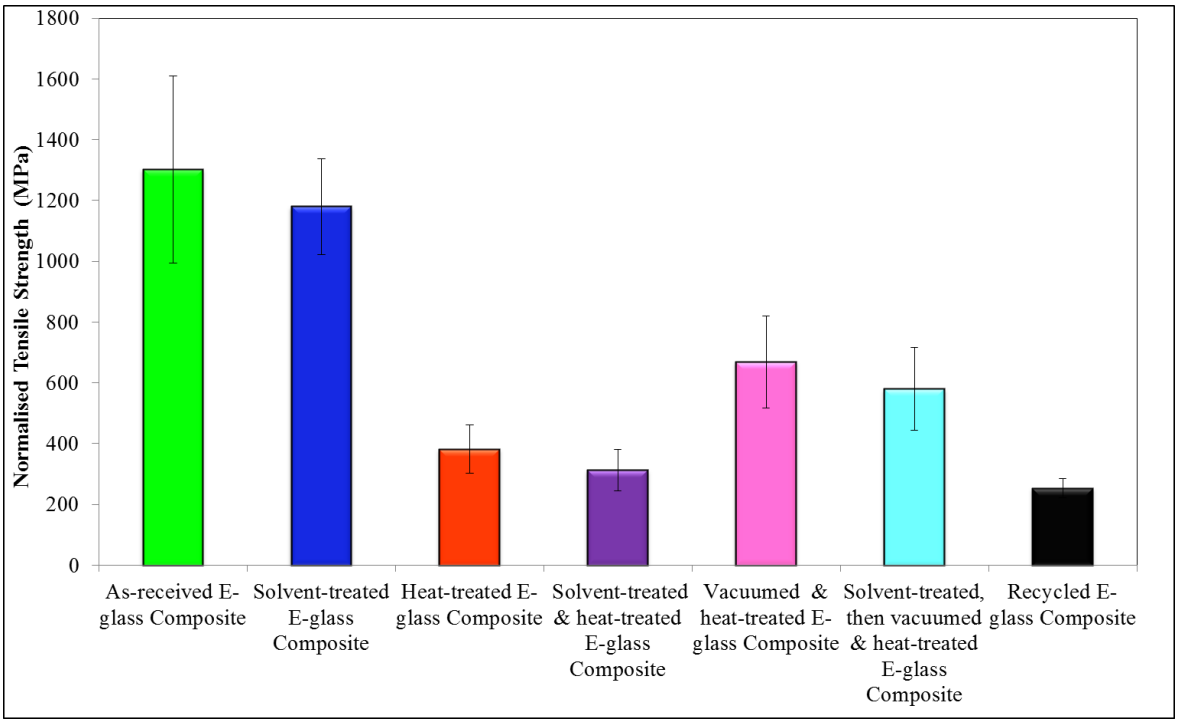

Figure 4.32 Summary of the tensile strengths for the composites manufactured in this current study using as-received E-glass fibres and reinforcement that were subjected to specified treatments. The data presented here were normalised.

(ii) Solvent treated E-glass fibre composites: A 31% reduction is observed in the tensile strength for the composites manufactured using solvent treated E-glass bundles. The reduction in the scatter in the samples where the solvent was used to extract part of the binder is unexpected. SEM micrographs presented previously indicated that not all the binder was removed after 72 hours of treatment with acetone at room temperature. Hence, it is possible that some degree of protection was still available to the majority of the filaments during manual subsequent handling. On the other hand, the other options to be

considered include: (a) The binder content and its variable distribution may have a role in the observed scatter. (b) Solvent treatment is known to remove the solvent-soluble components of the binder. Therefore, it is conceivable that this enabled the end-tab resin to penetrate and impregnate the fibres within the end-tab region more efficiently; thus enabling superior loading of the filaments. (c) The intrinsic variability in the filament diameters may have contributed to the observed scatter but this would have been similar for all the fibre bundles used in this study. (d) The part-removal of the acetone-soluble component of the binder may have permitted more efficient load-transfer between the matrix and the filaments.

(iii) Heat-treated E-glass FRC: The rational for selecting this temperature was that ASTM standard D 2584 stipulates this temperature for the resin burn-off experiments. It is conceivable that a lower temperature will suffice for oxidising the matrix to recover the fibres as part of a recycling strategy. The reduction in the tensile strengths for the E-glass fibres that were subjected to heat-treatment at 650 °C for two hours in air shows a reduction of approximately 82% when compared to the as-received bundle. The same comparison for the FRC manufactured from as-received and heat-treated fibres showed a reduction of 75%. A summary of the number of samples that were treated and subsequently tested are summarised in Table 4.8.

(iv) Solvent treatment followed by heat treatment at 650 °C for two hours: The reason for heat treating solvent-treated E-glass fibres was to investigate if the presence of the binder during heat treatment could have an influence on the subsequent tensile properties.

It is apparent from the data presented previously that the reduction in the tensile properties of the bundle is reflected in the properties of the composites. The reduction in tensile strength for the heat treated E-glass FRC was 78% and that for the solvent exposure, followed by heat treatment was 82%. In the current study, the presence of the binder did have significant influence on the heat treated E-glass as determined by the student T-test.

(v) Heat treatment at 650 °C conducted in a vacuum: The rationale for conducting the heat-treatment in a vacuum was to investigate if atmospheric conditions had any influence on the tensile strength. It is apparent from Figures 4.31 and 4.32 that the tensile strength of fibres heat treated in a vacuum had an average tensile strength of 529 MPa whereas that for bundles treated in air was 303 MPa. Previous researchers (Yang *et al.*, 2015; Jenkins *et al.*, 2015a; Jenkins *et al.*, 2015b; Thomason, 2012b; Petersen *et al.*, 2013; Thomason, 2012b; Bagherpour, 2012; Liu *et al.*, 2008; Plonka *et al.*, 2004a; Tomozawa and Han, 1991; Agrawal and Broutman, 1990; Cameron, 1968; Piggott, 1968; Sakka, 1957; Schmitz *et al.*, 1963; Thomas, 1960) have proposed the following reasons:

(a) as handling of the fibre bundles during sample preparation; (b) fatigue; (c) surface flaws on the fibre; and (d) atmospheric water or water vapour, which have been reported as agents that causes gradual fibre degradation may have contributed to a slight low in strength compared to the as-received fibre bundle

The reduction in the tensile strength for E-glass bundles at 450 °C, 550 °C and 650 °C was presented in Figure 4.20. It is possible that the temperature selected in the current study was

too high to infer any subtle mechanisms that could be responsible for the observed degradation in the mechanical properties.

(vi) Heat treatment at 650 °C after solvent extraction of the binder: Statistical analysis via the Student T-test suggests that the data sets for the heat-treated E-glass in air and in a vacuum belong to different populations. The conclusion that was reached after a similar analysis for the (a) E-glass bundles heat treated in vacuum and (b) those heat treated in a vacuum after solvent extraction was that they were from the same population. This suggests that the composition of the environment (oxygen, moisture content) plays a part in the degradation of heat-treated E-glass.

(vii) Composites manufactured from heat-treated E-glass fibres: Here, composites were fabricated and then the matrix was subjected to 650 °C in air for two hours. The unidirectional fibres were re-impregnated and the composite was manufactured. These fibres were extremely fragile and out of the 24 composites that were heat-treated and re-impregnated, only 20 of the composites were tested successfully. The reported scatter represents those that were tested successfully. The % reduction in the FRC when compared to the composites fabricated from the as-received E-glass fibres was 85%.

Table 4.8 Summary of the E-glass fibre composites that were produced and tested.

Sample	Duration of treatment in Acetone	Treatment Temperature and Time	Number of FRC Produced	Number of FRC Tested
As-received E-glass bundles			32	30
Solvent-treated E-glass bundle	72 hours	-	33	30
Heat-treated E-glass bundle		650 °C for 2 hours	35	30
Solvent-treated followed by heat treatment of E-glass fibre bundle	72 hours	650 °C for 2 hours	37	30
Vacuum & heat-treated of E-glass fibre bundle		650 °C for 2 hours	23	20
Solvent-treated, vacuum followed by heat treatment of E-glass fibre bundle	72 hours	650 °C for 2 hours	23	20
Recycled E-glass fibre		650 °C for 2 hours	26	20

Table 4.9 Summary of percentage strength loss of the fibre bundles when compared to the as-received E-glass fibre reinforced composite.

E-glass Fibre Bundle Types	(%) Degradation In the Tensile Strengths Relative to the As-received Composite
As-received	-
Solvent Treatment	31
Heat Treatment at 650 ℃	78
Solvent Treatment & then Heat Treatment at 650 ℃	82
Vacuum and Heat Treatment at 650 ℃	61
Solvent Treatment, Vacuum & then Heat Treatment at 650 ℃	66
Recycled (Composite manufactured using recovered E-glass fibres)	85

The data presented in Figure 4.33 compares the tensile strength of the composite (solid bars) and that of the fibre bundle per treatment. The general trend observed is that in all cases, a reduction in the tensile strength of the bundle is reflected in the tensile strength of the composites, as expected.

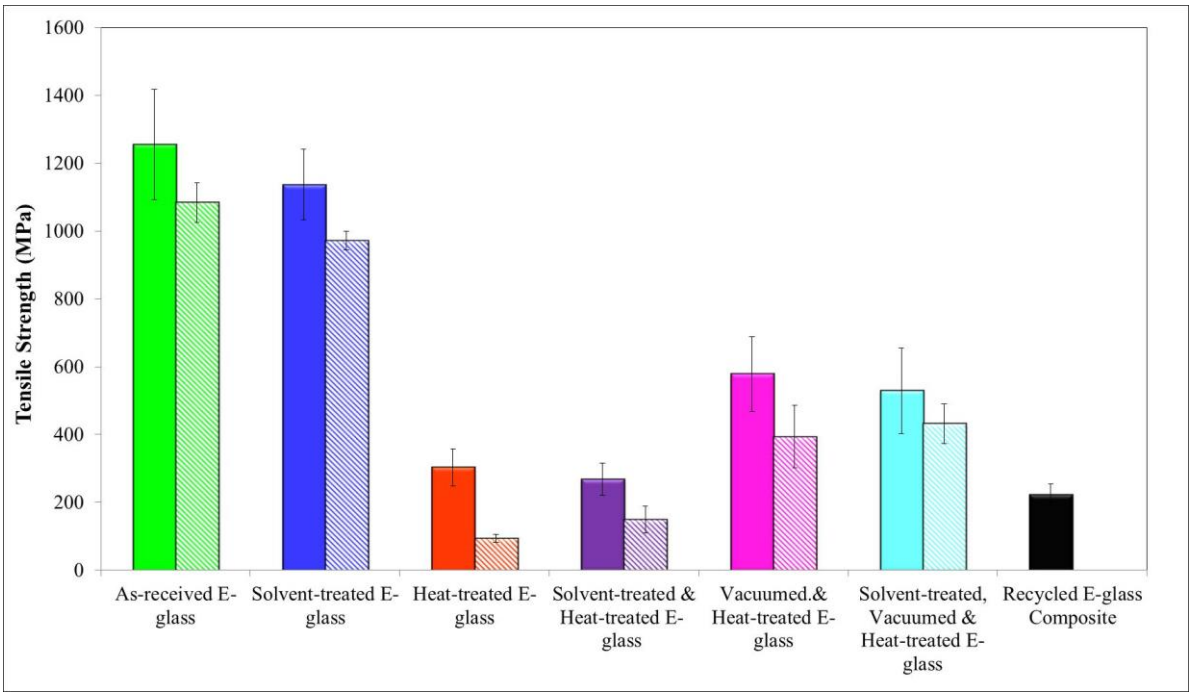

Figure 4.33 Tensile strength of as-received and various treatments of E-glass/epoxy composites and fibre bundles with the fibre bundles hashed.

Figure 4.34 illustrates the effect of the specified treatments on the un-normalised and normalised Young's modulus for all the composites investigated in this series of experiments. It was noted previously in Figure 4.26 that the effect of heat treatments at 450, 550 and 650 °C did not show any significant reduction in the Young's moduli. This observation is repeated in the case of the composites as seen in Figure 4.34 where the solid bars represent un-normalised data and the hashed bars indicate normalised data to 60% fibre volume fraction.

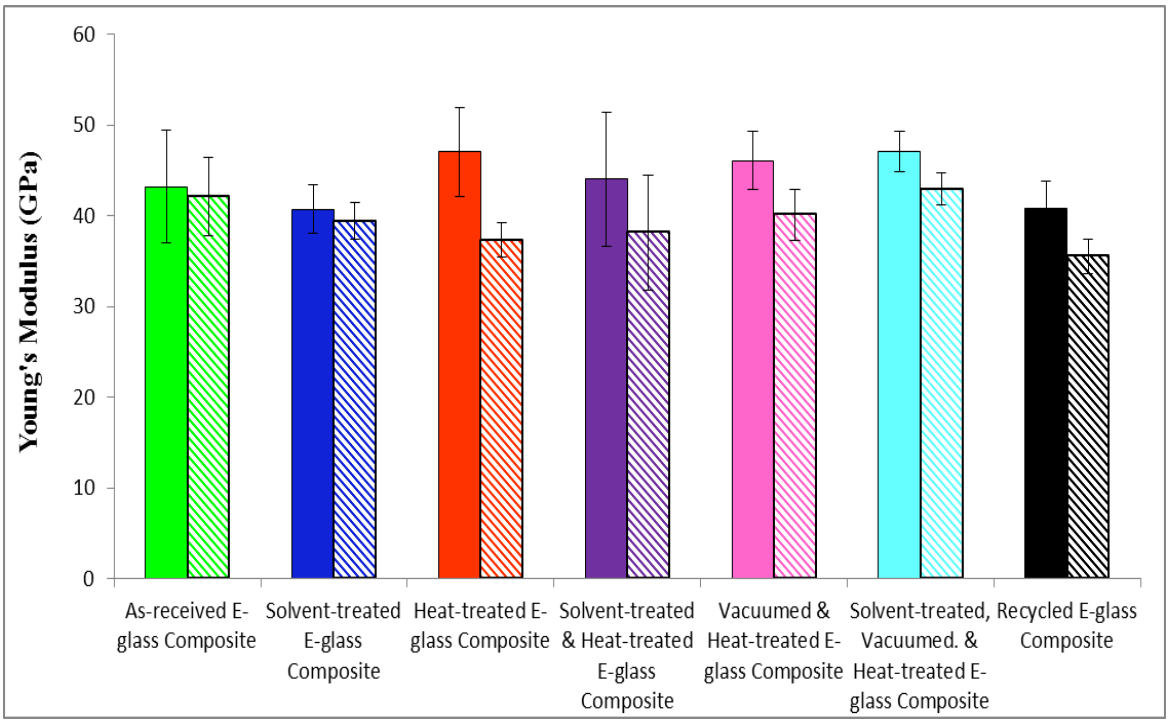

Figure 4.34 Un-normalised and normalised young modulus of the as-received and various treated E-glass/epoxy composites with normalised modulus hashed.

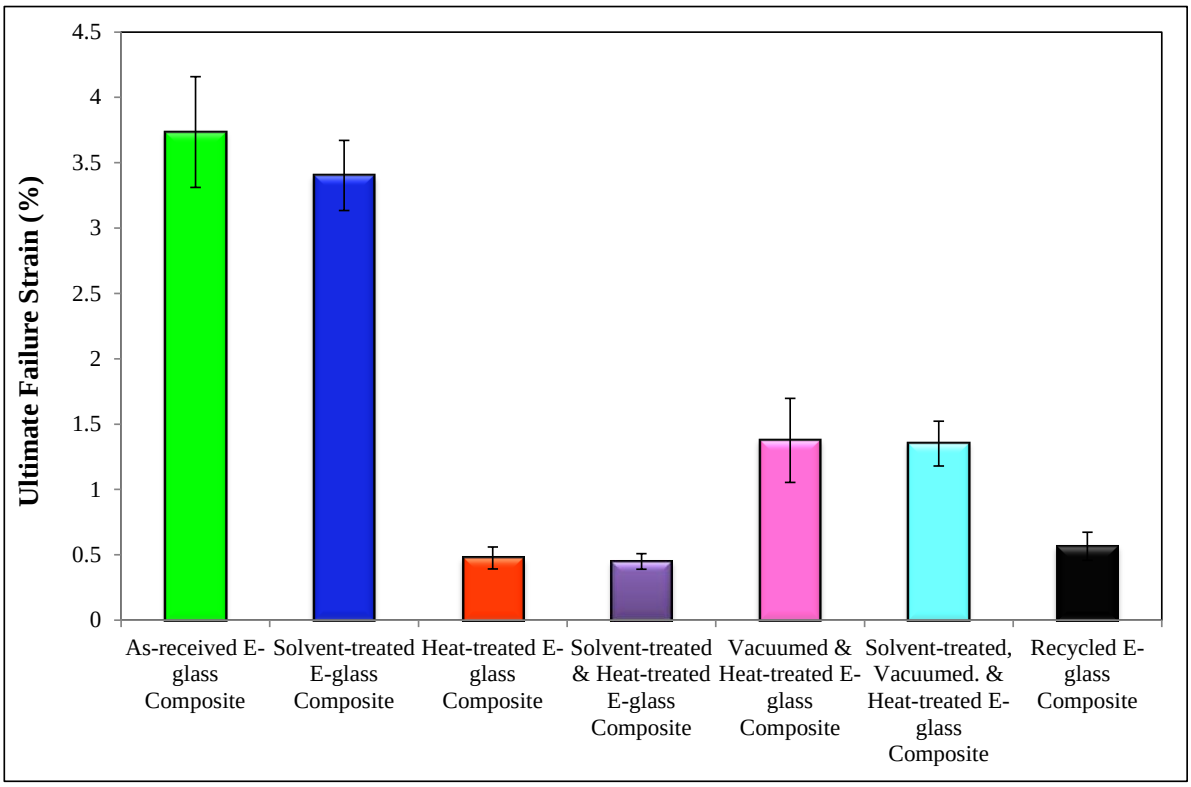

Figure 4.35 Ultimate failure strain data for E-glass composites tested in this series.

Figure 4.36 – 4.38 show SEM micrographs of the fractured composites for the as-received and thermally conditioned E-glass fibre. By examining the fracture mode, having considered the physical appearance of the fractured composites after testing; it can be seen from the micrographs that the as-received composites fractured by splitting along the longitudinal directions. Other composites produced from the thermally conditioned fibre bundles behaved slightly different. Composites produced from recycled fibres and fibres conditioned at 650 °C for two hours in air failed along the transverse direction with or without a trace of crack along the longitudinal direction. It was impossible to see any

fracture when the SEM of the flat surface of these samples were taken. In other words, the fractured fibres could only be seen when the observation was made along the transverse section. Contrary to this, as-received samples and composites produced from acetone-treated fibre bundles show the fracturing and splitting of the fibre filaments from the matrix along the longitudinal direction. The pattern of failure of composites made from fibre bundles conditioned in vacuum also has similarity with the as-received composites. The reasons for this have been discussed previously.

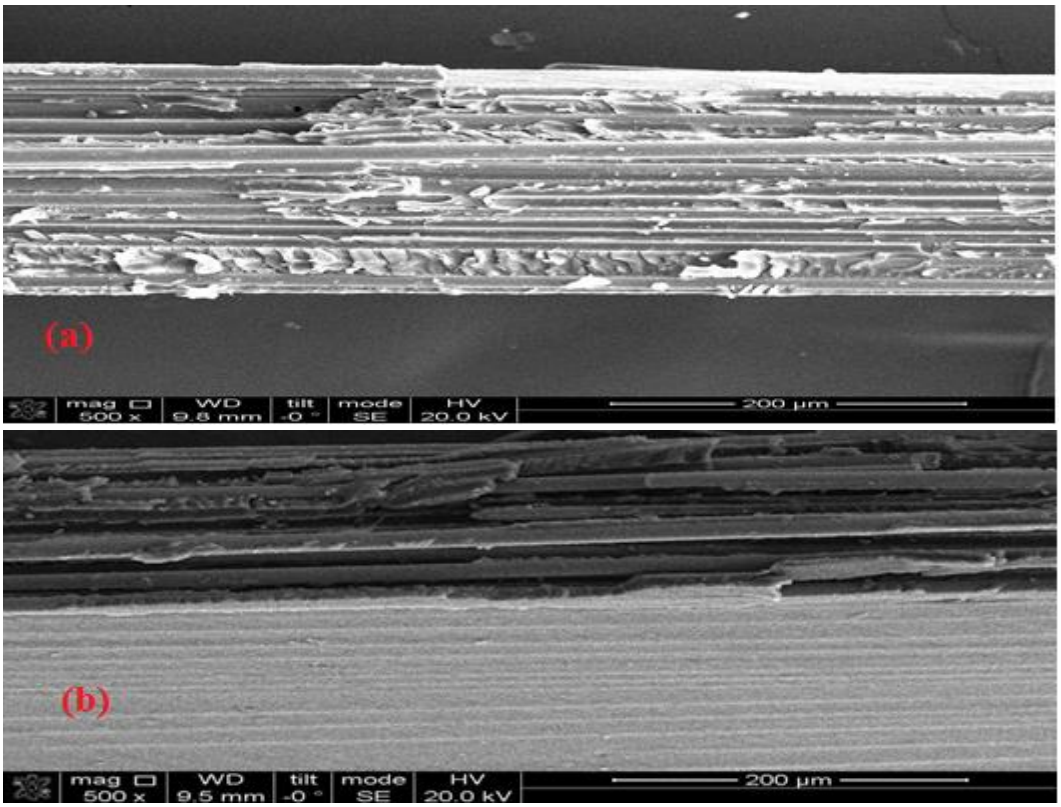

Figure 4.36 SEM images of fractured (a) as-received and (b) solvent-extracted E-glass/epoxy composites.

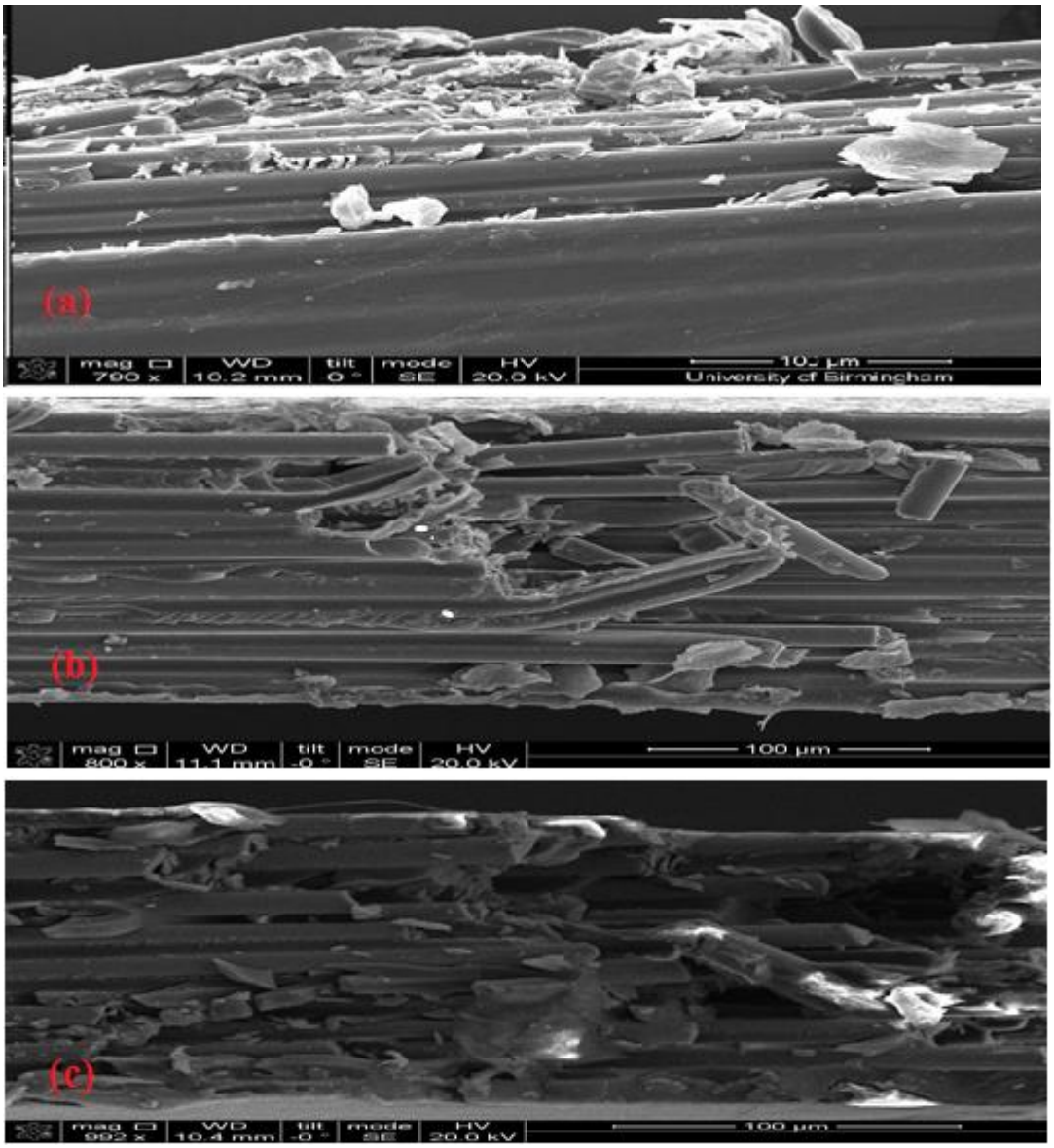

Figure 4.37 SEM images of fractured (a) heat-treated; (b) solvent-extracted and heat-treated; and (c) recycled E-glass/epoxy composites.

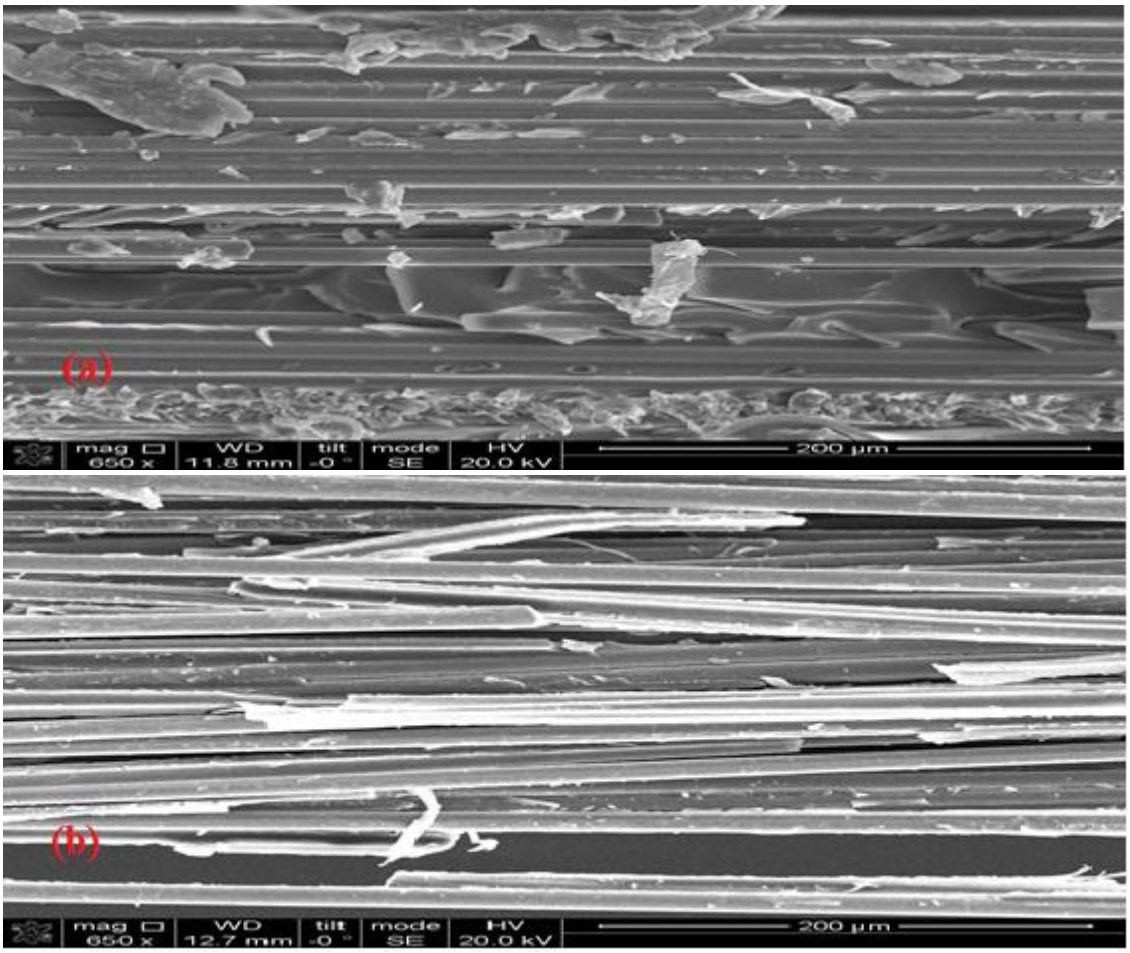

Figure 4.38 SEM images of fractured (a) solvent-extracted, vacuumed and heat-treated and (b) vacuumed and heat-treated E-glass/epoxy composites.

5 CONCLUSIONS

The rationale for undertaking this study was to investigate methods to minimise the reduction in tensile strength when E-glass fibres are subjected to binder removal and elevated temperatures. A new method for the partial removal of the binder was investigated involving fibre spreading. In this method, a custom-designed rig was used to enable the spreading of the filaments in a bundle where at the same time it resulted in de-cohesion and fragmentation of the binder.

Other methods to remove the binder were also investigated and these involved acetone extraction, heat treatment in air and in a vacuum. Since inter-filament interactions were identified in previous investigations as one of the primary causes for the degradation of tensile strength, the effect of using a lubricant was also investigated.

The fibre bundle test was used as the primary tool to study the degradation in the tensile properties of E-glass bundles in the as-received and treated conditions. A method was developed to manufacture composites using as-received and treated E-glass single bundles.

Binder removal using the fibre spreading technique did not lead to any degradation in the tensile properties. In fact, an apparent increase in the tensile strength was observed for the spread bundles when compared to the as-received bundle. It was concluded that this apparent increase in the tensile strength was due to: (i) more efficient impregnation and loading within the end-tabbed region of the single bundle; (ii) a greater degree of alignment

of the filaments in the spread bundles; (iii) the removal of fibre clusters as a consequence of removing excess binder. The average tensile strength for as-received 2400 Tex E-glass fibre bundles was 1.08 GPa and that for the spread bundle was 1.3 GPa. This finding has not been observed or reported previously.

Using these findings, the as-received properties of the E-glass bundle was used as the benchmark as far as the other surface treatments were concerned in this work. Heat treating E-glass bundles in air at 450 °C, 550 °C and 650 °C for two hours was found to decrease the tensile strength by 60%, 66%, and 90% respectively. Heating E-glass bundles in a vacuum at 650 °C for two hours resulted in a reduction of 63% in the tensile strength. It was observed that the strength of the fibre bundles degraded as the time of samples exposure to air increases (that is between the period of removing the sample from the vacuum > to being stored away in a desiccator > to being prepared for tensile testing). It was concluded that the moisture in the air led to the observed degradation in tensile properties. In other words, the E-glass bundles that were heated in air were also cooled in air. Whereas, the E-glass fibre bundles that were subjected to heating in a vacuum were sealed in quartz tubes and these were cooled in a vacuum.

After subjecting the E-glass bundles to the above-mentioned treatments (heating in air and vacuum, and solvent-based binder extraction), composites were fabricated and tensile tested. The reduction in the tensile properties of the composites was found to be proportional to that obtained for the fibre bundles at the corresponding fibre volume fractions. The reductions in the tensile strengths for composites manufactured using the

specified treatments when compared to composites manufactured using as-received fibres was as follows:

(i) solvent treatment lead to a reduction of 31%;

(ii) heat treatment in air at 650 ℃ for two hours resulted in a 78% reduction;

(iii) solvent treatment followed by heating in air, at 650 ℃ for two hours gave a reduction of 82%;

(iv) solvent treatment followed by heating in a vacuum, at 650 ℃ for two hours led to a reduction of 61%;

(v) heat treatment of as-received E-glass in a vacuum at 650 ℃ for two hours resulted in a reduction of 66%;

A method for filtering the AE data was proposed and implemented whereby the parameters used were “absolute energy” and the duration of the hits. This was found to remove spurious AE hits. These parameters were identified using oil-lubricated bundles.

6 RECOMMENDATIONS FOR FUTURE RESEARCH

(i) The following analytical tools were used to characterise the as-received and treated E-glass fibres; (a) diffraction scanning calorimetry – to investigate if crystallisation has occurred during the slow-cooling after exposure to 450, 550 and 650 °C. (b) X-ray diffraction – to determine if crystallisation has occurred during slow cooling. (c) Raman spectroscopy – to infer if crystallisation has occurred during slow cooling. (d) Surface ion mass spectroscopy – to determine if low atomic number element had diffused to the surface of the glass fibres that altering the stress field from compression to tension on the surface. Regrettably, consistent results could not be obtained using the above mentioned techniques. A focus and in-depth study should be undertaking using one or more of the above mentioned techniques in conjunction with E-glass fibre under controlled conditions.

(ii) A cold vapour mist was used to quench the heat-treated fibre. However, the rate of cooling that could be attained was insufficient to determine if crystallisation was an issue. It is recommended that instrumentation and experimental protocols be developed to enable E-glass fibres, to be heated to temperature above 450 °C followed by rapid quenching to simulate that achieved during the production of E-glass.

(iii) Whilst the end-tabbing operation was necessary, it was labour intensive and time consuming. A capstan-based technique for loading a single bundle should be used in future studies.

(iv) High resolution SEM and TEM should be used to study the consequences of heat treatment on the external and internal morphology of E-glass fibres.

(v) Note the location on the creel from which the sample was obtained. These samples should be treated at different temperatures.

(vi) Identify the length at which behaviour observed in 50 mm gauge length occurs.

(vii) Identify the variability in the diameter of fibre measured.

7 REFERENCES

AGRAWAL, B. D. & BROUTMAN, L. J. 1990. Analysis and performance of fiber composites. *Materials and manufacturing processes.* New York: John Wiley and Sons Inc.

AL-KHUDAIRI, O., HADAVINIA, H., WAGGOTT, A., LEWIS, E. & LITTLE, C. 2014. Characterising mode I/mode II fatugue delamination growth in unidirectional fibre reinforced polymer laminates. *Materials and Design,* 66**,** 93-102.

ANDERSONS, J., JOFFE, R., HOJO, M. & OCHIAI, S. 2002. Glass fibre strength distribution determined by common experimental methods. *Composites Science and Technology,* 62**,** 131-145.

ASOKAN, R., ARUMUGAM, V., SANTULI, C. & STANLEY, A. J. 2012. Acoustic emission monitoring of repaired composite laminates. *Reinforced Plastics & Composites,* 31**,** 1226-1235.

BAGHERPOUR, S. 2012. Fiber reinforced polyester composites. INTECH.

BAINES, M. & CARRUTHERS, J. 2013. Composite Materials: A resource efficiency action plan. *In:* HALLIWELL, S. (ed.) *The green construction board.* UK: Composites Trade Association, UK.

BAO, G., FAN, B. & EVANS, A. G. 1992. Mixed mode delamination cracking in brittle matrix composites *Mechanics of Materials,* 13**,** 59-66.

BAO, G. & SUO, Z. 1992. Remarks on crack-bridging concepts. *Journal of Applied Mechanics,* 45.

BAR-SINAI, Y., SPATSCHEK, R., BRENER, E. & BOUCHBINDER, E. 2014. On the velocity-strengthening behavior of dry friction. *Journal of Geophysical Research / Solid Earth,* 119**,** 1738 - 1748.

BARTENEV, G. M. 1968. Constitution and strength of glass fibers. *International Journal of Fracture Mechanics,* 5.

BEDANTA, S., BARMAN, A., KLEEMANN, W., PETRACIC, O. & SEKI, T. 2013. Magnetic Nanoparticles: A Subject for Both Fundamental Research and Applications144. *Journal of Nanomaterials,* 2013**,** 22 pp.

BERGMAN, B. 1984. On the estimation of the Weibull modulus. *Journal of Materials Science,* 3**,** 689-692.

BLAIR, W., FARKAS, E. G. & GOOCH, M. B. 2015. Composites. *In:* BLAIR, W. (ed.) *Specialty Materials Setor Update.* UK: William Blair & Company.

BOCK, M., UMATHUM, R., SIKORA, J., BRENNER, S., AGNOR, E. N. & SEMMLER, W. 2006. A faraday position sensor for interventional magnetic resonance imaging. *IOP Electronic Journal.*

BOTT, T. R. & BARKER, A. J. 1968. Defects on glass fiber surfaces *In:* EITEL, W. (ed.) *Glass Science.*

BREARLEY, W. & HOLLOWAY, D. G. 1963. *Phys. Chem. Glasses,* 4**,** 69.
BROWN, E. N., DAVIS, A. K., JONNALAGADDA, K. D. & SOTTOS, N. R. 2004. Effect of surface treatment on the hydrolytic stability of E-glass fiber bundle tensile strength. *Composites Science and Technology,* 65**,** 129-136.
BRÜCKEL, T. Introduction: Neutron Scattering in Contemporary Research. JCNS Neutron Laboratory Course, 2013 2 Sep 2013 - 13 Sep 2013, Jülich (Germany).
BUNSELL, A. R. & RENARD, J. 2005. *Series in material science and engineering - Fundamentals of fibre reinforced composite materials,* Bristol and Philadelphia, Institute of Physics Publishing.
CALVEZ, L., ROSE, M., MA, H. L., SANGLEBOEUF, J. C., GUIN, J.-P. & ZHANG, X. H. 2009. Strengthening of chalco-halide glasses by ion exchange. *Journal of Non-oxide and Photonic Glasses,* 1**,** 30-37.
CAMERON, N. M. 1960. An investigation of the factors likely to affect the strength and properties of glass fibres. *Physical Chem. Glass,* 1**,** 4-18.
CAMERON, N. M. 1968. The effect of environment and temperature on the strength of E-glass fibres. Part 2. Heating and ageing. *Glass Tech.,* 9**,** 121-130.
CARMAN, L. A. & PANTANO, C. G. 1990. Water-vapor adsorption on calcium-boroaluminosilicate glass fibers. *Journal of Non-Crystalline Solids,* 120**,** 40-46.
CARRE, H. & DAUDEVILLE, L. 1996. Numerical simulation of soda-lime silicate glass tempering. *Journal de Physique IV,* 1996**,** C1-175-C1-185.
CECH, V., PRIKRYL, R., BALKOVA, R., GRYCOVA, A. & VANEK, J. 2002. Plasma surface treatment and modification of glass fibers. *Composites Part A,* 33**,** 1367-1372.
CHAN, K. L. A. & KAZARIAN, S. G. 2016. Attenuated total reflection Fourier-transform infrared (ATR-FTIR) imaging of tissues and live cells. *The Royal Society of Chemistry,* 200166**,** 1850-1864.
CHANDA, M. & ROY, S. K. 2009. Plastics fabrication and recycling - Plastic engijneering series. London: Taylor & Francis Group-CRC Press
CHANG, N.-B. & PIRES, A. 2015. Sustainable solid waste management - A systems engineering approach. *In:* ZHOU, M. (ed.). New Jersey: John Wiley & Sons.
CHERIN, A. H. 1983. Optical Fibers *An introduction to optical fibers.* Shepherdstown, W.V. USA: McGraw-Hill.
CHUNG, D. D. L. 2001. Applied Materials Science. *Applications of engineering materials in structural, electronics, thermal, and other industries.* London: CRC Press LLC.
CICCOTTI, M. 2009. Stress-corrosion mechanisms in silicate glasses. *Journal of Phys. D.: Applied Phys.*
CLEMENTS, L. L. & MOORE, R. L. 1978. Composite properties for E-glass fibres in a room temperature curable epoxy matrix. *Composites***,** 93-99.
COLORADO, H. A., HIEL, C. & YANG, J.-M. 2013. Different fibers exposed to temperatures up to 1000 ºC. *In:* SINGH, D., SALEM, J., KIRIHARA, S. & WIDJAJA, S. (eds.) *Mechanical Properties and Performance of Engineering Ceramics and Composites VIII: Ceramic Engineering and Science Proceedings* New Jersey, USA: JohnWiley & Sons.

COOPER, A. R. & KROHN, D. A. 1969. Strengthening of glass fibers: II, Ion exchange. *Journal of American Ceramic Society*, 52.

CORNELISSEN, B. 2012. The role of friction in tow mechanics. *PhD Thesis, University of Twente*.

COWKING, A., ATTOU, A., SIDDIQUI, A. M., SWEET, M. A. S. & HILL, R. 1991. Testing E-glass fibre bundles using acoustic emission. *ournal of Materials Science,* 26**,** 1301-1310.

CREASY, T. S. 2000. A method of extracting Weibull survival model parameters from filament bundle load/strain data. *Composites science and technology,* 60**,** 825-832.

CUNLIFFE, A. M., JONES, N., & WILLIAMS, P. T. 2003. Pyrolysis of composite plastic waste. *Environmental technology*, 24**,** 653-663.

DALAI, R. P. & RAY, B. C. 2010. Loading rate sensitivity of fibrous composite materials. *International Conference on Recent Trends in Materials and Characterisation (RETMAC-2010).*

DAUDEVILLE, L. & CARRE, H. 1998. Thermal temperaing simulation of glass plates: Inner and edge residual stresses. *Jorn. of Thermal Stresses,* 21**,** 667-689.

DAVIS, K. M. & TOMOZAWA, M. 1994. Water diffusion into silica glass: structural changes in silica glass and their effect on water solubility and diffusivity. *Journal of Non-Crystalline Solids,* 185**,** 203-220.

DEROSA, R., GAUSTAD, G., TELFEYAN, E. & MAYES, J. S. 2004. Microscopical evaluation of recycled glass reinforced polymer matrix composites. *Microscopy and Analysis*, 18**,** ??-??

DONALD, I. W. 1989. Review: Methods for improving the mechanical properties of oxide glasses. *Journal of Materials Science*, 24**,** 4177-4208.

DURAI PRABBHAKARAN, T. R., TOM, A. L., MALTE CHRISTEN, M. & HANS LILHOLT, M., BO. Tensile and compression properties of hybrid composites - A comparative study. Proceedings of the 19th International Conference on Composite Materials (ICCM19), 2013 Canada. 1029-1035.

EC, B. 2005. "COM(2005) 666 final, Taking Sustainable Resource Use Forward: A Thematic Strategy on the Prevention and Recycling of Waste. *In:* EC, B. (ed.). Brussels.

FAUCHER, B. & TYSON, W. R. 1988. On the determination of Weibull parameters. *Journal of Materials Science***,** 1199-1203.

FAUDREE, M. C. & NISHI, Y. 2010. Tensile strength enhancement by shortening glass fibers with sub-millimeter length in bulk molding polymer compound. *Materials Transactions,* 51**,** 2304-2310.

FEIH, S., BOIOCCHI, E., MATHYS, Z., GIBSON, A. G. & MOURITZ, A. P. 2011. Mechanical properties of thermally-treated and recycled glass fibres. *Composites Part B,* 42**,** 350-358.

FEIH, S., MOURITZ, A. P., MATHYS, Z. & GIBSON, A. G. 2009. Strength degradation of glass fibers at high temperatures. *Journal of Material Science,* 44**,** 392-400.

FEIH, S., MOURITZ, A. P., MATHYS, Z., & GIBSON, A. G. 2010. Fire structural modeling of polymer composites with passive thermal barrier. *Fire Sciences,* 28**,** 141-160.

FERNANDO, G. F. & AL-KHODAIRI, F. A. A. (eds.) 2003. *The fatigue of hybrid composites,* Middx., England: Woodhead Publishing Ltd.

FRANCOIS, D., PINEAU, A. & ZAOUI, A. 2013. Mechanical Behaviour of Materials. *Fracture mechanics and damage.* New York: Springer Science+Business media.

FREIMAN, S. 2012. The Fracture of Glass: Past, Present, and Future. *International Journal of Applied Glass Science,* 3**,** 89-106.

GAO, L., ZAI, F., SU, S., WANG, H., CHEN, P. & LIU, L. 2011. Study and application od acoustic emission testing in fault diagnosis of low-speed heavy-duty gears. *Sensors,* 2011**,** 599-611.

GERARD, J. & KANDLIKAR, M. 2007. "Is European end-of-life vehicle legislation living up to expectations? Assessing the impact of the ELV Directive on green innovation and vehicle.". *Journal of Cleaner Production,* 15**,** 17-27.

GHOSH, S. B., JONES, F. R. & HAND, R. J. 2010. A novel indentation based method to determine the threshold stress intensity factor for sub-critical crack growth in glass. *Glass Tech.: Eur. J. Glass Sci. Techn. A,* 51**,** 156-160.

GONG, G., OLOFSSON, K., NYSTROM, B., JUNTIKKA, M., OXFALL, H. & LINDQVIST, K. 2016. Experimental verification of Re-Fib method for recycling fibres from composites. *Advanced Manufacturing: Polymer & Composite Science,* 2016**,** 27-33.

GOROWARA, R. L., KOSIK, W. E., MCKNIGHT, S. H. & MCCULLOUGH, R. L. 2001. Molecular characterization of glass fiber surface coatings for thermosetting polymer matrix/glass fiber composites. *Composites Part A: Applied Science and Manufacturing,* 32**,** 323-329.

GRIFFITH, A. A. 1921. The theory of rupture. *Phil. Trans. Royal Society (London)***,** 55-63.

GROSSE, C. U., & KRÜGER, M. 2006. Inspection and monitoring of structures in civil engineering. *The E-Journal of Non-Destructive Testing,* 11.

GUILD, F. J., PHILLIPS, M. G. & HARRIS, B. 1980. Acoustic emission studies of damage in GRP. *NDT & E International*.

GY, R. 2008. Ion exchange for glass strengthening. *Materials Science and Engineering,* B**,** 159-165.

HALDIMANN, M., LUIBLE, A. & OVEREND, M. 2008. Structural use of glass. *Structural Engineering Document.* Zurich, Switzerland: International Association for Bridge and Structural Engineering.

HALLIWELL, S. 2006. End of life options for composite waste: Recycle, reuse or dispose? *National Composite Network Best Practice Guide* [Online]. Available: http:/www.netcomposites.com.

HAMAD, K., KASEEM, M. & DERI, F. 2013. Recycling of waste from polymer materials: An overview of the recent works. *Polymer Degradation and Stability,* 98**,** 2801-2812.

HAMSTAD, M. A., AND MOORE, R. L. 1986. Acoustic emission from single and multiple Kevlar 49 filament breaks. *Journal of phys. D,* 20**,** 47.
HARRIS, B. 1999. Engineering composite materials. *The Institute of Materials, London.*
HE, J. & CLARKE, D. R. 1997. Determination of fibre strength distributions from bundle tests using optical luminescence spectroscopy. *The Royal Society,* 453**,** 1881-1901.
HENCH, L. L. & CLARK, D. E. 1978. Physical chemistry of glass surfaces. *Journal of Non-crystalline Solids,* 28**,** 83-105.
HILL, C. L., GUELETII, Y. V., MUSAEV, D. G., YIN, Q. & BOTAR, B. 2012. POLYOXOMETALATE WATER OXIDATION CATALYSTS AND METHODS OF USE THEREOF.
HILL, R. & OKOROAFOR, E. U. 1995. Weibull statistics of fibre bundle failure using mechanical and acoustic emission testing: the influence of interfibre friction. *Composites,* 26**,** 699-705.
HITCHON, J. W. & PHILLIPS, D. C. 1978. The effect of specimen size on the strength of CFRP. *Composites Part A.*
HOGAN, P. M. 1981. *Glass article strengthened by ion exchange substitution*. 118,193.
HOLLAWAY, L., CHRYSSANTHROPOULOS, M. K. & MOY, S. S. J. 2004. *Advanced Polymer Composites for Structural Applications in Construction,* Abington, Cambridge, England, Woodhead Publishing Limited.
HORNBOLL, L., KNUSEN, T., YUE, Y. & GUO, X. 2010. Heterogeneous enthalpy relaxation in glasses far from equilibrium. *Chemical Physics Letters,* 494**,** 37-40.
HORNBOLL, L. & YUE, Y. 2007. Enthalpy relaxation in hyperquenched glasses of different fragility *Journal of Non-Crystalline Solids,* 354**,** 1862-1870.
HU, H. & LIU, Y. 2010. High modulus, high tenacity yarns. *In:* ALAGIRUSAMI, A. D. (ed.) *Technical textile yarns.* Woodhead Publishing Limited.
HULL, D. & CLYNE, W. 1996. *An Introduction to Composite Materials,* Cambridge, Cambridge University Press.
ILANKEERAN, P. K., MOHITE, P. M. & KAMLE, S. 2012. Axial tensile testing of single fibres. *Modern Mechanical Engineering,* 2012**,** 151-156.
ISHIDA, H. & KOENIG, J. L. 1978. The reinforcement mechanism of fiber-glass reinforced plastics under wet conditions: A review. *Polymer Engineering and Science,* 18.
(ISO), I. O. F. S. 2009. Plastics - Determination of tensile properties *Part 5: Test conditions for unidirectional fibre reinforced plastic composites.* ISO.
ITO, S. & TOMOZAWA, M. 1982. Crack blunting of high-silica glass. *Journal of American Ceramic Society,* 65.
IVASHCHENKO, S., IVIRICO, J. L. E., CRUZ, D. M. G., CAMPILLO-FERNANDEZ, A., FERRER, G. G. & PRADAS, M. M. 2014. Bioactive organic-inorganic poly(CLMA-co-HEA)/silica nanocomposites. *Journal of Biomaterials Applications,* 0**,** 1-13.
IRFAN, M. S., MACHAVARAM, V. R., MAHENDRAN, R. S., SHOTTON-GALE, N., WAIT, C. F., PAGET, M. A., HUDSON, M. & FERNANDO, G. F. 2012. Lateral spreading of a fibre bundle via mechanical means. *Journal of Composite Materials,*

46**,** 311-330.JARVELA, P. K. 1984. Bending strength and static fatigue of glass fibre in different atmospheres by fibre loop test. *Journal of Materials Science,* 19**,** 2481-2487.
JAYATILAKA, A. D. S. & TRUSTRUM, K. 1977. Statistical approach to brittle fracture. *Journal of Materials Science,* 12**,** 1426-1430.
JENKINS, P. G., RIOPEDRE-MENDEZ, S., SAEZ-RODRIGUEZ, E., YANG, L. & THOMASON, J. L. 2015a. Investigation of the strength of thermally conditioned basalt and E-glass fibres. *20th International Conference on Composite Materials.* Copenhagen.
JENKINS, P. G., YANG, L., LIGGAT, J. J. & THOMASON, J. L. 2015b. Investigation of the strength loss of glass fibre after thermal conditioning. *Journal of Material Science,* 50**,** 1050-1057.
JIN, L., JIA, C.-L. & VREJOIU, I. 2014. Engineering 180° ferroelectric domains in epitaxial PbTiO3 thin films by varying the thickness of the underlying (La,Sr)MnO3 layer. *Applied Physics Letters,* 105**,** 132903.
JOB, S. 2013. Recycling glass fibre reinforced composites: history and progress. *Reinforced Plastics.* Elsevier.
JONES, F. R. 2001. Glass fibre *In:* HEARLE, J. W. S. (ed.) *High performance fibres.* Cambridge: Woodhead Publishing Ltd.
JONES, F. R. 2010. A review of interphase formation and design in fibre reinforced composites. *Journal of Adhesion Science and Technology,* 24**,** 171-202.
JONES, R. M. 1999. *Mechanics of composite materials,* Philadelphia, Taylor and Francis Inc.
KADOGAWA, Y. & YAMATE, T. 1971. Studies on the surface structure of chemically strengthened glasses: Part 1. Some properties of ion-exchanged glasses. *Tech. Rep. Kansai Univ.*
KALIDASS, R. & BALAJI, S. 2014. Tensile Test for Environmental Effect On Glass Fiber Composite Materials. *The International Journal of Engineering and Science,* 3**,** 23-27.
KAO, C., OLIVEUX, G., HALLAM, K., & GHITA, O. 2010. A mechanical study of glass fibres recovered from solvolysis process. *University of Exeter*.
KARLSSON, S. 2012. *Modification of float glass surfaces by ion exchange.* PhD, Linnaeus University.
KARLSSON, S., JONSON, B. & STALHANDSKE, C. 2010. The technology of chemical glass strengthening - a review. *Glass Tech.: Eur. J. Glass Sci. Techn. A,* 51**,** 41-54.
KENNERLEY, J. 1998. *Recycling fibres recovered from composite materials using a fluidised bed process.* PhD, University of Nottingham.
KENNERLEY, J. R., FENWICK, N. J., PICKERING, S. J. & RUDD, C. D. 1997. The properties of glass fibers recycled from the thermal processing of scrap thermoset composites. *Vinyl & additive technology,* 3.
KHALILI, A. & KROMP, K. 1991. Statistical properties of Weibull estimators. *Journal of Materials Science,* 26**,** 6741-6752.

KHENNANE, A. & MELCHERS, R. E. 2003. Durability of glass polymer composites subject to stress coorrosion. *Jouurnal of American Ceramic Society,* 2**,** 1090-0268.

KIM, T., OSHIMA, K. & KAWADA, H. 2013. Impact tensile properties and strength development mechanism of glass for reinforcement fiber. *Journal of Physics,* 451.

KINSELLA, M., MURRAY, D., CRANE, D., MANCINELLI, J. & KRANJE, M. 2001. Mechanical properties of polymeric composites reinforced with high strength glass fibers. International Comp.

KOIKE, A., TOMOZAWA, M. & ITO, S. 2007. Sub-critical crack growth rate of soda-lime-silicate glass and less brittle glass as a function of fictive temperature. *Journal of Non-Crystalline Solids,* 353**,** 2675-2680.

KORWIN-EDSON, M. L., HOFMANN, D. A. & MCGINNIS, P. B. 2012. Strength of high performance glass reinforcement fiber. *International Journal of Applied Glass Science,* 3**,** 107-121.

KOUVARAKOS, M. & HILL, E. V. K. 1996. Isolating tensile failure mechanisms in fiberglass epoxy from acoustic emission signal parameters. *Materials Evaluation,* 54.

LAMMON-HILINSKI, K., MORFESIS, A. & UNITES, T. P. 2001. *Photocatalytic filter with fiber glass mat carrier*. United States patent application.

LEE, S. M. 1993. Handbook of composite reinforcements. *In:* LEE, S. M. (ed.). California, USA: Wiley VCH Publisher Inc.

LETERRIER, Y. 2000. Life cycle engineering of composites. *Comprehensive Composite Materials.* Elsevier Science Ltd.

LEZZI, P. J., EVKE, E. E., AALDENBERG, E. M. & TOMOZAWA, M. 2015. Surface crystallization and water diffusion of silica glass fibers: Causes of mechanical strength degradation. *Journal of American Ceramic Society***,** 1-11.

LI, H. & TOMOZAWA, M. 1995. Effects of water in simulated borosilicate-based nuclear waste glass on their properties. *Journal of Non-Crystalline Solids,* 195**,** 188-198.

LIU, X., JONES, F. J., THOMASON, J. L. & ROEKENS, B. J. An XPS study of organosilane and sizing adsorption on E-glass fibre surface. 16th International Conference on Composite Materials, 2007 Kyoto, Japan.

LIU, X., THOMASON, J. L. & JONES, F. R. 2008. XPS and AFM study of interaction of organosilane and sizing with E-glass fibre surface. *The Journal of Adhesion,* 84**,** 322-338.

LIU, X. M., THOMASON, J. L. & JONES, F. R. 2009. XPS and AFM study of the structure of hydrolysed aminosilane on E-glass surfaces. Glasgow: Strathclyde University.

LOEWENSTEIN, K. L. 1962. *Glass Compositions.*

LOPEZ, F. A., MARTIN, M. I., ALGUACIL, F. J., RINCON, J. M., CENTENO, T. A. & ROMERO, M. 2012a. Thermolysis of fibreglass polyester composite and reutilisation of the fibre residue to obtain a glass-ceramic material. *Journal of Analytical and Applied Pyrolysis,* 93**,** 104-112.

LOPEZ, F. A., MARTIN, M. I., GARCIA-DIAZ, I., RODRIGUEZ, O., ALGUACIL, F. J. & ROMERO, M. 2012b. Recycling of Glass Fibers from Fiberglass Polyester Waste

Composite for the Manufacture of Glass-Ceramic Materials. *Journal of Environmental Protection,* 3**,** 740-747.

LU, X., ARRUDA, E. M. & SCHULTZ, W. W. 1998. The effect of processing parameters on glass fiber birefringence development and relaxation. *Journal of Non-Newtonian Fluid Mechanics,* 86**,** 89-104.

LUND, M. D. 2010. *Tensile Strength of Glass Fibres.* PhD, Aalborg University.

LUND, M. D. & YUE, Y. 2005. Influences of thermal and chemical ageing on the surface morphology and crystallization behaviour of basaltic glass fibre. *International Symposium on Glass.* Shanghai, China: Crystalline Solids.

MAHATO, K. K., BISWAL, M., RATHORE, D. K., PRUSTY, R. K., DUTTA, K. & RAY, B. C. Effect of loading rate on tensile properties and failure behaviour of glass fibre/epoxy composite. 5th National Conference on Processing and Characterisation of Materials, 2016. Materials Science Engineering.

MALLICK, K. K. & HOLLAND, D. 2013. A method of surface strengthening of soda lime aluminosilicate glasses bi Li and Al ion vapour treatment. *Journal of Material Science,* 2013**,** 5012-5021.

MANDERS, P. W. & CHOU, T.-W. 1983. Variability of carbon and glass fibers, and the strength of aligned composites. *Journal of Reinforced Plastics and Composites,* 2.

MATTEWSON, M. J. & KURKJIAN, C. R. 1987. Static fatigue of optical fibers in bending. *Journal of American Ceamic Society,* 70**,** 662-68.

MAURO, J. C., LOUCKS, R. J. & GUPTA, P. K. 2008. Fictive temperature and the glassy state. *Journal of American Ceramic Society,* 92**,** 75-86.

MAXWELL, A. S., BROUGHTON, W. R., DEAN, G. & SIMS, G. D. 2005. Review of accelerated ageing methods and lifetime prediction techniques for polymeric materials. Middlesex, united Kingdom: National Physical Laboratory.

MCGRAVEY, M. P. 2008. *An Investigation into the Structure and Performance of a Glass Fibre Size.* PhD, Durham University.

MCKINNIS, C. L. & SUTTON, J. W. 1959. the glassmelting process: II, glass structure andthe effects of "melting history" on glass properties. *Journal of American Ceramic Society*.

MICHALSKE, T. A. & FREIMAN, S. W. 1983. A molecular mechanism for stress corrosion in vitreous silica. *Journal of American Ceramic Society,* 66**,** 284-288.

MONNIER, T., DIA, S., GODIN, N. & ZHANG, F. 2012. Primary calibration of acoustic emission sensors by the method of reciprocity, theoretical and experimental considerations. *Journal of Acoustic Emission,* 30**,** 152-166.

MOURITZ, A. P., MATHYS, Z. 1999. Post-fire mechanical properties of marine polymer composites *Composites Structures,* 47**,** 643-653.

MURRAY, R. 2016. *Design and development of a new class of intra-filament hybrid composite.* PhD, University of Birmingham.

NAIMEH, K. 2004. Design principles for glass used structurally. Lund Universitet: Lund University.

NORDBERG, M. E., MOCHEL, E. L., GARFINKEL, H. M. & OLCOTT, J. S. 1964. Strengthening by ion exchange. *Journal of American Ceramic Society,* 47**,** 215-19.

NORIHIKO, T., ARAO, Y., NISHIWAKI, T., HIRAYAMA, N., NAKAMURA, K. & KAWADA, H. 2012. Experimental study on impact tensile property of glass fiber. *Advanced Composite Materials,* 21**,** 165-175.

OEHLER, A. & TOMOZAWA, M. 2004. Water diffusion into silica glass at a low temperature under high water vapor pressure. *Journal of Non-Crystalline Solids,* 347**,** 211-219.

OLIVEUX, G., BAILLEUL, J.-L. & LA SALLE, E. L. G. 2012. Chemical recycling of glass fibre reinforced composites using subcritical water. *Composites Part A,* 43**,** 1809-1818.

OSKOUEI, A. R., & AHMADI, M. 2009. Fracture strength distribution in E-glass fiber using acoustic emission. *Composites Materials,* 44**,** 693-705.

OSKOUEI, A. R. & MEHDI, A. 2010. Acoustic emission characteristics of mode I delamination in glass/polyester composites. *Journal of Composite Materials,* 44**,** 793-807.

OTHEGUY, M. E., GIBSON, A. G., ROBINSON, M., FINDON, E., CRIPPS, B., MENDOZA, A. O. & AGUINACO CASTRO, M. T. 2009. Recycling of end-of-life thermoplastic composite boats. *Plastic Rubber and Composites*.

PAHLER, G. & BRUCKNER, R. 1982. Mechanical properties and strujctural aspects of binary phosphate glass fibers. *Journal of Non-crystalline Solids,* 49**,** 487-496.

PARDINI, L. C. & MANHANI, L. G. 2002. Influence of the testing gage length on the strength, Young's Modulus and Weibull modulus of carbon fibres and glass fibres. *Material Research,* 5**,** 411-420.

PETERSEN, H. N., KUSANO, Y., BRONDSTED, P. & ALMDAL, K. Preliminary chacterization of glass fiber sizing. 34th International Symposium on Materials Science, 2013 Denmark. Technical University of Denmark.

PHOENIX, S. L. & WU, E. M. 1983. Statistics for the time-dependent failure of Kevlar-49/epoxy composites: micromechanical modeling and data interpretation. National Technical Information Service.

PICKERING, S. J. 2005. Recycling technologies for thermoset composite materials—current status. *Composites Part A: Applied Science and Manufacturing,* 37**,** 1206-1215.

PICKERING, S. J., KELLY, R. M., KENNERLEY, J. R., RUDD, C. D. & FENWICK, N. J. 2000. A Fluidized-bed Process for the Recovery of Glass Fibres from Scrap Thermoset Composites. *Composites Science and Technology,* 60**,** 509-523.

PICO, D., & BARTL, A. 2010. Chemical treatment of glass fibers after composite recycling process. *Institute of chemical engineering, Vienna university of technology*.

PIGGOTT, M. R. & YOKOM, J. C. 1968. The weakening of silica fibres by heat treatment. *Glass Tech.,* 9**,** 172-175.

PLONKA, R., MADER, E., GAO, S. L., BELLMANN, C., DUTSCHK, V. & ZHANDAROV, S. 2004. Adhesion of epoxy/glass fibre composites influenced by aging effects on sizings. *Composites Part A,* 35**,** 1207-1216.

R'MILI, M., BOUCHAOUR, T. & MERLE, P. 1996. Estimation of Weibull parameters from loose-bundle tests. *Composites Science and Technology,* 56**,** 831-834.

R'MILI, M. & LAMON, J. 2011. Investigation of subcritical crack growth using load relaxation tests on fibre bundles. *Acta Materials*, 59**,** 2850-2857.

R'MILI, M., MOEVUS, M. & GODIN, N. 2008. Statistical fracture of E-glass fibre using a bundle tensile test and acoustic emission monitoring. *Composites science and technology*, 68**,** 1800-1808.

RAY, B. C. 2005. Loading rate sensitivity of glass fiber-epoxy composite at ambient and sub-ambient temperatures. *Journal of Reinforced Plastics and Composites*.

REYNAUD, P., R'MILI, M. & FANTOZZI, G. 2007. Fatigue Behaviour of Ceramic Matrix Composites at High-Temperature. Institut National des Sciences Appliquées.

RIBEIRO, M. C. S., MEIRA-CASTRO, A. C., SILVA, F. G., SANTOS, J., MEIXEDO, J. P., FIUZA, A., DINIS, M. L. & ALVIM, M. R. 2013. Re-use assessment of thermoset composite wastes as aggregate and filler replacement for concrete-polymer composite materials: A case study regarding GFRP pultrusion wastes. *Resources, Conservation and Recycling*, xxx**,** xxx-xxx.

RYABOV, V. A. 1968. The role of surface in the physical and chemical properties of glass. *Glass Technology*, 9**,** 105-112.

SAKKA, S. 1957. Effects of reheating on strength of glass fibers. *Sawai Laboratory.* Japan: Kyoto University.

SAMBORSKY, D. D., MANDELL, J. F. & PANCASATYA, A. 2012. 3-D static elastiic constants and strength properties of a glass/epoxy unidirectional laminate. Department of Chemical and Biological Engineering, Montana State University, Bozeman.

SCHMITZ, G. K., METCALFE, A. G. & LONG, J. V. 1963. Exploration and evaluation of new glasses in fiber form. *NRL Project 62 R05 19A. Technical Memo.* San Diego 12, California: U.S. Naval Research Laboratory.

SGLAVO, V. M. 2015. Chemical strengthening of soda lime silicate float glass: Effect of small differences in the KNO_3 bath. *International Journal of Applied Glass Science*, 6**,** 72-82.

SHEN, J. & GREEN, D. J. 2004. Prediction of stress profile in ion exchange glasses. *J. Non Cryst. Solids*, 2004**,** 79-87.

SHOKRIEH, M. M., MOSALMANI, R. & MAJID, O. J. 2013. Strain rate dependent micromechanical modeling of reinforced polymers with carbon nanotubes. *Journal of Composite Materials*, 48**,** 3381-3393.

SHRIVASTAVA, A. K., & HUSSAIN, M. N. 2008. Effect of low temperature on mechanical properties of bidirectional glass fiber composites *Composites Materials*, 42**,** 2407-2432.

SMEDSKJAER, M. M., JENSEN, M. & YUE, Y. 2010. Effect of thermal history and chemical composition on hardness of silicate glasses. *Journal of Non-Crystalline Solids*, 356**,** 893-897.

SOLVANG, M., GROVE-RASMUSSEN, S. & FOLDSCHACK, M. R. 2014. *Melt Composition for the Production of Man-made Vitreous Fibres*. USA patent application.

STOCKHORST, H. & BRUCKNER, R. 1982. Deviation of structure between bulk and fiber glasses. *Journal de Physique Colloques,* 43**,** C9-451-C9-454.
STRICKLAND, J. 2011. How gorillas glass works. Corning Glass Works.
SURATWALA, T. I. & STEELE, R. A. 2003. Anomalous temperature dependence of sub-critical crack growth in silica glass. *Journal of Non-Crystalline Solids,* 316**,** 174-182.
SUTHERLAND, L. S., SHENOI, R. A. & LEWIS, S. M. 1998. Size and scale effects in composites: I. Literature review. *Composites Science and Technology,* 59**,** 209-220.
TANIGUCHI, N., ARAO, Y., NISHIWAKI, T., HIRAYAMA, N., NAKAMURA, K. & KAWADA, H. 2012 Experimental study on impact tensile property of glass fiber *Advanced Composite Materials,* 21.
TAYLOR, A. T., MATTHEWSON, M. J. & KURKJIAN, C. R. 1999. Strength degradation of silica fibers by acetone immersion. *SPIE Conference on Optical Fiber Reliability and Testing.* Boston, Massachusetts: SPIE.
THOMAS, W. F. 1960. An investigation of the factors likely to affect the strength and properties of glass fibres. *Physics and Chemistry of Glasses,* 1.
THOMAS, W. F. 1971. An investigation of the factors affecting the strength of glass fibre strand. *Journal of Glass Technology. ,* 12**,** 60 - 64.
THOMASON, J. L. Interfacial strength in themoplastic composites - at last an industry friendly measurement method? Proceedings of the 7th International Conference on Interfacial Phenomena in Composite Materials (IPCM7), 2001 Spain. Butterworh Heinemann.
THOMASON, J. L. 2007. Iinterfaces and interfacial effects in glass reinforced thermoplastics. *In:* SORENSEN, B. F., MIKKELSEN, L. P., LILHOLT, H., GOUTIANOS, S. & ABDUL-MAHDI, F. S. (eds.) *Interface Design of Polymer Matrix Composites -Mechanics, Modelling and Manufacturing.* Proceedings of the 28th Riso International Symposium on Materials Science ed. Roskilde, Denmark: University of Strathclyde.
THOMASON, J. L. 2012a. Glass fibre sizings: A review of the scientific literature. *Sizing application at the state of the art ECR glass fibre production facility of AFG Bahrain*
THOMASON, J. L. 2013. On the application of Weibull analysis to experimentally determine single fibre strength distributions. *Composites Science Tech.,* 2013**,** 74-80.
THOMASON, J. L., URE, J., YANG, L. & KAO, C. C. Mechanical study on surface treated glass fibres after thermal conditioning. ECCM15 - 15th European Conference on Composite Materials, June 2012 2012 Venice, Italy. 24-28.
THOMASON, J. L., YANG, L., KAO, C. C., JENKINS, P., SAEZ-RODRIGUEZ, E. & NAGEL, U. Regeneration of thermally recycled glass fibre for cost-effective composite recycling: Overview of the Recover Projects'. 16th European Conference on Composite Materials, ECCM16, 2014a Seville, Spain.
THOMASON, J. L., YANG, L. & MEIER, R. 2014b. The properties of glass fibres after conditioning at composite recycling temperatures. *Composites Part A,* 61**,** 201-208.
TOMOZAWA, M. 1985. Water in glass. *Journal of Non-Crystalline Solids,* 73**,** 197-204.

TOMOZAWA, M. & HAN, W. 1991. Water enttry into silica glass during slow crack growth. *Journal of Am. Cream. Soc.*, 74**,** 2573-76.
TRUSTRUM, K. & JAYATILAKA, A. D. S. 1983. Applicability of Weibull analysis for brittle materials. *Journal of Materials Science,* 18**,** 2765-2770.
TSAI, S. W. & WU, E. M. 1971. A general theory of strength for anisotropic materials. *Journal of Composite Materials,* 5**,** 58.
VARSHNEYA, A. K. 2010. The physics of chemical strenthening of glass: Room for a new view. *Journal of Non-Crystalline Solids,* 356**,** 2289-2294.
VIELI, O. A. 1967. *Cellular Glass and Method of Making Same*.
VIKRAM, N. & KUMAR, R. 2013. Review on fatigue-crack growth and finite element method. *International Journal of Scientific & Engineering Research,* 4.
WAIT, C. F. 2016. *Clean filament winding: Industrial site trials and product evaluation.* PhD, University of Birmingham.
WAKABAYASHI, H. & TOMOZAWA, M. 1989. Diffusion of water into silica glass at low temperature. *Journal of American Ceramic Society,* 72**,** 1850-55.
WALLENBERGER, F. T. 2010. Commercial and experimental glass fibers. *In:* WALLENBERGER, F. T. & BINGHAM, P. A. (eds.) *Fiberglass and Glass Technology*. Pittsburgh, PA 15237, USA: Springer Science Business Media, LLC.
WANG, L., KISTER, G., RALPH, B., TALBOT, J. D. R., & FERNANDO, G. F. 2003. Conventional E-glass fiber light guides: Self-sensing composite based on Sol-gel cladding. *Journal of smart materials and structures,* 13**,** 73 - 81.
WELSH, L. & HARDING, J. 1985. Effect of strain rate on the tensile failure of woven reinforced polyester resin composites. *Journal de Physique Colloques,* 46**,** C5-405-C5-414.
WIEDERHORN, S. M. & BOLZ, L. H. 1970. Stress corrosion and static fatigue of glass. *Journal of American Ceramic Society,* 53**,** 543-548.
WIERZHOWSKI, S. 1995. Chemistry of ion exchanges. Rensselaer. Available: http://www.rpi.edu/dept/chem-eng/Biotech-Environ/IONEX/chem.html.
WILLIAMS, P. T., CUNLIFFE, A. & JONES, N. 2005. Recovery of value-added products from the pyrolytic recycling of glass-fibre-reinforced composite plastic waste. *Journal - Energy Institute,* 78**,** 51-61.
WITTEN, E. 2014. The European GRP-market 2014. *In:* WITTEN, E. (ed.) *Composites market report 2014: Market developments, trends, challenges and opportunities.* Germany: Industrievereinig Verstarkte Kunststofee - Federation of Reinforced Plastics.
WU, W. F. & NI, C. C. 2006. Statistical aspects of some fatigue crack growth data. *Engineering Fracture Mechanics,* 74**,** 2952-2963.
YA, M., DEUBERNER, J. & YUE, Y. 2008. Enthalpy and anisotropy relaxation of glass fibers. *Journal of American Ceramic Society,* 91**,** 745-752.
YANG, L., SAEZ, E. R. & THOMASON, J. L. 2015. Can thermally degraded glass fibre be regenerated for closed-loop recycling of thermosetting composites. *Composites Part A,* 72**,** 167-174.

YANG, Y., BOOM, R., IRION, B., HEERDEN, D.-J. V., KUIPER, P. & WIT, H. D. 2011. Recycling of composite materials. *Chemical Engineering and Processing: Process Intensification,* xxx.

YOLKEN, H. T. & MATZKANIN, G. A. 2009. Nondestructive evaluation of advanced fiber reinforced polymer matrix composites. *NASA.* Hampton, Virginia: Texas Research Institute, Austin, Texas.

YUE, Y. 2004. Influence of physical ageing on the excessive heat capacity of hyperquenched silicate glass fibers. *Journal of Non-Crystalline Solids,* 348**,** 72-77.

YUE, Y. Z., CHRISTIANSEN, J. D. & JENSEN, S. L. 2002. Determination of the fictive temperature for a hyperquenched glass. *Chemical Physics Letters,* 357**,** 20-24.

ZAINUDDIN, S., HOSUR, M.V., ZHOU, Y., KUMAR, A., & JEELANI, S. 2009. Durability study of nanophased FRP composites under synergestic exposure exposure conditions. *Material Science & Engineering,* 507**,** 117-123.

ZANGENBERG, J. & BRONDSTED, P. 2015. Fatigue life in textile composites used for wind energy engineering. *In:* CARVELLI, V. & LOMOV, S. V. (eds.) *Fatigue of Textile Composites.* Amsterdam: Woodhead Publishing

ZHANDAROV, S. & MADER, E. Estimation of the local interfacial strength parameters of carbon nanotube fibers in an epoxy matrix from a microbond test data. European Polymer Congress, 2015 Dresden. 54-57.

ZINCK, P., MADER, E. & GERARD, J. F. 2001. Role of silane coupling agent and polymeric film former for tailoring glass fiber sizings from tensile strength measurements. *Journal of Materials Science,* 36**,** 5245-5252.